



MINISTÉRIO DA CIÊNCIA, TECNOLOGIA, INOVAÇÕES E COMUNICAÇÕES  
**INSTITUTO NACIONAL DE PESQUISAS ESPACIAIS**

sid.inpe.br/mtc-m21b/2017/04.18.17.29-TDI

**UNDERSTANDING FLOODING PROCESSES OF  
LARGE WETLANDS OF THE BOLIVIAN AMAZON  
THROUGH IN SITU OBSERVATION, REMOTE  
SENSING AND NUMERICAL MODELING**

Alex Ovando Leyton

Doctorate Thesis of the Graduate  
Course in Earth System Science,  
guided by Drs. Javier Tomasella,  
and Celso von Randow, approved  
in May 04, 2017.

URL of the original document:

<<http://urlib.net/8JMKD3MGP3W34P/3NNFSM5>>

INPE  
São José dos Campos  
2017

**PUBLISHED BY:**

Instituto Nacional de Pesquisas Espaciais - INPE

Gabinete do Diretor (GB)

Serviço de Informação e Documentação (SID)

Caixa Postal 515 - CEP 12.245-970

São José dos Campos - SP - Brasil

Tel.:(012) 3208-6923/6921

E-mail: pubtc@inpe.br

**COMMISSION OF BOARD OF PUBLISHING AND PRESERVATION  
OF INPE INTELLECTUAL PRODUCTION (DE/DIR-544):**

**Chairperson:**

Maria do Carmo de Andrade Nono - Conselho de Pós-Graduação (CPG)

**Members:**

Dr. Plínio Carlos Alvalá - Centro de Ciência do Sistema Terrestre (CST)

Dr. André de Castro Milone - Coordenação de Ciências Espaciais e Atmosféricas (CEA)

Dra. Carina de Barros Melo - Coordenação de Laboratórios Associados (CTE)

Dr. Evandro Marconi Rocco - Coordenação de Engenharia e Tecnologia Espacial (ETE)

Dr. Hermann Johann Heinrich Kux - Coordenação de Observação da Terra (OBT)

Dr. Marley Cavalcante de Lima Moscati - Centro de Previsão de Tempo e Estudos Climáticos (CPT)

Silvia Castro Marcelino - Serviço de Informação e Documentação (SID) **DIGITAL LIBRARY:**

Dr. Gerald Jean Francis Banon

Clayton Martins Pereira - Serviço de Informação e Documentação (SID)

**DOCUMENT REVIEW:**

Simone Angélica Del Ducca Barbedo - Serviço de Informação e Documentação (SID)

Yolanda Ribeiro da Silva Souza - Serviço de Informação e Documentação (SID)

**ELECTRONIC EDITING:**

Marcelo de Castro Pazos - Serviço de Informação e Documentação (SID)

André Luis Dias Fernandes - Serviço de Informação e Documentação (SID)



MINISTÉRIO DA CIÊNCIA, TECNOLOGIA, INOVAÇÕES E COMUNICAÇÕES  
**INSTITUTO NACIONAL DE PESQUISAS ESPACIAIS**

sid.inpe.br/mtc-m21b/2017/04.18.17.29-TDI

**UNDERSTANDING FLOODING PROCESSES OF  
LARGE WETLANDS OF THE BOLIVIAN AMAZON  
THROUGH IN SITU OBSERVATION, REMOTE  
SENSING AND NUMERICAL MODELING**

Alex Ovando Leyton

Doctorate Thesis of the Graduate  
Course in Earth System Science,  
guided by Drs. Javier Tomasella,  
and Celso von Randow, approved  
in May 04, 2017.

URL of the original document:

<<http://urlib.net/8JMKD3MGP3W34P/3NNFSM5>>

INPE  
São José dos Campos  
2017

Cataloging in Publication Data

---

Ovando Leyton, Alex.

Ov1u Understanding flooding processes of large wetlands of the bolivian Amazon through in situ observation, remote sensing and numerical modeling / Alex Ovando Leyton. – São José dos Campos : INPE, 2017.

xxvi+149 p. ; (sid.inpe.br/mtc-m21b/2017/04.18.17.29-TDI)

Thesis (Doctorate in Earth System Science) – Instituto Nacional de Pesquisas Espaciais, São José dos Campos, 2017.

Guiding : Drs. Javier Tomasella, and Celso von Randow.

1. Flood mapping. 2. Satellite altimetry. 3. Hydrology.  
4. Wetlands. I.Title.

CDU 551.311.2:528.8(84)

---



Esta obra foi licenciada sob uma Licença [Creative Commons Atribuição-NãoComercial 3.0 Não Adaptada](https://creativecommons.org/licenses/by-nc/3.0/).

This work is licensed under a [Creative Commons Attribution-NonCommercial 3.0 Unported License](https://creativecommons.org/licenses/by-nc/3.0/).

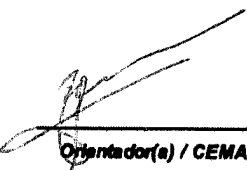
Aluno (a): **Alex Ovando Leyton**  
"UNDERSTANDING FLOODING PROCESSES OF LARGE WETLANDS OF THE BOLIVIAN AMAZON  
THROUGH IN SITU OBSERVATION, REMOTE SENSING AND NUMERICAL MODELING"

Aprovado (a) pela Banca Examinadora  
em cumprimento ao requisito exigido para  
obtenção do Título de **Doutor(a)** em  
**Ciência do Sistema Terrestre**

Dra. Luz Adriana Cuartas Pineda

  
\_\_\_\_\_  
Presidente / CEMADEN / São José dos Campos - SP

Dr. Javier Tomasella

  
\_\_\_\_\_  
Orientador(a) / CEMADEN / Cachoeira Paulista - SP

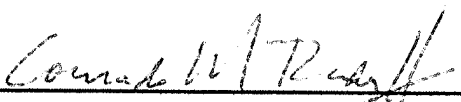
Dr. Celso von Randow

  
\_\_\_\_\_  
Orientador(a) / INPE / São José dos Campos - SP

Dr. Jean-Michel Martinez

  
\_\_\_\_\_  
Convidado(a) / IRD-HYBAM / Toulouse - FR

Dr. Conrado de Moraes Rudorff

  
\_\_\_\_\_  
Convidado(a) / CEMADEN / São José dos Campos - SP

**Este trabalho foi aprovado por:**

maioria simples

unanimidade

São José dos Campos, 04 de Maio de 2017



*“Between earth and earth's atmosphere, the amount of water remains constant; there is never a drop more, never a drop less. This is a story of circular infinity, of a planet birthing itself”*

- Linda Hogan -



*(In Portuguese)*

*À Graciela, minha esposa.*



## AKNOWLEDGMENTS

*(In Portuguese):*

O presente estudo representa o esforço e entusiasmo de muitas pessoas, cuja colaboração e amizade, fizeram deste percurso não só uma aprendizagem científica, mas também humana.

Agradeço ao Instituto Nacional de Pesquisas Espaciais e ao Centro de Ciência do Sistema Terrestre pela oportunidade e suporte.

Aos Drs. Javier Tomasella e Celso vonRandow: obrigado pelas orientações e pela confiança depositada em mim.

Ao Dr. Jean-Michel Martinez do IRD e OS-HYBAM pelas valiosas contribuições neste trabalho.

Aos Gerard Cochoneau (IRD), Philippe Vauchel (IRD), Stephan Calmant (LEGOS) e Jocelia Santos da Silva (UEA), Daniel Andrés Rodriguez (CCST-INPE), José Lazaro Siqueira Jr. (CCST-INPE) e Doyle McKey (CEF – Montpellier) pela disponibilidade e qualidade das discussões que contribuíram para este trabalho.

Ao Dr. Marc Pouilly (IRD) pela disponibilidade e suporte brindados.

Às Angela Harada e Mariana Santos (PG-CST) pela paciência e eficiente assistência brindadas.

Aos colegas doutorandos e professores do CCST, com quem tive a oportunidade de aprender e caminhar junto.

À Coordenação de Aperfeiçoamento de Pessoal de Nível Superior (CAPES) agradeço pelo apoio financeiro para a realização do doutorado.



## ABSTRACT

The Amazonian wetlands of Bolivia, known as the Llanos de Moxos, are believed to play a crucial role in regulating the upper Madeira hydrological cycle, the most important southern tributary of the Amazon River. In addition to its rich natural diversity, the Llanos were the setting for many complex pre-Columbian societies. Because the area is vast and sparsely populated, the hydrological functioning of the wetlands is poorly known. In this thesis we show the feasibility of using multi-temporal flood mapping, based on optical (MODIS M<sup>\*</sup>D09A1) and satellite altimetry (ENVISAT RA-2 and SARAL AltiKa altimeters) to characterize and monitor flood dynamics and to optimize floodplain simulations within a hydrological model (MHD-INPE model). Initially we analyzed the hydrometeorological configurations that led to the major floods of 2007, 2008 and 2014 in the upper Madeira Basin; Then, with the inclusion of altimetric information, which provided a vertical component for the two-dimensional flood maps, we analyzed the flood dynamics for the whole 2001-2014 period, including both extension and water stage variations that allowed to have initial surface water storage estimations. Finally, we critically analyzed how numerical modeling of the wetlands can be improved using additional remote sensing techniques. Our results showed that large floods are the result of the superimposition of flood waves from major sub-basins of the region and the strong influence of the occurrence of intense rainfall over saturated areas. We had identified relevant features of the flood regime, identifying three groups with particular characteristics in function of its connectivity and dependence to the Andes and piedmonts or to local processes and classified the hydraulic function of the wetlands based on remote sensed imagery. Finally, we demonstrate that remote sensing information is of major importance for improving floodplain simulations using hydrological models. However, there are still clear limitations in the existent remote sensed products for achieving seamless predictions of the hydrological behavior of the Llanos under changing climate.

Key-words: Flood mapping. Satellite Altimetry. Hydrology, Wetlands



# **COMPREENDENDO OS PROCESSOS DE INUNDAÇÃO DE GRANDES PLANÍCIES DE INUNDAÇÃO DA AMAZÔNIA BOLIVIANA POR OBSERVAÇÃO SITU, SENSOREAMENTO REMOTO E MODELAGEM NUMÉRICA.**

## **RESUMO**

As extensas terras úmidas da Amazonia Boliviana, conhecidas como Llanos de Moxos, desempenham um papel crucial na regulação do ciclo hidrológico do Alto Madeira, o mais importante tributário do sudoeste da Bacia Amazônica. Além de sua riqueza e diversidade natural, os Llanos de Moxos foram o cenário para o desenvolvimento de complexas sociedades pré-colombianas. Devido a área ser extensa e pouco povoada, o funcionamento hidrológico destas terras úmidas é pouco conhecido. Nesta tese mostrou-se a viabilidade do uso de mapeamento multitemporal baseado em imagens ópticas (MODIS M\*D09A1) e altimetria por satélite (ENVISAT RA-2 and SARAL AltiKa) para caracterizar e monitorar dinâmicas de inundação e otimizar simulações de planícies de inundação dentro de um modelo hidrológico (o modelo MHD-INPE). Inicialmente analisamos as configurações hidrometeorológicas que levaram aos grandes eventos de inundação dos anos 2007, 2008 e 2014 no Alto Madeira. Em seguida, com a inclusão de informação altimétrica, que forneceu o componente vertical aos mapas de inundação bidimensionais, analisamos as dinâmicas de inundação para o período 2001-2014, incluindo extensão e variações de profundidade das inundações, o que permitiu estimar de armazenamento de água superficial nas planícies. Finalmente analisamos criticamente como a simulação numérica das planícies pode ser otimizada com informação de sensoriamento remoto. Identificamos, baseados em informações de sensoriamento remoto e altimetria, três zonas diferenciadas em função de sua conectividade e dependência aos Andes ou a processos locais. Finalmente, demonstramos que a informação de sensoriamento remoto é de grande importância para a melhoria de simulações de planícies de inundação. No entanto, ainda existem limitações claras nos produtos de sensoriamento remoto para alcançar previsões exatas do comportamento hidrológico dos Llanos de Moxos.

Palavras-chave: Mapeamento inundações. Altimetria Satelital. Hidrologia.



## LIST OF FIGURES

Figure 2.1 - The upper Madeira Basin in Bolivia, RAMSAR sites and elevation map. ....	8
Figure 2.2 - Contrast between observed land cover change in 2008 and a land cover change scenario for 2050. ....	14
Figure 2.3 - Satellite ground tracks of ENVISAT and JASON-1 missions. ....	20
Figure 3.1 – Observational network in the study area. ....	29
Figure 3.2 - Detail of ALOS-PALSAR mosaics with the respective revolution date. ....	32
Figure 3.3 - ALOS PALSAR images preparation steps ....	34
Figure 3.4 - Multitemporal Radar backscatter behavior at L-band, for different landscapes in the Llanos de Moxos floodplain. ....	35
Figure 3.5 – ALOS-PALSAR Classification flowchart. ....	36
Figure 3.6 - PALSAR Classification flowchart, based in contrasts with the dry season image. ....	37
Figure 3.7 – Details of segmentation results. ....	38
Figure 3.8 -- MIR reflectance of a Savanna unit in the Mamore floodplain. ....	40
Figure 3.9 - Multitemporal variation of MIR reflectance within different land cover units. ....	41
Figure 3.10 - MODIS classification flowchart, based in MIR and NIR reflectance values. ....	42
Figure 3.11 – Validation of flood extension estimates. ....	43
Figure 3.12 - Relation between MODIS and PALSAR flood estimates in a savanna unit. ....	45
Figure 3.13 - Comparison between MODIS and PALSAR flood estimations. ..	45
Figure 3.14 – Monthly rainfall anomalies in the Upper Madeira. ....	47
Figure 3.15 - Hydrographs for different discharge stations: long term monthly mean discharge and during extreme flood events. ....	49
Figure 3.16 - Time-variation of the flooded area in the study area during period 2001–2014 ....	53
Figure 3.17 - Time-variation of the flooded area during the 2007, 2008 and 2014 flood events. ....	54
Figure 3.18 - Flood dynamics for the 2007, 2008 and 2014 events. ....	56

Figure 3.19 - Relationship between flooded area and water stage at Puerto Siles during the three floods.....	59
Figure 3.20 – Comparison of water stages of the Mamoré and Ibaré Rivers. .	61
Figure 4.1– Satellite tracks, measurement points and Location of altimetric virtual stations along floodplains in the Llanos de Moxos;.....	70
Figure 4.2 – Detail of the different basins and subbasins according to Pfafstetter (1989).....	71
Figure 4.3 - Comparison between water stage variations in floodplain and in the river mainstream.....	78
Figure 4.4 - Flood frequency and R-B Flood maps.....	82
Figure 4.5 - Water stage and flooded fraction time series. ....	84
Figure 4.6 – Signatures from water stage time series .....	86
Figure 4.7 – Box-Whisker and scatter plots from different flood signatures. ....	88
Figure 4.8 - Clustering results of flood signatures. ....	89
Figure 4.9 - Flooded area and surface water storage in floodplains during 2003-2014 period. ....	90
Figure 4.10 - Contrast between flooded area and surface water storage in floodplains with and without Andean connection.....	91
Figure 4.11 - Contrast between flooded area and surface water storage in floodplains with and without Andean connection.....	92
Figure 5.1 – a) Schematic representation of water flow between floodplain cells; b) and between river channel and floodplain.....	100
Figure 5.2 – Schematic relationship between volume VFP, area AFP and water stage HFP within a model cell. ....	102
Figure 5.3 - MHD-INPE model cell discretization .....	104
Figure 5.4 - Estimation of the flooded fraction for a model grid cell (25 km)..	105
Figure 5.5 - Modeled and observed streamflow in 4 sites within the study area. ....	109
Figure 5.6 - Comparison between total flooded areas estimated by the MHD-INPE model and mapped with MODIS MOD09A1 data.....	110
Figure 5.7 - Estimates of total flooded area by the MHD-INPE model and mapped with MODIS-MOD09A1 during flood peaks. ....	111

Figure 5.8 – Spatial representation of flooded areas as estimated by the MHD-INPE model and by MODIS MOD09A1 data. ....	112
Figure 5.9 - Flooded fraction as a function of water stage based in SRTM and satellite altimetry in different sites. ....	113



## LIST OF TABLES

Table 4.1 - Major basins, subbasins and codification of AVS .....	72
Table 4.2 - Maximum flooded area in the different tributaries, and subbasins division .....	80
Table 5.1 - Model performance expressed in NSE, RSR and PBIAS.....	108



## LIST OF ABBREVIATIONS

- ALOS - Advanced Land Observation Satellite
- ANA - Brazilian Water Agency
- AOI - Area of Interest
- BIOBAB - Aquatic BIO-diversity of the Bolivian Amazon Basin
- CEPAL - Comisión Económica para América Latina y el Caribe
- CMIP - Coupled Inter-comparison Project
- DN - Digital Numbers
- ELN - Equivalent Number of Looks
- ENVISAT - Environmental Satellite
- GCM - Global Circulation Model
- G-POD - European Space Agency Grid Processing on Demand
- ICESat - (Ice, Cloud, and land Elevation Satellite
- IIRSA - Initiative for the Integration of South American  
Infrastructure
- INMET - Brazilian National Institute of Meteorology
- INPE - Brazilian National Institute for Space Research
- IPH - Instituto Pesquisas Hidraulicas Universidad Federal Rio  
Grande do Sul
- IWRM - Integrated Water Resources Management
- JAXA - Japanese National Space Agency
- JERS - Japanese Earth Resources Satellite
- LLJ - Low Level Jet
- MGB - Modelo de Grandes Bacias -
- MHD - Modelo Hidrologico Distribuido -
- MIR - Mid Infra Red
- MODIS - Moderate Resolution Imaging Spectroradiometer
- NASA - National Aeronautics and Space Administration
- NDVI - Normalized Difference Vegetation Index
- NIR - Near Infra Red
- OBIA - Object Based Image Analysis
- PALSAR - Phased Array L-band Synthetic Aperture Radar

- SACZ - South Atlantic Convergence Zone
- SAMS - South American Monsoon System
- SAR - Synthetic Aperture Radar
- SARAL - Satellite with ARGOS and ALTIKA
- SENHAMI-BO - Bolivian Meteorology and Hydrology National Service
- SENHAMI-PE - Peruvian Meteorology and Hydrology National Service
- SO HYBAM - Geodynamical, hydrological and biogeochemical control of erosion/alteration and material transport in the Amazon basin
- SST - Sea Surface Temperature
- SSTA - Sea Surface Temperature Anomalies
- SWAT - Soil and Water Assessment Tool
- SWOT - Surface Water and Ocean Topography mission
- TIPNIS - Territorio Indígena y Parque Nacional Isiboro-Sécure
- TM - Thematic Mapper
- UDAPE - Unidad de Análisis de Políticas Sociales y Económicas
- WWF - World Wildlife Fund

## CONTENTS

1	INTRODUCTION.....	1
1.1	Research question, objectives and thesis outline.....	3
1.2	Thesis outline .....	5
2	WETLANDS OF THE BOLIVIAN AMAZON – AN ECOLOGICAL PATRIMONY WHICH IS WORTH TO UNDERSTAND .....	7
2.1	Location and characteristics.....	7
2.2	Water ecosystem services .....	10
2.3	Environmental change threats.....	11
2.4	Challenges and perspectives for understanding wetlands hydrology .....	16
2.4.1	The role of remote sensing and numerical models.....	18
2.4.2	Knowledge about the hydrology of the Bolivian Amazon wetlands ....	23
3	EXTREME FLOOD EVENTS IN THE BOLIVIAN AMAZON LOWLANDS.	27
3.1	Introduction .....	27
3.2	Methods .....	28
3.2.1	Data .....	28
3.2.1	Flood mapping .....	32
3.3	Results and discussion.....	46
3.3.1	Hydrological regime of the upper Madeira Basin .....	46
3.3.2	Hydrometeorological context of the 2007, 2008 and 2014 flood events in the upper Madeira Basin .....	46
3.3.3	Flood dynamics in the Llanos during the 2007, 2008 and 2014 events.....	52
3.3.4	Hydrological functioning of the Llanos.....	59
3.4	Conclusions.....	62
4	SATELLITE ALTIMETRY AND MULTITEMPORAL FLOOD MAPS TO SUPPORT PROCESS UNDERSTANDING .....	65

4.1	Introduction .....	65
4.2	Methods .....	66
4.2.1	Multitemporal flood maps .....	66
4.2.2	Altimetric water stage time series .....	67
4.2.3	Surface water storage in floodplains .....	75
4.3	Results .....	75
4.3.1	The complex flooding processes.....	75
4.3.2	Flood extension, variability and frequency .....	79
4.3.3	Water depth in floodplains.....	83
4.4	Discussion and conclusions .....	93
5	TOWARDS INTEGRATING SPATIAL HYDROLOGY AND HYDROLOGICAL MODELING .....	97
5.1	Introduction .....	97
5.2	Methods .....	97
5.2.1	The MHD-INPE model .....	97
5.2.2	Model parameterization.....	103
5.2.3	Water stage and flood extent .....	105
5.2.4	Model evaluation/validation.....	106
5.3	Results .....	108
5.3.1	Discharge and flooded area .....	108
5.3.2	Differences between modeled and remote sensing derived flood estimations at cell grid level.....	111
5.4	Discussion and conclusions .....	115
6	GENERAL DISCUSSION AND CONCLUSIONS .....	119
6.1	About the methods .....	119
6.1.1	Multitemporal flood mapping.....	119
6.1.2	Satellite altimetry in floodplains.....	120
6.1.3	Multi-temporal flood maps and satellite altimetry .....	120
6.1.4	Integrating remote sensing and hydrological modeling .....	121
6.2	Conclusions.....	122

REFERENCES.....	125
APPENDIX 1 .....	145



## 1 INTRODUCTION

Wetlands are the fragile interface between land and water; they perform relevant functions in the environment by playing a role in hydrological processes and biogeochemical cycles (FRASER; KEDDY, 2005; JUNK, 2013). They buffer extreme floods or droughts, support innumerable species and abundant biomass and provide habitat for a wide variety of flora-fauna and several services to riverside communities such as transportation, fisheries and agriculture (FRASER; KEDDY, 2005; MITCH; GOSSELINK, 2007; JUNK, 2013). Many wetlands are located in the tropics where optimum environmental conditions (radiation, temperature and precipitation) together with the regular enrichment in organic matter brought by seasonal floods, create one of the world's most productive ecosystems (MITCH; GOSSELINK, 2007).

Tropical South America is characterized by large watersheds (Amazon, Orinoco, Magdalena, Parana-Paraguay, São Francisco), by a very long coastline and by the uplands (Andean mountain range and the highlands of Guyana and Central Brazil). Large portions of these watersheds are flat and poorly drained floodplains exposed to monomodal flood pulses (e.g. in the Amazon and its large affluents) or multimodal (e.g. in streams and small rivers) (JUNK; FURCH, 1993). The noticeable rainfall seasonality, the variability of streamflow discharge and wetland water availability determines that most of wetlands in tropical South America belong to the floodplain category (JUNK; FURCH, 1993). According to Junk et al., (1989), floodplains consist of areas that are periodically inundated by the lateral overflow of rivers or lakes, and/or local precipitation or groundwater rise (sheet floods), changing the physicochemical environment with different biota responses and determining characteristic community structures.

The Amazon wetlands constitute the largest freshwater ecosystem in the tropics and they are represented by a diversity of plant communities varying from different types of savannas or aquatic macrophytes to wetland forests (JUNK, 2013). Carbon cycle studies indicate that the undisturbed forest of Amazonia

may be a strong sink of carbon, whereas the wetlands may act as a source of carbon into the atmosphere (RICHEY et al., 2002; ABRIL et al., 2014). Extensive wetlands and lakes may play role in global or regional climate and are strongly important in floods and biogeochemical processes regulation, since they retain different types of water and sediments from upstream (JUNK; FURCH, 1993).

Wetlands of the Bolivian Amazon, known widely as Llanos de Moxos, are of great importance for hydrological and biogeochemical cycles for the whole Amazon: The proximity and influence of the Andes determines a high spatial and temporal variability of floods, which even includes multi flood peaks in some rivers. The great proportion of herbaceous wetlands in the region (savannas), the highest among the Amazon (DE CARVALHO; MUSTIN, 2017) define a wide floodable area, of about 150000 km<sup>2</sup> (HAMILTON; SIPPEL; MELACK, 2004; HESS et al., 2015b).

The importance of this region is reflected in its recognition as Ramsar<sup>1</sup> site, considered the world's largest protected wetland in the world (WWF 2013). Although the Bolivian Amazon wetlands have aroused interest, mainly across the scientific community, its ecological importance is not well acknowledged by the government and society in general. This is the situation of most of the South American wetlands, where, as described by Wittmann et al., (2015), the lack of proper knowledge about its functioning, definition and delimitation is an obstacle to its conservation and management. There is an urgent need then, to develop proper tools and methods to assess the functionality of these ecosystems and the services they provide.

Despite being the largest savanna wetland the Amazon, the Llanos de Moxos have been little studied, especially from the hydrological point of view. The lack of dense hydrologic and meteorological observational network, derived from the

---

<sup>1</sup> The Convention on Wetlands of International Importance, called Ramsar convention, is an intergovernmental treaty that provides the framework for national action and international cooperation for the conservation and wise use of wetlands and their resources. The treaty was adopted in the Iranian city of Ramsar in 1971 (<http://www.ramsar.org>)

remoteness and large extension of these wetlands, may be pointed as the main constraint for this. In the last decades, the role of remote sensing to overcome these constraints has proven to be crucial; most of the knowledge regarding different hydrological aspects is a result of the active and passive sensors in complementarity with in situ information. Although the limited data availability also had constrained the implementation of hydrological models, there are relevant examples that demonstrate its feasibility when combined or integrated with remote sensing information.

In this study, the combination of multi-temporal flood maps (from MODIS-M\*D09A1 data) and floodplain water level time series derived from satellite altimetry (ENVISAT RA2 & SARAL AltiKa altimeters) allow to answer, for the first time, key questions about the hydrological functioning of the Llanos de Moxos: Providing new insights regarding the influences of extreme climatic conditions in the region, contributing to reduce the gaps between common perception and scientific evidence about extreme floods the region; Answering previous hypothesis regarding the dynamics of the floods in region; Providing initial estimations of the floodplains role in streamflow regulation through surface water storage; and exploring the feasibility for improving hydrological models.

This study is of relevance for understanding the wetlands role in providing ecosystem services and constitutes a preparatory information for future altimetry projects such as the SWOT (DURAND et al., 2010), which is expected to provide information of continental waters in an unprecedented way and support hydrological modeling.

## **1.1 Research question, objectives and thesis outline**

Research questions:

- What are the temporal and spatial hydrological patterns that explain the magnitude and duration of extreme flood events?

- Is there any characteristic that allows differentiating between endogenous and exogenous flood processes?
- What is the role of the Llanos de Moxos in water storage and streamflow regulation?
- It is possible to improve wetland simulation in hydrological models using multitemporal flood maps and satellite altimetry in the study area?

General objective:

To understand flooding processes of large wetlands of the Bolivian Amazon through in situ observation, remote sensing and numerical modeling.

Specific objectives:

- To perform a multitemporal flood mapping using both optical MODIS and radar (ALOS-PALSAR) data and to analyze streamflow and meteorological data for the period 2001-2014, in order to assess the temporal and spatial hydrological patterns that explain the magnitude and duration of extreme flood events.
- To retrieve water stage variations within floodplains using satellite altimetric data from ENVISAT-Ra2 and SARAL-AltiKa altimeters, in order to characterize flood dynamics in terms of water stage variations.
- To combine Multitemporal maps and satellite altimetry information in order to estimate quantify water storage in floodplains.
- To analyze the results of hydrological model in order to assess the feasibility of integrating remote sensing and numerical models to better understand wetland's hydrology.

## 1.2 Thesis outline

This document is organized in six main sections:

**Chapter 1:** With a brief background of the topic, research questions and objectives.

**Chapter 2:** This section contains a brief description of the Bolivian Amazon wetlands (the study area), location, main hydrological, climatic and physiographic characteristics. In order to highlight the relevance of the Llanos de Moxos, a characterization of the ecosystem services that these wetlands provide is presented. Then we briefly explain the main environmental change threats and its possible impacts in the hydrological processes. Finally we describe the challenges and perspectives for understating the wetlands hydrology using remote sensing and numerical models.

**Chapter 3:** This chapter, contains an analysis of the hydrometeorological context of the 2007, 2008 and 2014 floods in the upper Madeira Basin and the dynamics of the Llanos de Moxos during those major floods events. Previous hypothesis regarding the flood processes in the region are initially discussed. The analysis was done using multitemporal flood maps and observational data.

**Chapter 4:** In this chapter we present the inclusion of satellite altimetry as a key complementary information for the two-dimensional multitemporal flood maps. We analyze the flood dynamics for the whole 2001-2014 period, including both extension and water stage variations that allowed to have initial surface water storage estimations. More insights for the hypothesis regarding the flood processes are provided.

**Chapter 5:** This chapter addresses the feasibility of using remote sensing information for improving numerical models. We critically analyze the results of the MHD-INPE model and discuss about model constraints in floodplain simulation and the potential contribution of flood maps and satellite altimetry.

**Chapter 6.** Discussion and conclusions



## **2 WETLANDS OF THE BOLIVIAN AMAZON – AN ECOLOGICAL PATRIMONY WHICH IS WORTH TO UNDERSTAND<sup>2</sup>**

### **2.1 Location and characteristics**

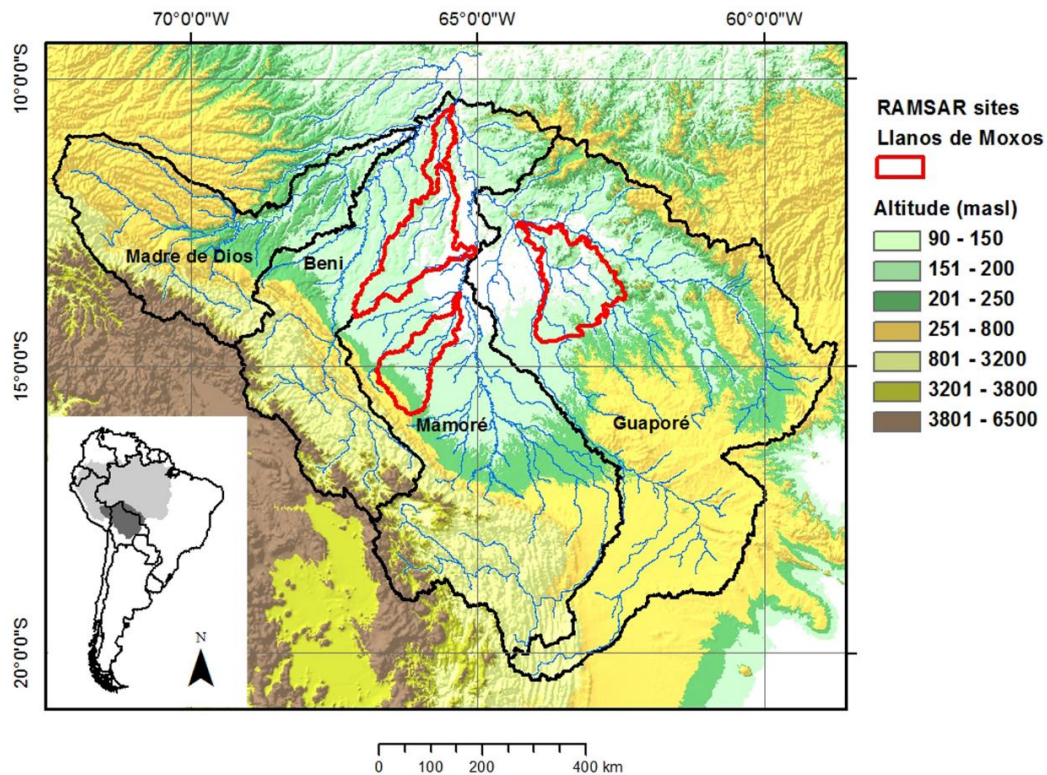
The Bolivian wetlands, “Llanos de Moxos”, is a vast savanna floodplain of approximately 150000 km<sup>2</sup> (HAMILTON; SIPPEL; MELACK, 2004) located in the Mamoré-Beni-Guaporé (Iténez) rivers fluvial system, between the eastern Andes, the adjacent Amazon alluvial fans and the Precambrian Brazilian shield (Figure 2.1). The mean altitude at the “Llanos” is approximately 150 m with a mean slope less than 10 cm per km (GUYOT, 1993). The natural vegetation is mixed: grassland and savannah vegetation in seasonally flooded areas, and evergreen tropical forests in non-flooded areas, although deforestation has converted part of the forest areas to pasture (HAMILTON; SIPPEL; MELACK, 2004).

The hydrological dynamics of the “Llanos” is controlled by four major sub-basins (Figure 2.1): the Guaporé (Iténez), the Mamoré, the Beni and the Madre de Dios, which define the upper Madeira River Basin, the main southern tributary of the Amazon. Although the Madre de Dios River is outside the geographical region that delimits the “Llanos”, the hydrological behavior of that river has a strong influence on the wetlands during major floods.

---

<sup>2</sup> This chapter is based in the publication: OVANDO, A.; TEJADA, G.; TOMASELLA, J. Environmental Change and Water Ecosystem Services in the Bolivian Amazon Lowlands (Llanos de Moxos). GLP newsletter, v. 12, p. 30–36, 2016

Figure 2.1 - The upper Madeira Basin in Bolivia, RAMSAR sites and elevation map.



Major sub-basins are delimited by black polygons Bolivian amazon wetlands; official RAMSAR sites delimitation within Llanos de Moxos (red polygons) and elevation map.

Source: by the author

Altitudes in the four sub-basins range from 90 to 6500 meters above sea level (masl), where it is possible to differentiate three geomorphological regions: the lowlands (< 800 masl), the Andean slope (800 to 3200 masl) and the high Andes (3200 to 6500 masl). The seasonality of precipitation in the Bolivian Amazon is governed by the South American Monsoon System (SAMS) composed of the Low Level Jet (LLJ), the Chaco low pressure system and the South Atlantic Convergence Zone (SACZ) (MARENGO et al., 2004). SAMS determines the moisture transport from the Atlantic Ocean southwards through the Amazon during the rainy season (November to March), and it is estimated

that 70% of the total annual precipitation occurs during these months (NAVARRO; MALDONADO, 2004). Precipitation during dry months (June to September), if present, is generated mainly by cold frontal advections from the Antarctic anti-cyclone (NAVARRO; MALDONADO, 2004). Incoming moisture from the Atlantic is deflected by the Andes, determining a particular spatial rainfall distribution across the Bolivian Amazon. The annual values in the lowlands vary southwards: from 2000 mm year<sup>-1</sup> in the northern part of the region to 1500 mm year<sup>-1</sup> in the central lowlands and 800 mm year<sup>-1</sup> in the southern part (ROCHE; FERNANDEZ-JAUREGUI, 1988).

Rainfall variability westwards is highly influenced by the Andes: east-oriented Andean slopes capture moist warm air forming a humid belt (ESPINOZA VILLAR et al., 2009). In the piedmonts (<1500 masl), rainfall values range from 6000 mm year<sup>-1</sup> in the Mamore Basin, 4000 mm year<sup>-1</sup> in the Beni Basin, to 1700 mm year<sup>-1</sup> in the Mamoré (ROCHE; FERNANDEZ-JAUREGUI, 1988). Rainfall decreases with altitude from 800-1000 mm year<sup>-1</sup> in the Andean summits of the Beni and Madre de Dios basins (>4500 masl) to 450 mm year<sup>-1</sup> in the upper Mamoré basin (~2500 masl) (ROCHE; FERNANDEZ-JAUREGUI, 1988).

The strong contrast between dry and rainy season leads to annual variability in discharge. In the Andes and piedmonts, hydrographs have multiple peaks and lows, denoting a rapid response to rainfall. Downstream, the hydrograph is smoothed and floods occur generally during summer (ROCHE; FERNANDEZ-JAUREGUI, 1988; RONCHAIL et al., 2003, 2005). Interannual variability in streamflow may influence flood intensity and extension depending on the meteorological conditions in the Andean slopes-piedmonts and within the lowlands (ESPINOZA VILLAR et al., 2009). Thus, variable sources of floodwaters that include distinct upland watersheds and local precipitation result in high variability in both the magnitude of the flooding and droughts (HANAGARTH, 1993; HAMILTON; SIPPEL; MELACK, 2004).

## 2.2 Water ecosystem services

Freshwater is considered as the bloodstream of the biosphere, driving critical processes and functions in forests, woodlands, wetlands, grasslands, croplands and other terrestrial ecosystems while keeping them resilient to change (FALKENMARK, 2003). Wetlands, besides providing fresh water, regulation and cultural services, support a rich biodiversity and human populations. Water is a key driver in the delivery of many ecosystem services, including provisioning services (domestic use, irrigation, power generation and transportation), as well as supporting, regulatory and cultural services (AYLWARD; BANDYOPADHYAY; BELAUSTEGUIGOTIA, 2005; BOLEE, 2011).

Human livelihood and wellbeing, along the Amazon, is strongly dependent on local landscape, ecosystem functionality and the multiple services they provide (BOLEE, 2011). Like other wetlands in Amazonia, the Llanos de Moxos, because of its size and remoteness, is poorly monitored. These wetlands are believed to be a vital piece of the overall health of the entire Amazon and it has recently designated by the RAMSAR convention as a wetland of international importance (WWF, 2013). The multiple Water Ecosystem Services that they provide are not yet properly characterized and quantified. Also, the environmental change impacts in the hydrological cycle, that may compromise these ecosystems functions and services, are still poorly unknown.

In general, Amazonian wetlands play a crucial role at the watershed scale because they are the most important source of biodiversity in the ecosystem (JUNK, 1997) and because they modulate water fluxes. Amazon wetlands affect the basin sediment load, modifying water and dissolved and particulate material fluxes from upland watersheds through river drainage networks (GUYOT et al., 1996; JUNK; WORBES, 1997; DUNNE et al., 1998; MELACK; FORSBERG, 2001). Water residence time in wetlands alters river discharge due to the exchange of water between river and floodplain, and it promotes large evaporative losses (BONNET et al., 2008). In addition, water residence time in Amazon wetlands is crucial in the regulation of biogeochemical and biotic processes (JUNK; BAYLEY; SPARKS, 1989; VIERS et al., 2005; BOUCHEZ et

al., 2012) and consequently carbon dioxide (CO<sub>2</sub>) and methane (NH<sub>4</sub>) emissions (RICHEY et al., 2002; KAYRANLI et al., 2010; ABRIL et al., 2014). Both sediments and biogeochemical dynamics depend on the spatial and temporal patterns of hydrology, which, in addition to rainfall distribution, are also influenced by the topography, soil and vegetation (MERTES et al., 1995). It is known that the Bolivian Amazon wetlands retain different types of water and sediments from upstream (GUYOT, 1993). These processes imply complex interactions of black water, generated in the lowlands, and sediment loaded white water from the Andes (BECK et al., 2008). Black and white water interactions, together with the high water storage capacity of the floodplains, are determinant for nutrients cycle, sediment weathering and consequently the ecology, spatial segregation of vegetation and ecosystems (POUILLY et al., 2004).

Most of the waterways in the Bolivian Amazon has national relevance since they belong to bi-oceanic corridors (ALURRALDE et al., 2008). The Ichilo-Mamore, Itenez-Madera and Beni-Madre de Dios corridors are the most relevant waterways. Also secondary rivers are used for transportation, merchandise exchange between disperse communities in the BA lowlands (VAN DAMME, 2002).

In addition to its rich natural diversity, the Llanos were the setting for many complex pre-Columbian societies. Vestiges of these cultures, spread over the floodplains, constitute an example of human adaptation to aquatic environments (LOMBARDO et al., 2013).

### **2.3 Environmental change threats**

Climate change and variability as well as human activities are impacting water processes and increasing the pressure to ecosystems and the services they provide. As exposed by Castello; Macedo (2016), hydrological alterations may trigger a wide range of impacts in Amazon freshwater ecosystems, many of which have complex feedbacks and synergic interactions. Cumulative impacts of dams, infrastructure and climate change can substantially alter

biogeochemical cycling, transport of organic and inorganic matter, freshwater community composition and productivity (CASTELLO; MACEDO, 2016).

Sea surface temperature anomalies (SSTA) are believed to be influencing extreme flood events in the Bolivian Amazon (RONCHAIL et al., 2005). For example, the unprecedented rainfall over the Madeira Basin during the rainy season of 2013-2014, was related to warm conditions in the Pacific-Indian and sub-tropical south Atlantic, and exceptional warm conditions in the Atlantic Ocean, which favored the humidity transport over South western Amazonia (ESPINOZA et al., 2014). The increased frequency of extremes in the Amazon has led Gloor et al., (2013) to suggest an intensification of the hydrological cycle starting from the 90s, which is responsible for “progressively greater differences in Amazon peak and minimum flows”.

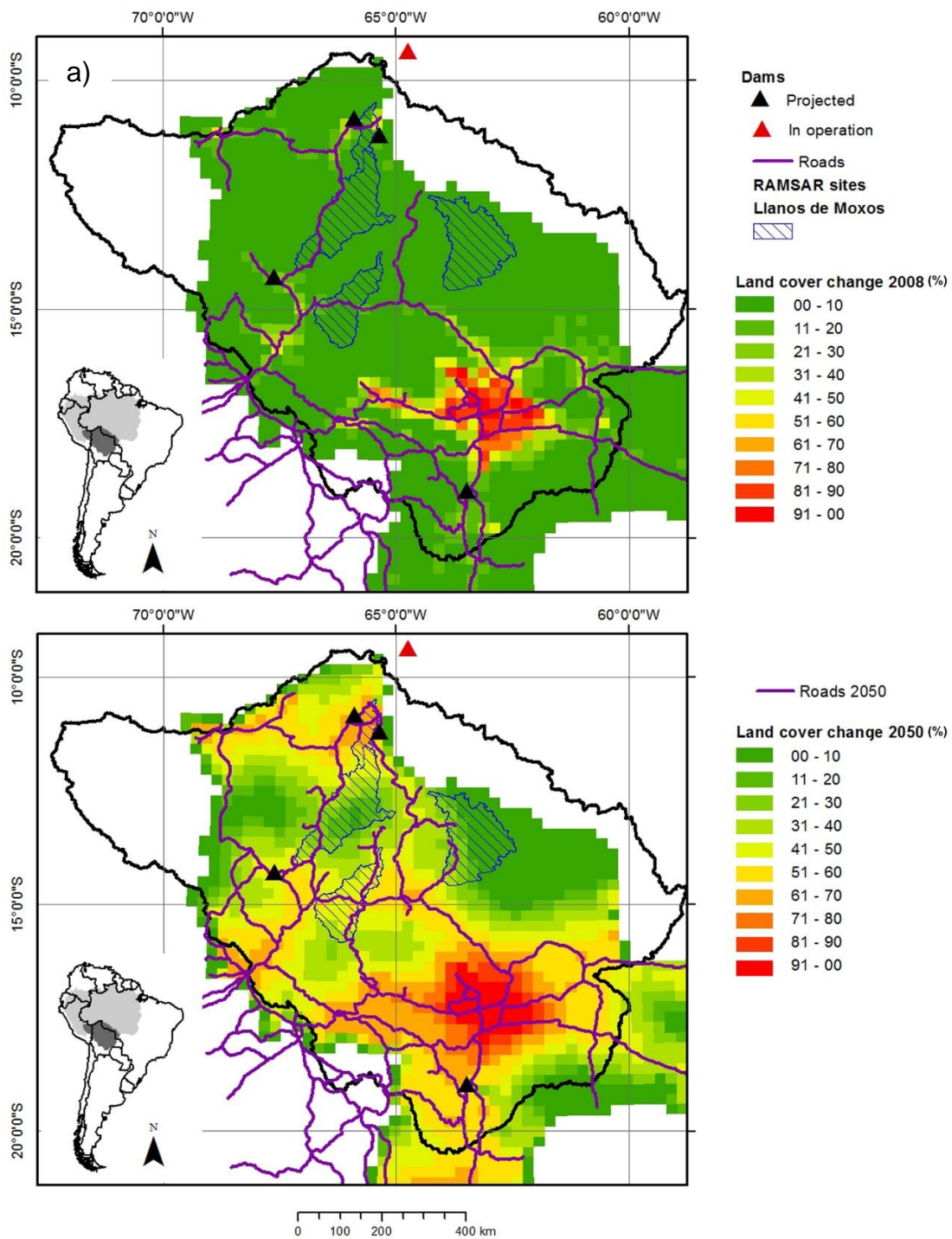
It has been shown that these extreme events have the potential to cause serious disruptions in the ecological functioning of the Amazon forest ecosystems (PHILLIPS et al., 2009) and alter the normal functioning of the wetlands, pushing the physiological adaptations and behavioral changes of living organisms beyond their resilience limits (JUNK, 2013). In addition, they compromise the livelihoods of riverine communities, which are dependent on the flood pulses (TOMASELLA et al., 2013; PINHO; MARENGO; SMITH, 2015).

According to (SEILER; HUTCHES; KABAT, 2013) who had analyzed 35 Global Circulation Models (GCMs) from the 3<sup>rd</sup> and 5<sup>th</sup> Coupled Inter-comparison Project (CMIP3/5), the Bolivian Lowlands are likely to have an annual precipitation decrease of -9% for the 2010-2099, this reduction attain to -19% during drier months (June to November). Results from Regional circulation Models (RCMs) in Bolivia (SEILER, 2009) exhibits and accentuation of the precipitation regime in the lowlands: more precipitation during the rainy season and less precipitation during the dry season. Severe economic and social impacts were reported after extreme events of 2007, 2008 and 2014 in the Bolivian lowlands (CEPAL, 2008; UDAPE, 2015), but little is known about impacts in the ecosystems.

Land change may potentially impact precipitation, river discharge and groundwater recharge in different forms intensities and scales, as demonstrated by numerical models by (SAMPAIO et al., 2007; COE; COSTA; SOARES-FILHO, 2009; MEI; WANG, 2009; DAVIDSON et al., 2012). Also, deforestation in riparian areas reduce filtration of terrestrial inputs flowing into the river system, causing erosion reducing water quality and altering aquatic primary production (WILLIAMS; FISHER; MELACK, 1997) while disrupting food webs and altering habitats for plant and animal species (FORSBERG et al., 1993; BOJSEN; BARRIGA, 2002; MACEDO et al., 2013). Deforestation in the Bolivian lowlands between 2000-2010 achieved 1.8 Million ha, being 56% in the central portion of the Bolivian Amazon (CUÉLLAR et al., 2012). According to Tejada et al., (2016), the projected deforestation for 2050, following the current trends in extractivism and land reclamation for agriculture, might affect 41% of the Bolivian Amazon basin (Figure 2.2). It is clear then, that identifying deforestation impacts in the wetlands hydrology is a pending task.

Sediment load and transport into the river systems following deforestation and mining activities may derive in water pollution with severe impacts on ecosystems and public health. Sediments from deforested areas in medium and upper portions of the watersheds are deposited in large floodplain environments activating mercury pollution (MAURICE-BOURGOIN et al., 2000; ACHA et al., 2005; OVANDO, 2012).

Figure 2.2 - Contrast between observed land cover change in 2008 and a land cover change scenario for 2050.



This is the worst scenario in terms of deforestation since road construction, oil extraction, mechanized agriculture and cattle ranching dominate the economy with little environmental governance; Main projected and operating dams (a and b), and contrast between current road network (a) and projected road network for 2050 (b).

Source: Tejada et al., (2016).

Roads constitute a significant hazard for ecosystems functionality and hydrology as well as a major driving factor for land use changes. In general, linear structures like roads, highways, power lines and gas lines interact with natural stream networks at the landscape scale, this interaction may impact biological and ecological processes in stream and riparian systems (JONES et al., 2000). The major ecological effects of roads, according to Forman & Alexander (1998), are: species disturbance, fragmentation of habitats and hydrologic and erosion effects. The bi-oceanic corridor and the highway across the TIPNIS (Territorio Indígena y Parque Nacional Isiboro-Securo) protected area are examples of current road projects, under the Initiative for the Integration of South American Infrastructure (IIRSA) ([www.iirsa.org](http://www.iirsa.org)), with undetermined impacts in the Llanos de Moxos

Also under IIRSA, massive hydroelectric dams are operating or in their initial projecting stages. The Cachuela Espezanza dam in the Beni River, Hidroeléctrica Binacional dam in the Madera River and Rositas in the Rio Grande River are the most representative dam projects in the Bolivian Amazon. In the Brazilian side, Santo Antonio and Jirau dams are already in operation. Dams in the region may impact the wetlands functionality in several ways: changes in water stage (level) can be observed even hundreds of kilometers upstream, with a consequent loss in flow velocity that could alter flood dynamics in a large area (POUILLY et al., 2009a); Sediment flow may be constrained deriving in enhanced sediment deposition-transformation and then mercury pollution (PÉREZ et al., 2009). The spread of vector borne diseases like malaria, leishmanioses, dengue, yellow fever and others may be enhanced since large areas may remain flooded for more time (ARNÉZ, 2009); The natural cycles of organic matter decomposition in floodplains may increase greenhouse gases emissions (CO<sub>2</sub> and CH<sub>4</sub>) (POUILLY et al., 2009b); The dams will form an artificial barrier to fish migration and mobilization, impacting on fish spawning–reproduction and local economy (VAN DAMME et al., 2010). Even dams in the Andean Amazon zone may alter the connectivity between Andes and the floodplains (FINER; JENKINS, 2012). Hydroelectrical dams in white water rivers are believed to impact sediment dynamics and river floodplain

morphology (FEARNSIDE, 2013) with unexpected consequences in incubation, growth rates, development time of some species (LUBIANA; FERREIRA JÚNIOR, 2009). With these examples, we can see that relevant efforts had been done to understand the potential impacts of dams; but a comprehensive evaluation of the applicability of dams, considering the wetland functionality and the Andes-Amazon connectivity, is still a critical need.

#### **2.4 Challenges and perspectives for understanding wetlands hydrology**

In order to tackle environmental change, water managers and policy makers require holistic assessments integrating biophysical and social science at different scales. Addressing vulnerability through the principles of the Integrated Water Resources Management (IWRM) may allow understanding the system, its key variables and relationships in a holistic way (MITCHELL, 2005). According to the Global Water Partnership (GLOBAL-WATER-PARTNERSHIP, 2003), IWRM is “a process which promotes the coordinated development and management of water, land related resources in order to maximize the resultant economic and social welfare in an equitable manner without compromising the sustainability of vital ecosystems”. IWRM makes possible to link environmental change with aspects of water use, water quality, management, conservation, ecosystem functionality, social-cultural values and the relevance of institutions relating to water (BELLAMY JA; JOHNSON, 2000; PLUMMER; LOE; ARMITAGE, 2012). It is a broad axis for analysis, it encompasses a wide and holistic range of potential impacts with many subsystems and particular impacts to take into account in function of the scale of study and actors perceptions.

It is noticeable that, in the context of global environmental change, the relevance of non-climatic factors is growing concern; initially non-climatic factors were limited to a socio-economic domain, then the term “non-climatic drivers” is included accounting for demographic, economic, technologic and biophysical drivers (FÜSSEL; KLEIN, 2006). Still, even though there is much more than climate change threatening the Llanos de Moxos, most of the initiatives for addressing vulnerability in Bolivian lowlands are focused mainly in climate

change drivers.. This means that it is necessary to include a wider set of non-climatic factors in order to highlight potential aggregated impacts, especially when addressing water resources.

As exposed by Wittmann et al., (2015), there is an urgent need for scientific research in South American wetlands, from its functioning, definition and delimitation to the proper assessment of potential environmental change impacts, which allow supporting conservation or management policies. This is the case of the Llanos de Moxos, whose ecological importance is not acknowledged by the government and society in general. Pertinent socio-economic and physical information is required to assess the functionality of these ecosystems and the services they provide. It is worth to highlight that even being the largest savanna wetland the Amazon, the Llanos de Moxos have been little studied when compared, for example, with Brazilian savannas (DE CARVALHO; MUSTIN, 2017).

The lack of pertinent knowledge regarding the hydrological functioning of these large wetlands has led to confusion and misinterpretation of the causes of major economic impacts in the region. The most notorious and recent examples of that are those referred to the causes of extreme flood events during 2014, when diverse hypotheses and erroneous perceptions have resulted in political administrative inconveniences. In this opportunity the Bolivian media emphasized the hypothesis that large floods in central floodplains were the result of the operation of large dams in the Brazilian side (Jirau and Santo Antonio hydropower plants). This situation even derived even in meetings between political and environmental authorities of both countries. Other hypotheses refer to the deforestation in the Andes and the consequential sediment load into floodplains as the main factor the large floods in 2014 (OSAVA, 2014) and climate change (CIPCA, 2014). Thus, there is an urgent need for developing proper tools and methods for understanding the hydrology of the upper Madeira and to avoid misperceptions and political tensions.

#### **2.4.1 The role of remote sensing and numerical models**

Quantitative and qualitative information are of primary importance: Remote sensing data together with streamflow data and, hydrologic-hydrodynamic models may provide spatial information about the hydrological functioning of the wetlands in this region, mainly provisioning and regulatory services. Information for cultural and supporting services is limited, constituting a relative new field of research that needs to be promoted. An accurate representation of the hydrological-hydrodynamic processes may derive in simulations under different scenarios of climate change-variability, land use and water management, providing the possibility to estimate their impacts on water ecosystem services.

The usefulness of satellite images for monitoring flooding from space has been known for about 40 years (SCHUMANN; DOMENEGHETTI, 2016). The advent and development of optical and microwave remote sensing systems, together with analysis algorithms permit to assess wetlands from a new perspective (MELACK; HESS, 2010). Many of the new developments in this field have been achieved studying large wetlands among the Amazon, mainly in terms of wetland vegetation, water properties, fluvial dynamics, flood extension, water stage and climate impacts in ecosystems and human societies.

Relevant examples of applications of optical systems, mainly using Landsat Thematic Mapper (TM) or MODIS images, for studying wetlands in the Amazon are available: Experiences in mapping wetland vegetation can be found in (BRONDIZIO et al., 1996; NOVO; SHIMABUKURO, 1997; RENO et al., 2011); fluvial dynamics assessed by vegetation succession states in (KALLIOLA et al., 1992); floodplain spatial patterns of geomorphology, hydrology and vegetation in (CHARRIÈRE et al., 2004; PLOTZKI; MAY; VEIT, 2012); limnological parameters like turbidity, suspended sediments or chlorophyll concentration in (ALCANTARA et al., 2008; RUDORFF; GALVAO; NOVO, 2009; DE LUCIA LOBO et al., 2012); flood extension and dynamics and its relations with climatic conditions in (ARRAUT; SILVA; NOVO, 2013). Moreover, recent near real time flood detection initiatives, based on moderate resolution images such as the NASA's Global Flood Mapping project <http://oas.gsfc.nasa.gov/floodmap/> or the

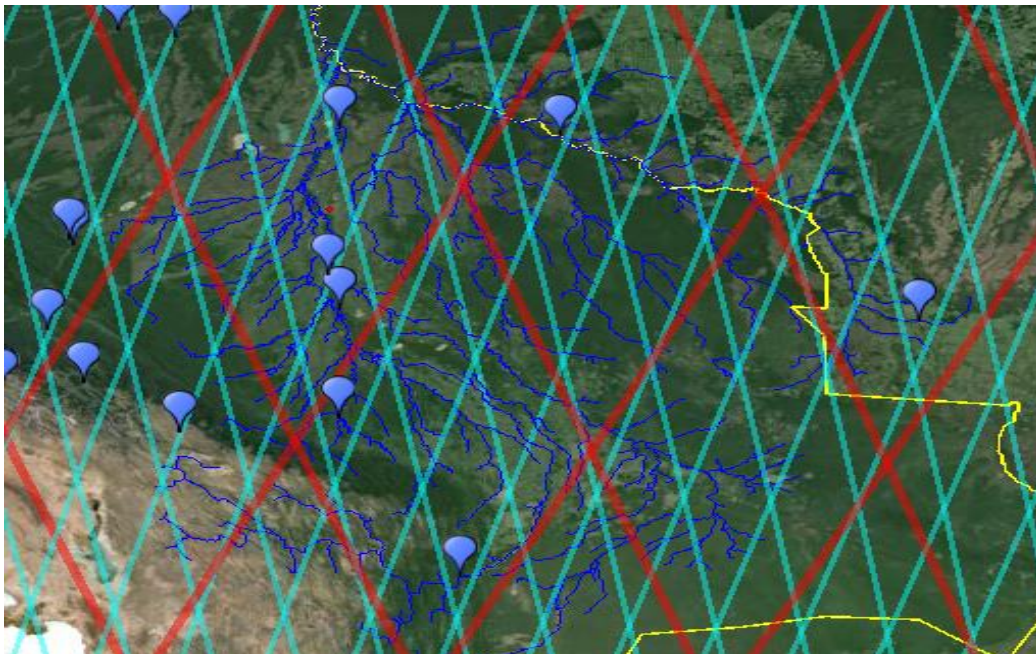
Flood Observatory <http://floodobservatory.colorado.edu/> that are providing crucial information for understanding extreme flood events, since they acquire images twice daily at global scale. Also, by mosaicking hundreds of images from different sensors during a time slot, it is possible to monitor changes in fluvial dynamics, wetland ecotones and water bodies in an unprecedented way, as demonstrated by Pekel et al., (2016), in a case study under the framework of the Earth Engine Platform (<https://earthengine.google.com/>), which integrates Landsat TM and Sentinel-1 collections. Nevertheless, the use and applications of optical remote sensing is constrained by persistent cloud cover or smoke (SCHUMANN; MOLLER, 2015) and the influence of dense forest canopy that limits the detection of flooding in wetland forests (MELACK; HESS, 2010).

Microwave systems are a suitable alternative to complement or substitute optical sensors since they can penetrate dense forest canopies, are much less influenced by clouds and can be implemented over several environments where optical sensors are limited (MELACK; HESS, 2010; SCHUMANN; MOLLER, 2015). Applications of microwave systems, mainly Synthetic Aperture Radar (SAR), to map floods and vegetation types in Amazon wetlands can be found in several studies (HAMILTON; SIPPEL; MELACK, 2004; MARTINEZ; LE TOAN, 2007; BOURREL; PHILLIPS; MOREAU, 2009; SARTORI et al., 2011; ARNESEN et al., 2013). Operational flood mapping using microwave systems is also limited, the European Space Agency Grid Processing on Demand (G-POD) tool (MATGEN et al., 2011) is a noticeable exception. Nevertheless, microwave systems still have relevant challenges, for studying wetlands hydrology, mainly as a result of long revisit times, effects of high winds, rain and urban areas (SANTOS DA SILVA et al., 2015b). Active remote sensing systems have also their constraints, mainly referred to their inability to provide good spatial and temporal coverage as the optical systems does (MARTINEZ; LE TOAN, 2007; ARRAUT; SILVA; NOVO, 2013).

Despite being designed initially for ocean and polar surveys, satellite radar altimeters also allow addressing water stages and hydrological properties of wetlands in a promising way (SCHUMANN; DOMENEGHETTI, 2016). Early applications of satellite altimetry in monitoring inland waters date from the 90s

(e.g. KOBLINSKY et al., 1993; BIRKETT, 1995). Recent studies in the Amazon (CALMANT; SEYLER, 2006; FRAPPART et al., 2006; KOSUTH; BLITZKOW; COCHONNEAU, 2006; SEYLER et al., 2009; JUNG et al., 2010; DASILVA et al., 2012) provide relevant examples of its feasibility and accuracy of satellite altimetry. Ongoing altimetry missions provide information in diverse footprint sizes, accuracy levels, spatial resolution, and temporal frequencies (i.e. Jason-2, Jason-3, Argos, ENVISAT and SARAL). Indeed, when dealing with wetlands, most of the limitations altimetry missions are generally related to the insufficient spatial coverage and revisit time. In Figure 2.3 is possible to see the differences between ENVISAT and Jason missions. In the case of ENVISAT the revisit time is 35 but the spatial coverage is better when compared with Jason, with 10 days revisit time. Future missions like SWOT, to be launched in 2020, Sentinel-3 and ICESat-2 will enhance the coverage and quality of earth observation data and represent an auspicious opportunity for remote sensing applications in continental waters (SCHUMANN; DOMENEGHETTI, 2016).

Figure 2.3 - Satellite ground tracks of ENVISAT and JASON-1 missions.



Blue lines represent the ENVISAT ground track orbit while red lines correspond to JASON-1 tracks. The blue drops are altimetric virtual stations in main rivers from SO HYBAM network.

Source: [www.aviso.altimetry.fr](http://www.aviso.altimetry.fr)

Hydrological and hydraulic models provide the means to study the interactions between the hydrometeorological regime and the floodplains ecological systems. However, in watersheds with large floodplains, modeling is constrained by the difficulty to attain an accurate numerical representation of the interchange between river banks and floodplains (PAZ; TUCCI; COLLISCHONN, 2010). Conventional models typically have a one-dimensional (1D) structure that represents river hydrodynamics in a simplified form of Saint Venant, kinematic wave or Muskingum equations (COE; COSTA; HOWARD, 2008; HALL et al., 2011; PAIVA; COLLISCHONN; TUCCI, 2011). This may derive an inappropriate simulation of important aspects of river hydraulics in floodplains where other three dimensional effects occur (BATES et al., 1997).

More accurate simulations may be achieved by implementing three dimensional (3D) or two dimensional (2D) hydrodynamic models, but they are limited by the computational cost and topographic data availability (PAZ; TUCCI; COLLISCHONN, 2010). Alternatively, a combination of 1D model, for the simulation of the main stream flow, with 2D models simulating the flow along the floodplain, is proved to be an interesting approach to deal with those constraints (BATES; DE ROO, 2000). Relevant improvements in floodplain simulation are the model for the Pantanal with a 2D raster component (PAZ; TUCCI; COLLISCHONN, 2010) and a full hydrodynamic model implemented in the Amazon basin (PAIVA; COLLISCHONN; TUCCI, 2011; PAIVA; COLLISCHONN; BUARQUE, 2012; PAIVA et al., 2013a), demonstrating that it is possible to achieve a good representation of floodplains in large scale hydrological models, despite the limited river geometry data and floodplain characterization.

The growing demand to improve our understanding on flood processes and to develop more reliable flood forecasting systems over large scales, have motivated the development of diverse methods for integrating remote sensing and hydrologic-hydraulic models. Remote sensing techniques allow to map different kind of wetland vegetation, water quality and to detect floods extend

and dynamics, but these information do not represent the whole catchment and all the processes within (WILSON et al., 2007b) According to Schumann et al. (2009), remote sensing and models are highly complementary and their integration is feasible in different modalities: i) the retrieval and modeling flood hydrology information from remote sensing observations (e.g. discharge, flood extent and area, and water stage) as in the case of (GUIMBERTEAU et al., 2012); ii) the use remote sensing data, mainly satellite altimetry, to calibrate and validate hydrodynamic models as in (WILSON et al., 2007a; GETIRANA, 2010; PAIVA et al., 2013b; GARAMBOIS et al., 2016; PARIS et al., 2016); iii) the potential of remote sensing to understand and improve model structures (ALSDORF, 2003; ALSDORF et al., 2007);and iv) the usefulness of remote sensing data assimilation in models (LEON et al., 2006; DURAND et al., 2008).

Flooded area is commonly used to assess model performance through spatial comparison. Comparisons under deterministic or probabilistic approaches, that implies flood extent comparison during flood events, wet or dry seasons or during longer periods, allow to achieve better model calibration (ARONICA; BATES; HORRITT, 2002; DI BALDASSARRE; SCHUMANN; BATES, 2009; WESTERHOFF et al., 2013; GIUSTARINI et al., 2015). Assimilation of flood extent by models is a topic that deserves further attention, relevant examples using high-order vibrational or kalman Filter techniques (ANDREADIS; SCHUMANN, 2014; LAI et al., 2014). As exposed by Schumann and Domenengheti, (2016), two main problems in assimilating flood information have to be taken into account: The first is localization, since the flood estimation from remote sensing is highly localized which causes a wear-off of its effects in the model (e.g. MATGEN et al., 2007); The second is the inherent two-dimensionality,,the lack of water level information, which implies the application of smoothing techniques (e.g, ANDREADIS; SCHUMANN, 2014; LAI et al., 2014), or indirect flood extent assimilation (e.g. MATGEN et al., 2007).

The increasing studies of the assimilation of water level information from satellite altimetry, encourages about the potential of this new research field. As exposed before, the limitations are related to the ground-track spacing and revisit times. Schumann and Domenengheti, (2016), illustrates about significant

studies that employ satellite altimetry data to calibrate and validate models (BIANCAMARIA et al., 2009; BIRKINSHAW et al., 2010; GETIRANA, 2010), in river discharge estimations and water level data assimilation (DURAND et al., 2008; MICHAILOVSKY; MILZOW; BAUER-GOTTWEIN, 2013; TOURIAN et al., 2016). Schumann and Domenengheti, (2016) also identifies that the lack of a systematic selection and extraction of altimetry data limits its application and operability. Considering that most of the satellite altimetry applications in continental waters are focused mainly in rivers, while little number of studies are focused explicitly in wetlands, the previously pointed limitations are expected to be more evident when dealing with large floodplains, where the influence of vegetation stage, soil moisture and other factors are expected to difficult water level estimations from altimetry data.

#### **2.4.2 Knowledge about the hydrology of the Bolivian Amazon wetlands**

Many studies regarding the hydroclimatology of the Bolivian Amazon were based in information from the existing in situ observational network in combination with other climatic information like Sea Surface Temperature (SST) in the Atlantic and Pacific oceans or global and regional circulation models. Among the most relevant in this field we can mention: A description of the hydroclimatology of the southwestern amazon – upper Madeira Basin (RONCHAIL et al., 2003; MOLINA-CARPIO et al., 2017); An assessment of SST and its particular influence on the Mamore floodplains (RONCHAIL et al., 2005); The role of SST and the extreme floods of 2014 (ESPINOZA et al., 2014) and Climate variability and climate change in Bolivia (SEILER; HUTCHES; KABAT, 2012)(SEILER; HUTCHES; KABAT, 2013).

The contribution of remote sensing and numerical modeling for understanding the hydrological functioning of the Bolivian Amazon wetlands is of big relevance, since the last decades. Indeed, much of the knowledge on this subject is a result of the use and application of remote sensing techniques in complementation also with in situ observational information.

At the end of the 1990s, a description of the flood dynamics using both radar (RADARSAT) and Landsat ERS images was done under the framework of a research initiative entitled BIOBAB -Aquatic BIO-diversity of the Bolivian Amazon Basin- (BOURREL; PHILLIPS; MOREAU, 2009). Later, at the beginning of the 2000s, flood extent estimation for the Llanos de Moxos were assessed using the Scanning Multichannel Microwave Radiometer (Nimbus-7 satellite), (HAMILTON; SIPPEL; MELACK, 2002, 2004). More recently, fluvial dynamics using Landsat TM and Google Earth images were assessed by Plotsky (2014). Near real time flood estimations, from the NASA's Global Flood Mapping project and the Flood Observatory, are also available for this area. Studies encompassing the whole Amazon have also provided relevant information about the wetland extension, vegetation and other characteristics, (e.g. HESS et al., 2003, 2015) who has estimated the floodplains extension and vegetation cover using dual season (JERS-1 Mosaics). The use of remote sensing to assess vegetation cover or land use change has wider applications and many studies about Bolivian amazon and its wetlands are available in the literature. Examples of the use of remote sensing techniques to asses flood characteristics, in this case based on floristic and vegetation composition rather than on direct water detection, can be found in (JUNK; FURCH, 1993; CRESPO; VAN DAMME, 2011) who had provided flood extent estimations for this region.

Despite the limitations of hydrometeorologic, topographic, pedologic and thematic information for hydrological-hydrodynamical modeling, several distributed model applications are available from the 2010s decade. In 2012, Escurra et al., (2014) have implemented the Soil Water Assessment Tool (SWAT) to simulate the monthly water balance from 1997 to 2008, as well as the water balance projected to 2050 for the entire Bolivian Amazon (Upper Madeira); however in this experience, no specific routines were used for the simulation of floodplains. Later, Villazon; Inturias, (2015), had employed a distributed WFLOW model ([www.openstreams.nl](http://www.openstreams.nl)) for a portion of the central Mamoré Basin, in this case the model included specific analysis for floods forecasting. Also, models implemented for the whole Amazon and for the

Madeira basin, had included specific routines for the floodplains in Moxos, that is the case of the MGB-IPH model (PAIVA et al., 2013b) or the MHD-INPE model (SIQUEIRA-JÚNIOR; TOMASELLA; RODRIGUEZ, 2015).



### 3 EXTREME FLOOD EVENTS IN THE BOLIVIAN AMAZON LOWLANDS<sup>3</sup>

#### 3.1 Introduction

The Bolivian Amazon wetlands have been affected by extreme flood events. In terms of impacts and magnitude, the floods of 2007, 2008 and 2014 caused significant economic impacts and a large number of fatalities. According to CEPAL, (2008), the floods of 2007 and 2008 caused losses of approximately \$US 220 million in Bolivia, with approximately 250000 affected people and 49 fatalities. The major flood of 2014 left 340000 people affected, 64 fatalities, and 49000 km<sup>2</sup> of crops lost. The losses in the livestock sector in the Beni Department reached \$US 111 million with 350000 people affected (FUNDACIÓN-MILENIO, 2014).

Sea surface temperature anomalies (SSTA) are believed to be influencing extreme flood events in the Bolivian Amazon (RONCHAIL et al., 2005). Higher than normal rainfall in the region has been related to a weak meridional sea surface temperature gradient (RONCHAIL et al., 2005). For this reason, the floods of 2007 and 2008 have been associated with El Niño and La Niña events, respectively (CEPAL, 2008), although the atmospheric processes associated with these extremes remain undocumented. The unprecedented rainfall over the Madeira Basin during the rainy season of 2013-2014, on the other hand, was related to warm conditions in the Pacific-Indian and subtropical south Atlantic, and exceptional warm conditions in the Atlantic Ocean, which favored the humidity transport over South western Amazonia (ESPINOZA et al., 2014). These features induced an anti-cyclonic anomaly over subtropical South America during January 2014, which enhanced rainfall over the Madeira Basin drainage area (ESPINOZA et al., 2014).

---

<sup>3</sup> This chapter is based in an adapted version of the publication: OVANDO, A.; TOMASELLA, J.; RODRIGUEZ, D. A.; MARTINEZ, J. M.; SIQUEIRA-JUNIOR, J. L.; PINTO, G. L. N.; PASSY, P.; VAUCHEL, P.; NORIEGA, L.; VON RANDOW, C. Extreme flood events in the Bolivian Amazon wetlands. *Journal of Hydrology: Regional Studies*, v. 5, p. 293–308, 2016.

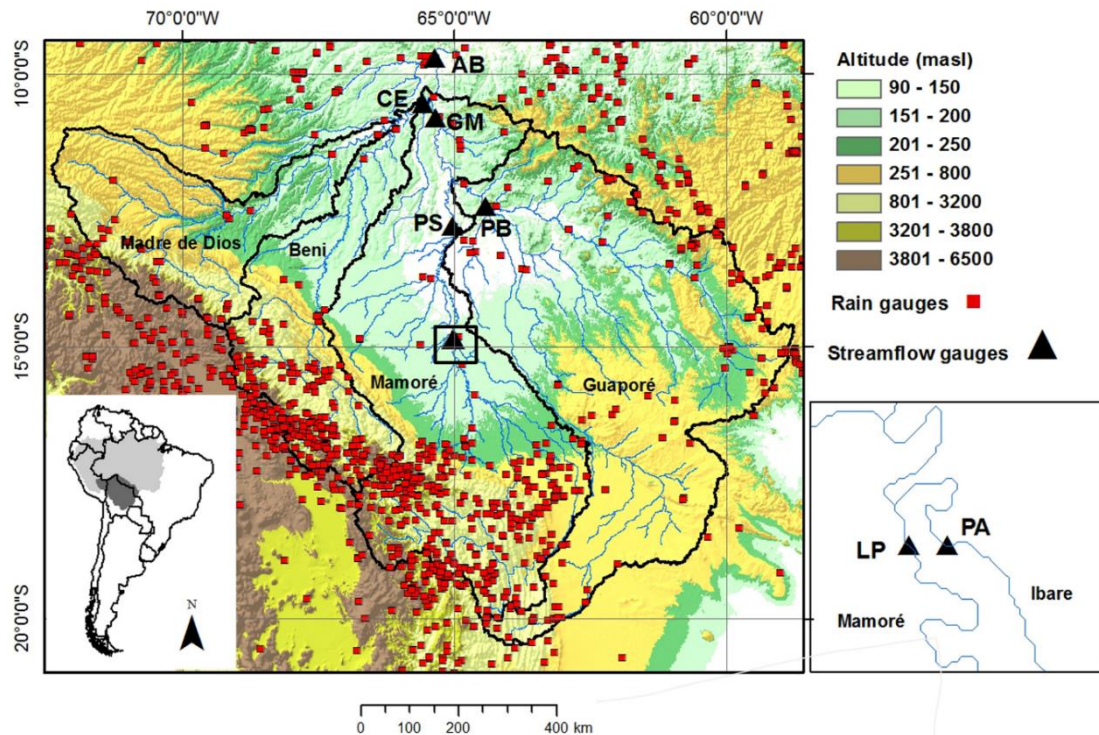
In this chapter, we have analyzed the hydrometeorological context of the 2007, 2008 and 2014 floods in the upper Madeira Basin and the dynamics of the Bolivian wetlands during those major floods events. We critically assess the temporal and spatial hydrological patterns that explain the magnitude and duration of those floods, both in the main rivers and wetlands. To achieve these goals, we have integrated hydrological and rainfall data from several sources in Bolivia, Brazil and Peru. Considering that the study region is vast and isolated, we complemented the scarce hydrometeorological data with multitemporal flood maps based on the use of nouvelle remote sensing techniques. This study brings new insights to previous studies regarding the influences of extreme climatic conditions in the region, and it is a contribution to reducing the gap between common perception and scientific evidence regarding the floods in the region.

## **3.2 Methods**

### **3.2.1 Data**

We used hydrometeorological data from different sources in Bolivia, Brazil and Peru. Rainfall data integrated information from the Brazilian National Institute of Meteorology (INMET), the Brazilian National Institute for Space Research (INPE) and discharge and water level data from the Brazilian Water Agency (ANA). Rainfall data from Bolivia and Peru were respectively extracted from the Bolivian and Peruvian Meteorology and Hydrology National Service – SENAMHI-BO and SENHAMI-PE. Hydrological data was made available by the Project "Geodynamical, hydrological and biogeochemical control of erosion/alteration and material transport in the Amazon basin" – SO HYBAM, which network is operated with SENAMHI-BO and SENHAMI-PE. These data were qualified for analyzing the temporal and spatial distribution of rainfall anomalies over the study region using the climatology for the period 1970-1990 derived by (SIQUEIRA-JÚNIOR; TOMASELLA; RODRIGUEZ, 2015).

Figure 3.1 – Observational network in the study area.



The red dots represent rain gauge locations; black triangles indicate the following gauge stations: Abunã—AB, Cachuela Esperanza—CE, Guajará-Mirim—GM, Príncipe da Beira—PB, Puerto Siles—PS, Puerto Almacén—PA and Los Puentes—LP (see right inset for detailed location)

Source: by the author

The dynamics of the “Llanos” was analyzed using data from the stations listed in Table 3.1. The Abunã gauging station is located downstream from the confluence of the Beni, Abuna and Mamoré Rivers (Figure 3.1), which join to form the Madeira River. The Beni River rises in the hillslopes of the Bolivian Andes northward, and it receives the discharge from the Madre de Dios River, which rises in the Peruvian Andes and flows eastward. The discharge at the Cachuela Esperanza gauge station, located downstream of this confluence, indicates the contribution of the northwestern part of the study area. The Mamoré River born in the Bolivian Andes, to the south of the study area, drains the precipitation falling over the western part of the basin and flows toward the north through the “Llanos”, where the Puerto Siles gauge station is located, to finally meet the Guaporé (Iténez) river at the Bolivian-Brazilian border. The

Guaporé River drains the southeastern part of the study area, receiving the contribution of several streams from Bolivia and Brazil, including the semi endorheic Parapeti basin. Upstream of the confluence of the Guaporé with the Mamoré, the Principe da Beira gauging station is located, whereas downstream of this confluence, the representative gauge station is Guajar -Mirim.

Table 3.1 - List of stations used to characterize the hydrological behavior of the study area.

<b>Code</b>	<b>Station</b>	<b>Longitude</b>	<b>Latitude</b>	<b>River</b>	<b>Drainage area (km<sup>2</sup>)</b>	<b>Mean discharge 1984-2014 (m<sup>3</sup>s<sup>-1</sup>)</b>
<b>PS</b>	Puerto Siles	-65.03	-12.78	Mamor�	230047	4157.00
<b>PB</b>	Pr�ncipe da Beira	-64.42	-12.43	Guapor�	341000	2233.10
<b>CE</b>	Cachuela Esperanza	-65.57	-10.54	Beni/Madre de Dios	281000	8074.00
<b>GM</b>	Guajar�-Mirim	-65.35	-10.79	Mamor�/Guapor�	609000	7247.60
<b>AB</b>	Abun�	-65.36	-9.70	Madeira	921000	15857.06
<b>LP</b>	Los Puentes	-65.04	-14.88	Mamor�	153000	-

Source: by the author

Finally, exchange between the wetlands floodplain and the Mamor  main-stem was analyzed using water stage data from the stations of Los Puentes, located in the Mamor  River, and Puerto Almac n, which records data from the Ibare River, a tributary of the Mamor  in the Llanos area. Both stations are operated by the Service for the Improvement of Amazon Navigation – SEMENA – Bolivia.

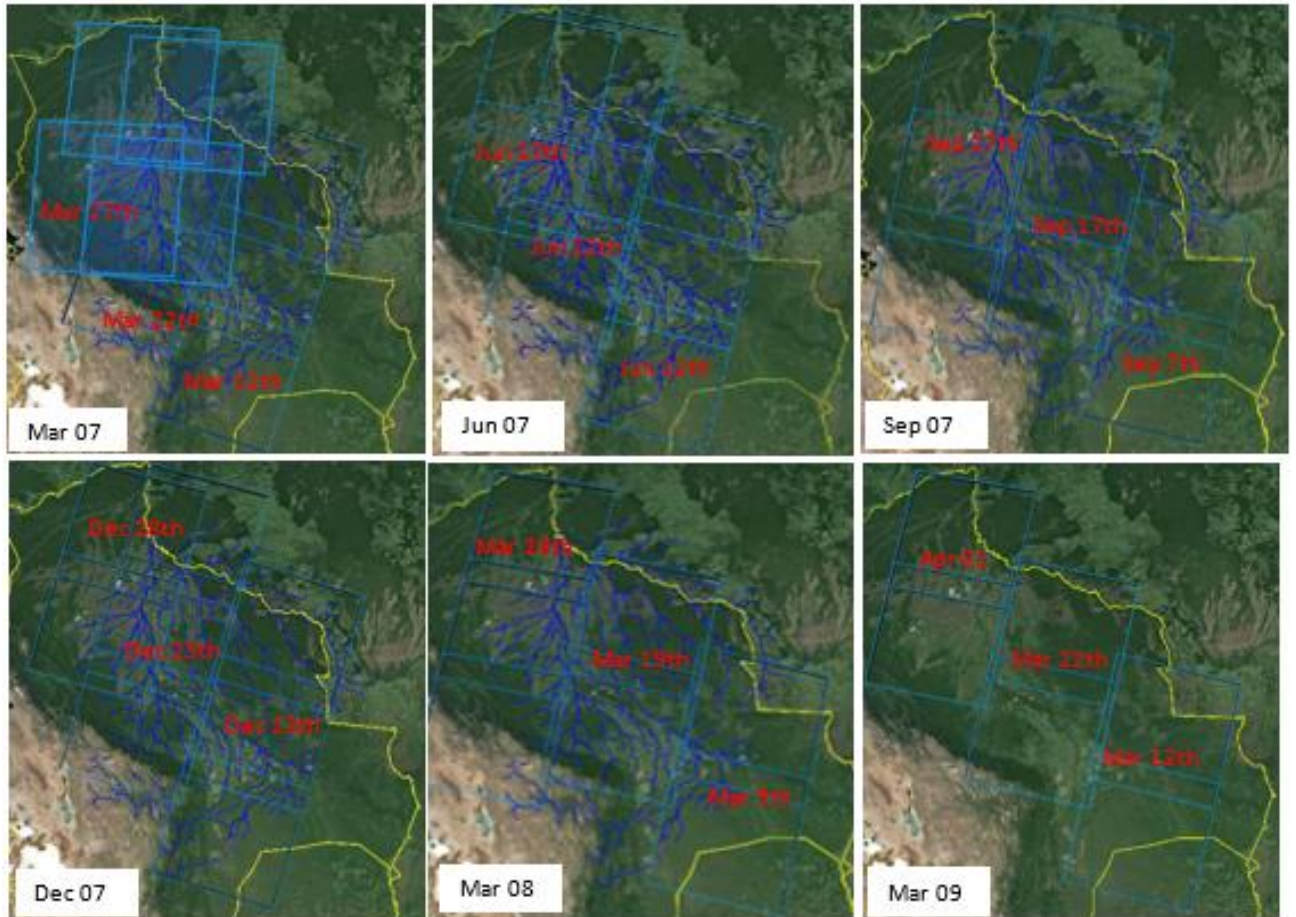
Because the onset of the wet season in the study area is between mid-October and mid-November, the floods of 2007, 2008 and 2014 were respectively described for the following periods: October 2006-September 2007, October 2007-September 2008 and October 2013-September 2014.

Multi-temporal maps of flooded area for the floods of 2007, 2008 and 2014 were derived using both active and optical systems: MODIS (Moderate Resolution Imaging Spectroradiometer) and PALSAR (Phased Array Synthetic Aperture Radar). MODIS data include seven spectral bands in the 400 nm to 2500 nm

spectral region at 500 m spatial resolution (<http://modis.gsfc.nasa.gov>). The near infrared (NIR- 841-576 nm) and middle infrared (MIR – 1230-1250 nm) channels make it possible to capture the variation of the floodplain surface during the hydrological cycle as a function of vegetation growth, water availability and flooding. We used the MODIS M\*D09A1 surface reflectance 8-day composite product because it provides the best available pixel in an 8-day period, reducing the amount of data to analyze and the effects of gaseous absorption, aerosol scattering and other atmospheric artifacts. Terra and Aqua MODIS M\*D09A1 images for the slot 01/01/2001- 09/09/2014 were collected from public repositories (<https://lpdaac.usgs.gov/>), resulting in 2248 images.

PALSAR is an active L-band sensor aboard the Land Observation Satellite (ALOS) launched in 2006 by the Japanese National Space Agency (JAXA). PALSAR data make it possible to detect water under vegetation canopy due to the L band double bounce effect with relative independence from atmospheric conditions (WOODHOUSE, 2005). Forty-five PALSAR ScanSar HH images were selected to cover most of the floodable areas in the Bolivian Amazon while capturing different flood stages (dry, wet and intermediate) and to have homogeneous coverage in terms of acquisition dates (Figure 3.2, Appendix 1 - Figure A1). Thus, six mosaics from March 2007 to March 2009 were generated.

Figure 3.2 - Detail of ALOS-PALSAR mosaics with the respective revolution date.



Source: Modified from [ursa.asfdaac.alaska.edu](http://ursa.asfdaac.alaska.edu)

### 3.2.1 Flood mapping

For the PALSAR images, the previous image treatment included data transformation-correction, registration, mosaicking and filtering (Figure 3.3). Image transformation is the process of converting a linear amplitude image into a radiometrically calibrated power image. Then, the original digital numbers (original pixel values - DN) were transformed into sigma values ( $\sigma^0$ ), which is the ratio of the incoming and backing power in a patch of ground.

$$\sigma_0 = a_2(DN^2 - a_1N_r) \quad (3.1)$$

where  $N_r$  is the noise offset and  $a_1$  and  $a_2$  are scale and linear conversion factors determined during the calibration of the processor. To analyze the backscatter response for different land cover units, the values resulting from equation 1 were converted into dB values using the following equation:

$$\text{dB} = 10 \cdot \log_{10}(\sigma_0) \quad (3.2)$$

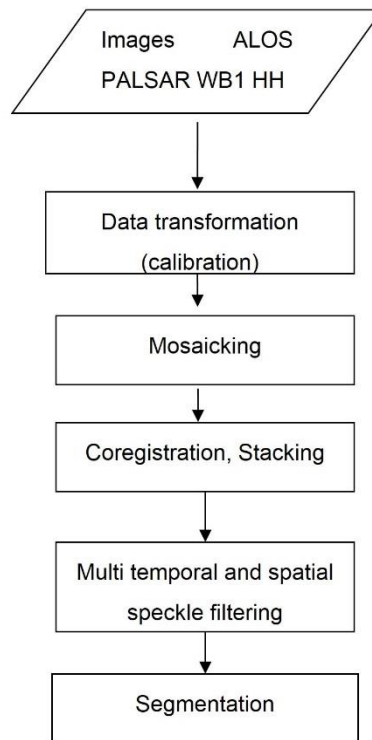
Mosaics covering the study area were assembled for every date, and then, once coregistered, multitemporal and spatial speckle reduction filters were applied. To increase the equivalent number of looks (ENL) by exploiting the temporal information available in the time series for each pixel, we applied a multitemporal filter developed by (QUEGAN et al., 2000). For a sequence of  $N$  registered multitemporal images with intensity at position  $(x,y)$  in the  $k$ th image denoted by  $I_k(x,y)$ , the temporal filtered images are given by:

$$j_k(x, y) = \frac{E[I_k]}{N} \sum_{i=1}^N \frac{I_i(x,y)}{E[I_i]} \quad (3.3)$$

$k= 1, \dots, N$ , where  $E[I]$  is the local mean value of pixels in a window centered at  $(x, y)$  in image  $I$ .

This filter makes possible to improve ENL and at the same time to preserve spatial resolution. Additional conventional filtering is classically applied to further improve the ENL in order to achieve appropriate radiometric stability (MARTINEZ; LE TOAN, 2007).

Figure 3.3 - ALOS PALSAR images preparation steps



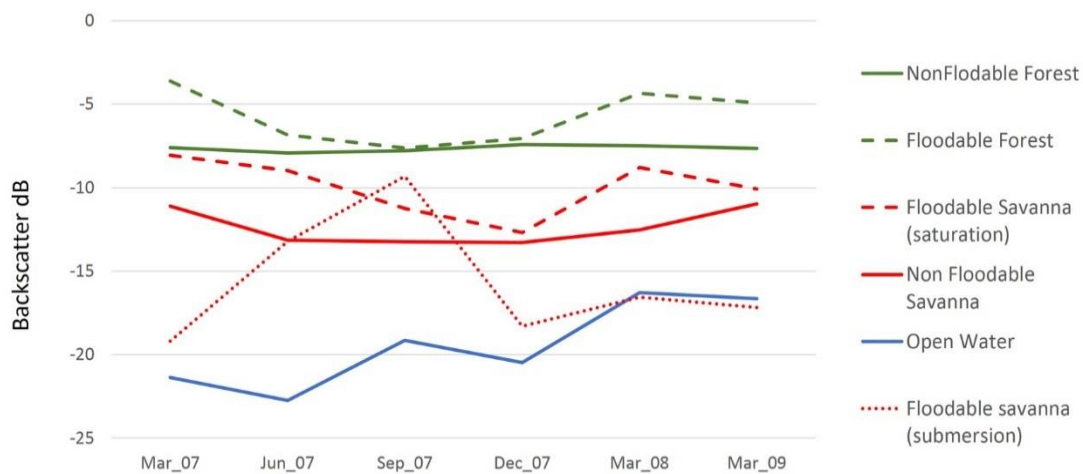
Source: by the author

Image treatment and analysis of MODIS images followed these steps: i) cloud masking, using ancillary pixel information provided by the MODIS-M\*OD09A1 product; ii) selection and delineation of sampling areas - AOI considering a variety of land cover units along the study area; iii) reflectance analysis for each of the selected AOI by automated procedures; and v) development of classification criteria using key values and thresholds of infrared bands.

Spectral analysis of MODIS reflectance and PALSAR backscatter signatures provided key information regarding its temporal variation along the floodplains. Radar backscatter over wetlands depends on different environmental conditions at the moment of the acquisition: soil moisture content, soil roughness, vegetation moisture, vegetation structure and flood coverage. Figure 3.4 shows the backscatter variability over floodable and non-floodable areas in the Llanos de Moxos. The dry season signature makes possible to discriminate between different land cover types: savannas (with backscatter values between -14dB and -9 dB); forests (~ -8 dB); and open water areas (~ -20 dB). Over forests, a

3-dB increase is characteristic of the microwave double-bounce reflection between the vegetation and the flooded surface beneath the forest (DOBSON et al., 1992; LE TOAN et al., 1992; MARTINEZ; LE TOAN, 2007). For savannas, the backscatter variations are more complex and depend on the respective heights of the water surface and of the vegetation cover. If the flood level lies below the vegetation top, double bounce interaction may occur leading to a significant increase in the radar backscatter. In this case, the flood level may not exceed 1 meter high, depending on the vegetation density and height, and we call this stage “saturation”. If the flood level reaches the top of the vegetation, the microwave is mainly reflected by the water surface and the backscatter show strong decrease down to -20 dB. We call this stage “submersion” as most of the savanna vegetation is drowned.

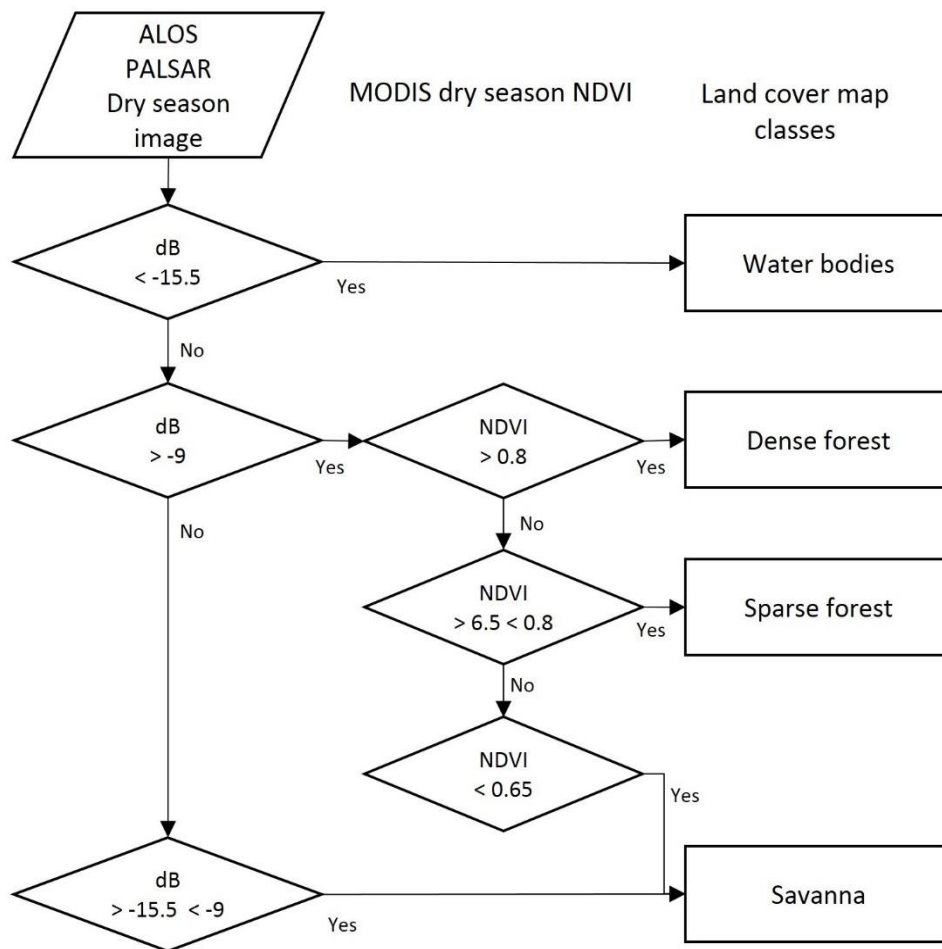
Figure 3.4 - Multitemporal Radar backscatter behavior at L-band, for different landscapes in the Llanos de Moxos floodplain.



Source: by the author

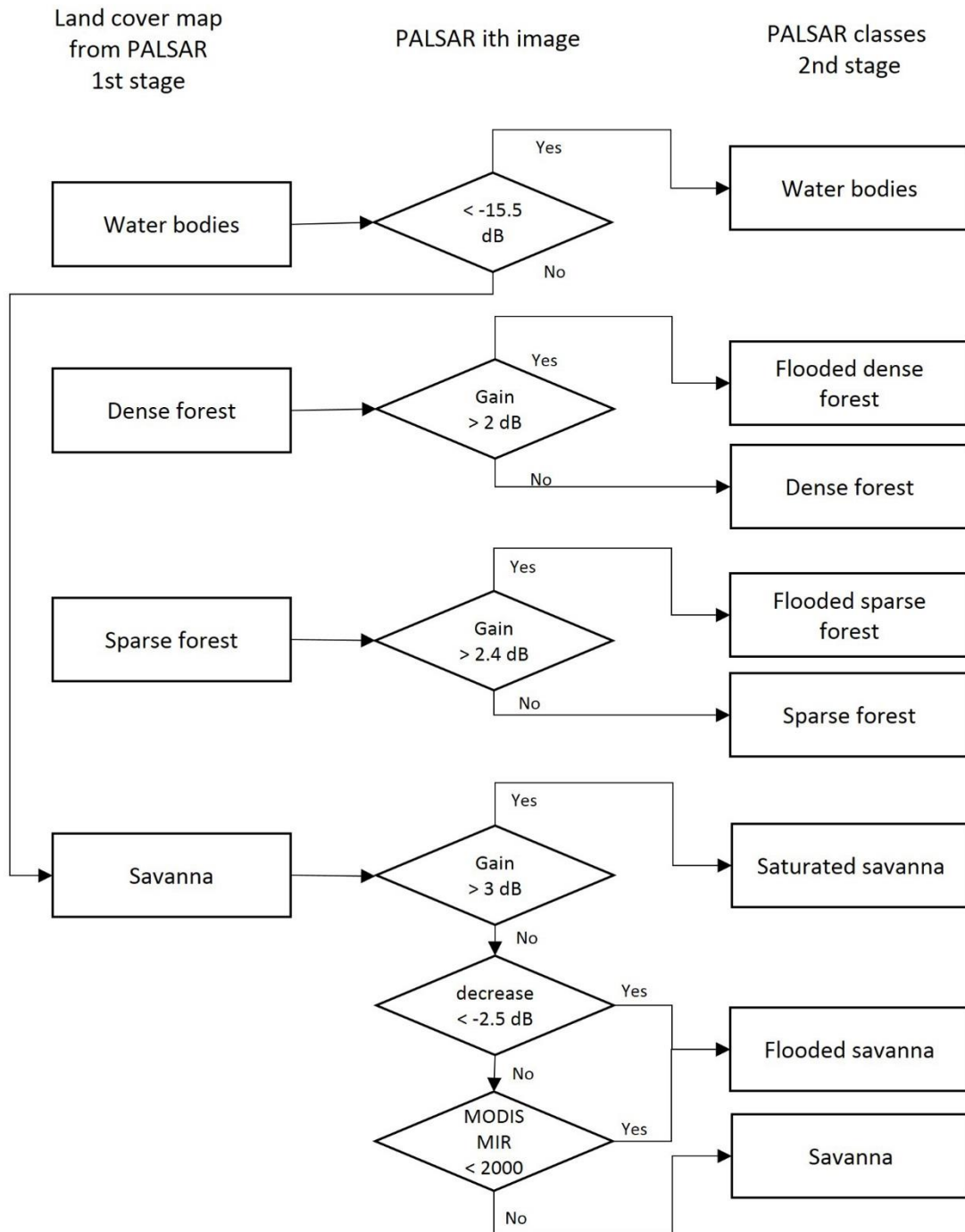
Initially, different vegetation classes are distinguished taking into account the backscatter level and its temporal variation (Absolute Change described in section 3.2.2) and MODIS-derived NDVI that allows to discriminate dense and sparse forest from saturated savannas and its flooding susceptibility (Figure 3.5). Then, the flood status for every land unit is determined by contrasting backscatter from every image with a referential dry season image, leading to a more complex class definition (Figure 3.6).

Figure 3.5 – ALOS-PALSAR Classification flowchart.



Source: by the author

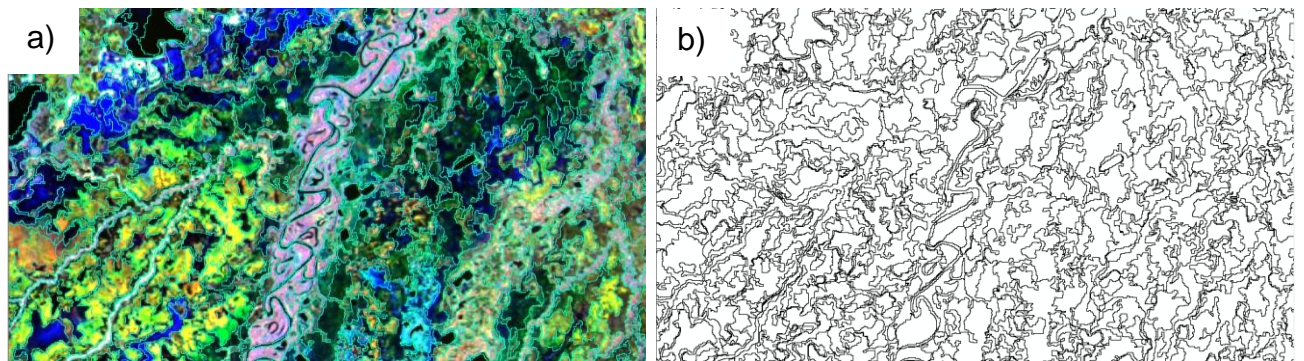
Figure 3.6 - PALSAR Classification flowchart, based in contrasts with the dry season image.



Source: by the author

Classification was based on an object-based image analysis (OBIA) approach (BLASCHKE, 2010), using segments or clusters-based mapping algorithms rather than pixel-based schemes. Image segmentation was achieved by exploring spatial connectivity and spectral similarity between pixels in order to form groups of homogeneous pixels. The statistical mean was computed at the cluster level and then used in the flood mapping algorithm. Spatial segmentation was performed in the PALSAR image dataset since it present the finest spatial resolution, and was subsequently applied on the MODIS images that were registered to the same geometry. This procedure generated smoother maps without excessive outlier pixels, and, in the case of the MODIS images, it tackled the lack of information resulting from extensive cloud cover in most of the wet season images. We applied the eCognition software (TRIMBLE, 2011) to perform the segmentation, using the Multiresolution segmentation method, giving all the layers the same weight, and assigning weights of 0.4 and 0.8 to shape and color (compactness) parameters, respectively (Figure 3.7 and Figure A2 in Appendix 1).

Figure 3.7 – Details of segmentation results.



a) ALOS PALSAR RGB composition (Mar07, Dec07, Sep07); d) segmentation results with parameters multi shape =.0 and color = 0.8.  
Source: by the author

Classification algorithms and data analysis for both the ALOS-PALSAR and MODIS systems were performed based on their respective backscatter and reflectance temporal variation. Temporal changes between dry and wet seasons are related directly to the progression of flooding. Initially, by using the

dry season signals and total change estimations, different land cover types are defined; then, the signal change between dry and wet season is used as a flood indicator.

For PALSAR images, the temporal variation across the time series is estimated by an Absolute Change (AC) estimator algorithm (QUEGAN; LE TOAN, 1998). It estimates the logarithm of the ratio between any date within the multi-date data set (QUEGAN et al., 2000) according to Equations 3.4 and 3.5.

$$AC = 10 \log \left| \frac{2}{2^N - 1} \sum_{i=1}^N \sum_{j>i} R_{ij} \right| \quad (3.4)$$

$$\text{With } R_{ij} = \max \left( \frac{i}{j}, \frac{j}{i} \right) \quad (3.5)$$

The AC computes the total unsigned backscatter change using the maximum ratios for every possible image couple. Then, the ratios are summed and normalized by the number of images. The AC provides positive values in decibels, which in combination with dry season radar signals and dry season MODIS NDVI values, allows the initial land cover to be obtained with four robust classes: water bodies, dense forests, sparse forests, and savannas. Then, the flood status for every land unit is determined by contrasting backscatter from every image with a referential dry season image, leading to a more complex class definition. If the backscatter signal changes until a fixed threshold, then the unit is classified as saturated or flooded. Submerged areas present a dramatic backscatter decrease, while saturated zones show increasing return as a function of vegetation structure. This second step gives birth to a more complex class definition that splits each vegetation class in either flooded / non-flooded sub-class, see Appendix 1 – Figure A3 for details of MODSI and ALOS PALSAR signals.

The classification of optical images is based on the radar image typology in terms of spatial clustering and vegetation type. Thresholding the MIR and NIR channels allows one to discriminate flood status classes, also with a more complex class definition. Figure 3.8 shows an 8-day reflectance times series over the 2001-2014 period (MIR band from MODIS-M\*D09A1) of a savanna cluster in the Llanos de Moxos floodplain. Spectral analysis of the reflectance

within the floodplain shows that the reflectance varies seasonally as a function of vegetation growth, water availability and flooding. Reflectance over savannas show increasing values from the first half year to the second half, with eventually, very low values in the first quarter of the year, for example at the beginning of 2007, 2008, 2010, 2011 and 2014. The reflectance increase (from 0.25 to 0.40) is typical of the vegetation development in low to intermediary biomass areas as a function of increasing soil coverage by the vegetation driven by increasing water and solar radiation availability. For some years, a decrease of the reflectance can be noticed during the last quarter of the year matching the end of the dry season. Low reflectance values, beneath 0.15-0.2 are associated with vegetation flooding and/or submersion leaving little or no vegetation element beneath the water surface.

Figure 3.8 -- MIR reflectance of a Savanna unit in the Mamore floodplain.

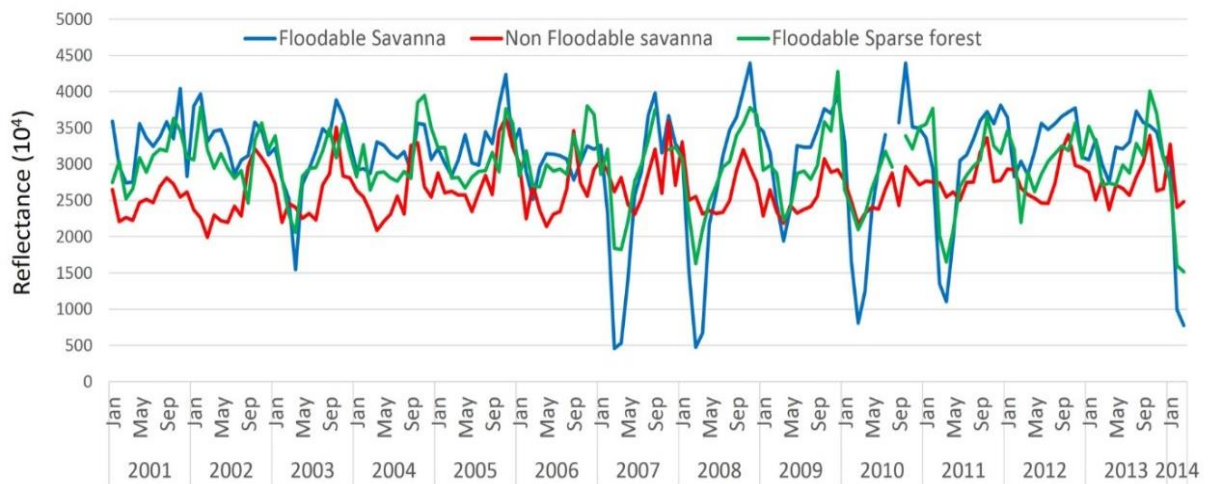


Source: by the author

Figure 3.9 shows MIR 8-day reflectance time-series for two savanna and one forest cluster. It is possible to distinguish a significant reflectance reduction during flood events (for example 2003, 2007 and 2014) for one savanna cluster. During flood events, the reflectance decreases until values below 0.2 (floodable savannas) or below 0.25 (floodable sparse forests). In the case of non flooded units, the reflectance variation remains more stable. Thus, using the radar

image typology in terms of spatial clustering and vegetation type and thresholding the MIR and NIR channels, different flood status classes are identified (Figure 3.10).

Figure 3.9 - Multitemporal variation of MIR reflectance within different land cover units.



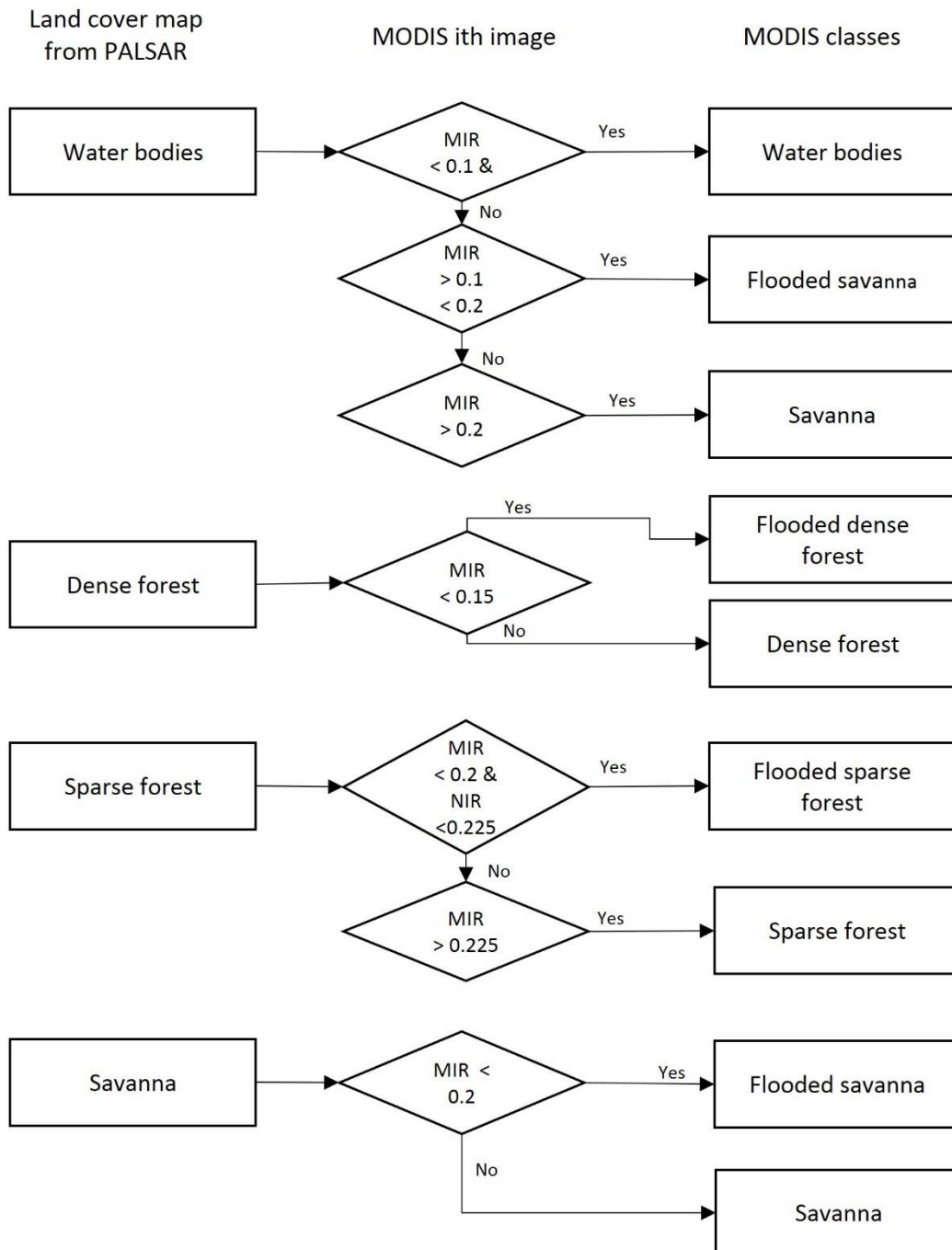
Details of MIR reflectance over a floodable savanna (blue lines); Non floodable savanna (red lines); and floodable sparse forest (green lines).

Source: by the author

We evaluated the robustness of the flood mapping based on the MODIS time series by comparing the resulting areas estimates with the areas assessed from an independent dataset. To achieve this objective, we analyzed PALSAR L-band SAR times series in order to compare the flooded savannas area and the flooded forested area estimates for five different flood stages including rising flood (December 2007), flood peak (March 2007, March 2008, March 2009) and decreasing flood (June 2007). As L-band microwave is known to penetrate deeply the vegetation cover and the PALSAR images stand as the best dataset allowing for a reliable estimates of the flooded area under forest cover. Comparison between SAR data and MODIS data is not straightforward as there is no SAR sensors acquiring images with the same time frequency and spatial resolution than MODIS. Furthermore, visible and infrared light and radar microwave do not interact the same way with the vegetation, the soils and the water surface. In this way, we do not expect both SAR and MODIS flood

estimates to match perfectly but we assume that their comparison is a fair assessment of the robustness of MODIS-derived flood maps.

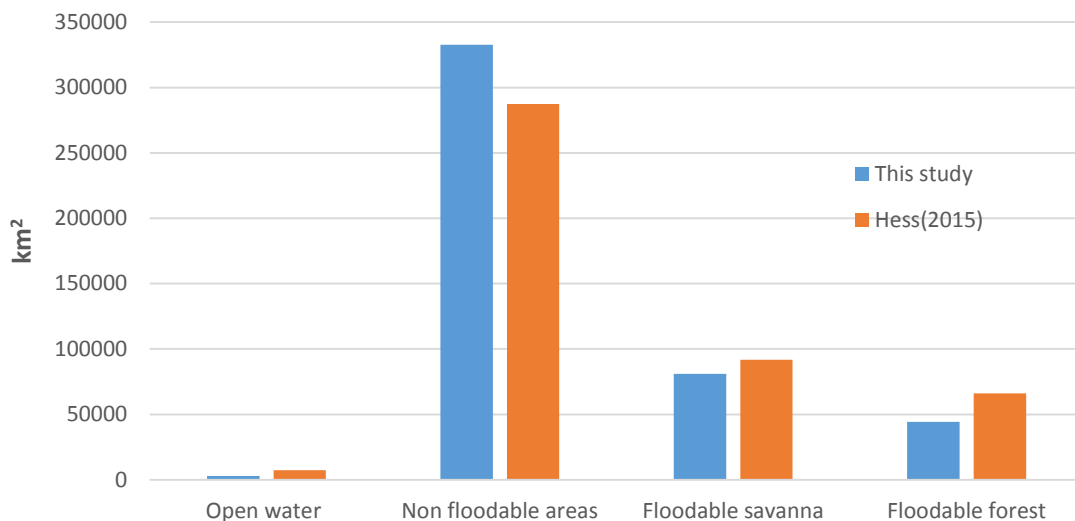
Figure 3.10 - MODIS classification flowchart, based in MIR and NIR reflectance values.



Source: by the author

The Land Cover Map was compared with the Amazon Wetland Extent and Vegetation Type and Dual-season Flooding State Map derived by (HESS et al., 2015a), considering our study area. Both maps were regrouped into compatible classes: Water bodies, Floodable forest, Floodable savannas and Non-floodable areas. Figure 3.11 shows that, despite the differences in the classification techniques and acquisition dates, there is a close similarity in both floodable and non-floodable areas and in the vegetation type units. We concluded that the ALOS PALSAR initial classification is robust since it represents both the wetlands vegetation cover type and flood exposure.

Figure 3.11 – Validation of flood extension estimates.



Comparison between Potential Maximum Flood Extension Map from this study and the Amazon Wetland Extent and Vegetation Type and Dual-season Flooding State Map of Hess et al. (2015).

Source: by the author

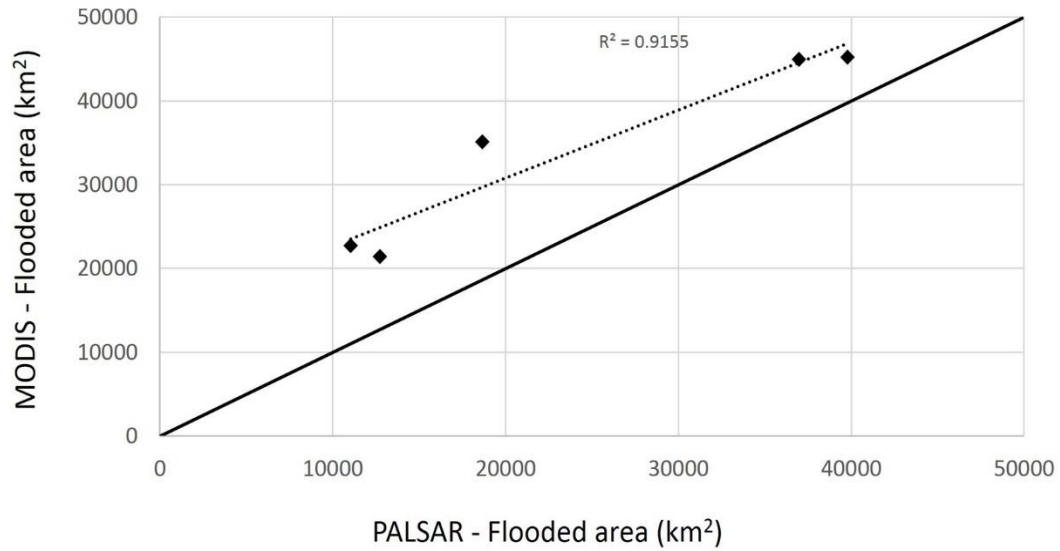
In order to have an estimate of the accuracy and capabilities of MODIS sensor to detect floods, we compared the MODIS and SAR-derived flood maps for March 2007, June 2007, December 2007, March 2008 and March 2009. Figure 3.12 shows the flooded area assessed using MODIS and PALSAR for the savanna theme. Over a large range of flooded conditions (from 11,000 km<sup>2</sup> up

to 39,000 km<sup>2</sup>), both sensors agree well ( $r^2 = 0.91$ ), even though a systematic underestimation of the flooded area by MODIS is observed, with a mean relative difference of 33%. This bias is likely to be introduced by the different physics involved in the light/microwave interaction with the landscape. Over marsh vegetation in another Amazonian floodplain, Martinez and Le Toan (2007) have reported lower classification accuracy of L-band SAR data (of about 70 %) than for flooded forest that usually is higher than 90 %. Indeed, over low vegetation, the radar backscatter penetrates down to the soil and the resulting values are less robust to detect flood-induced changes.

We further investigated the extent of the flooded areas beneath dense vegetation, i.e. mainly alluvial forest. Optical data do not penetrate dense vegetation cover and flood estimates based on sensors such as MODIS are known to produce non robust estimates for such forested areas. Additionally, we wanted to assess the relative flooded area outside and beneath vegetation. Figure 3.13 compares the flooded areas retrieved over savanna, sparse forest and dense forest for the same dates than for Figure 3.12. In the case of Flooded Sparse Forest the relative difference between MODIS and PALSAR-derived estimates is of 39%, and, as expected, MODIS estimations of Flooded Dense Forest are almost null with a difference of 96% in comparison to SAR estimates.

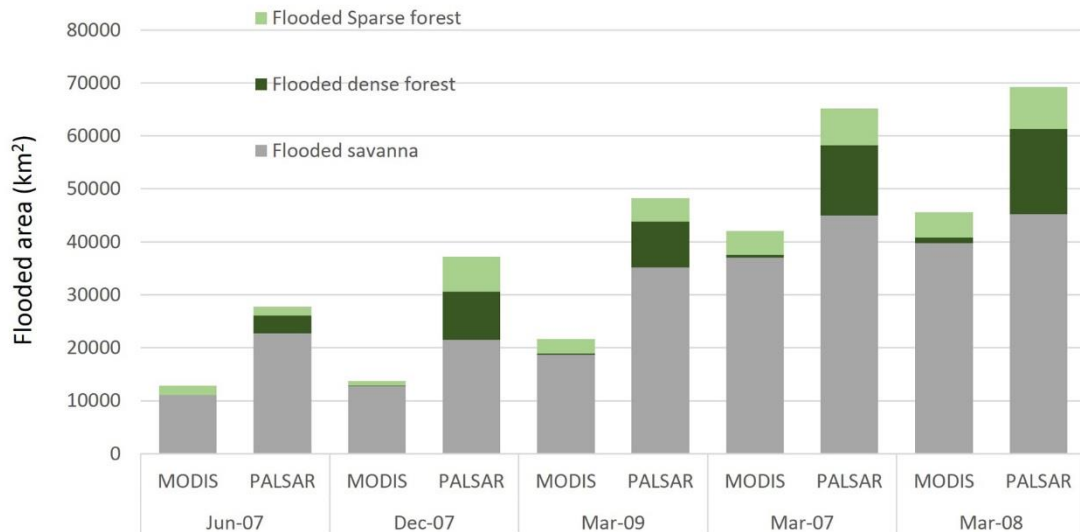
From these comparisons, we conclude that the MODIS flooded-savanna estimate produce robust estimates. Furthermore, as the flooded savanna theme represent most of the flooded areas in the Llanos region, our multitemporal MODIS-based flooded area estimates stand as a reliable index for flood condition in the region.

Figure 3.12 - Relation between MODIS and PALSAR flood estimates in a savanna unit.



Source: by the author

Figure 3.13 - Comparison between MODIS and PALSAR flood estimations.



In the figure, it is possible to distinguish that major differences are referred to flooded forest.

Source: by the author

### **3.3 Results and discussion**

#### **3.3.1 Hydrological regime of the upper Madeira Basin**

In addition to the contrasting differences in seasonal discharge of the sub-basins of the upper Madeira River due to differences in climate regime, the hydrological response is quite distinctive mainly because of the topographic characteristics of the middle and lower drainage areas. Because the Madre de Dios River has steeper topography and smaller contribution area compared with the other sub-basins, its hydrological response is faster and characterized by spiky behavior, and it has a strong influence on the peak and shape of the flood waves of the Beni River. The Mamoré River, on the other hand, flows along the vast “Llanos” wetlands, which reduces the peaks and significantly delays the travel time of the flood waves coming from the Andes. This explains why the peak discharge at Cachuela Esperanza station in the Madre de Dios-Beni River system occurs, on average, 54 days before the peak in Guajará-Mirim station in the Mamoré-Guaporé river system.

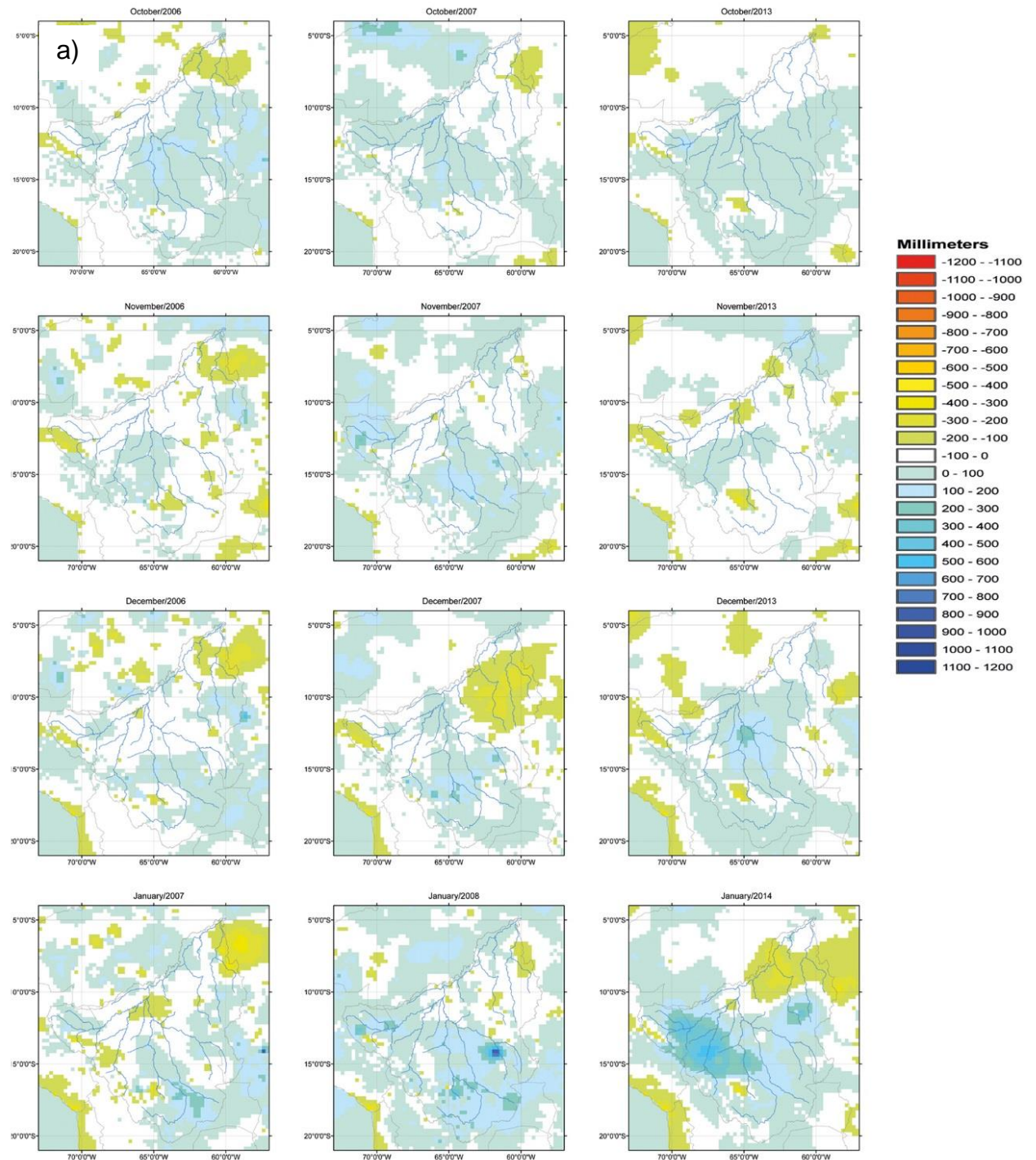
In the Madeira River, at the Abunã station, peak discharges occurs, on average, 8 days after Cachuela Esperanza and 46 days before the peak in the Mamoré-Guaporé river system. The time difference between the peaks of the Madre de Dios-Beni river system, coming from the west part of the study area, and the Mamoré-Guaporé River system, coming from the east, attenuates the discharge of the upper Madeira and prevent the occurrence of extremely high river levels at Abunã station.

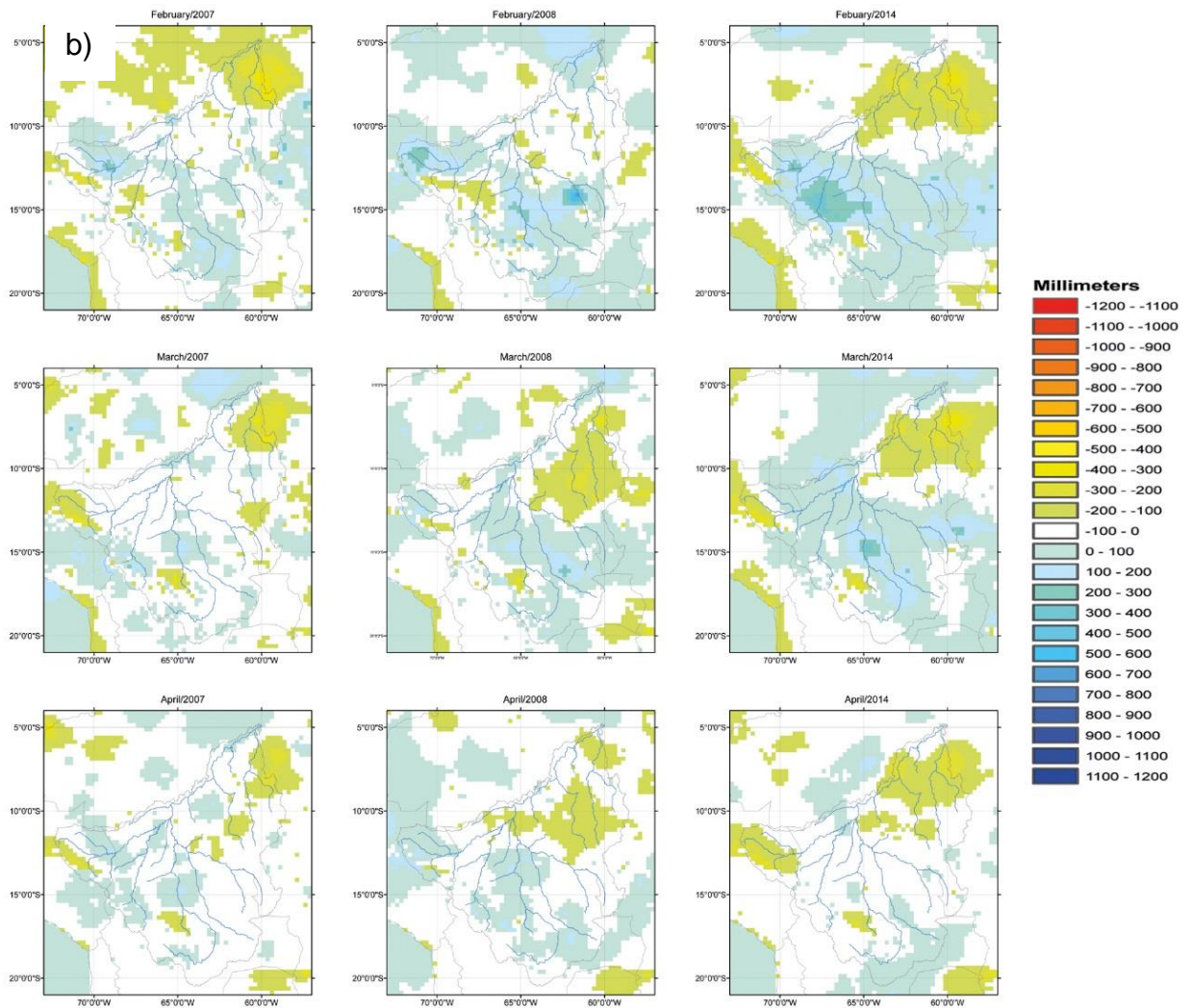
#### **3.3.2 Hydrometeorological context of the 2007, 2008 and 2014 flood events in the upper Madeira Basin**

Flood events are reported periodically in the Llanos because this area is naturally exposed and dependent on regular annual flood pulses. However, the extreme characteristics of the 2007, 2008 and 2014 flood events created serious concerns in local communities not only because of their magnitude but most importantly because they were concentrated in less than a decade. To analyze these extreme events, Figure 3.14 shows rainfall anomalies for the wet season periods associated with the three events, that is, October 2006-March

2007, October 2007-March 2008 and October 2013-March 2014. In addition, Figure 3.15 shows daily discharges during 2007, 2008 and 2014 against the long-term mean discharges of the period 1984-2014.

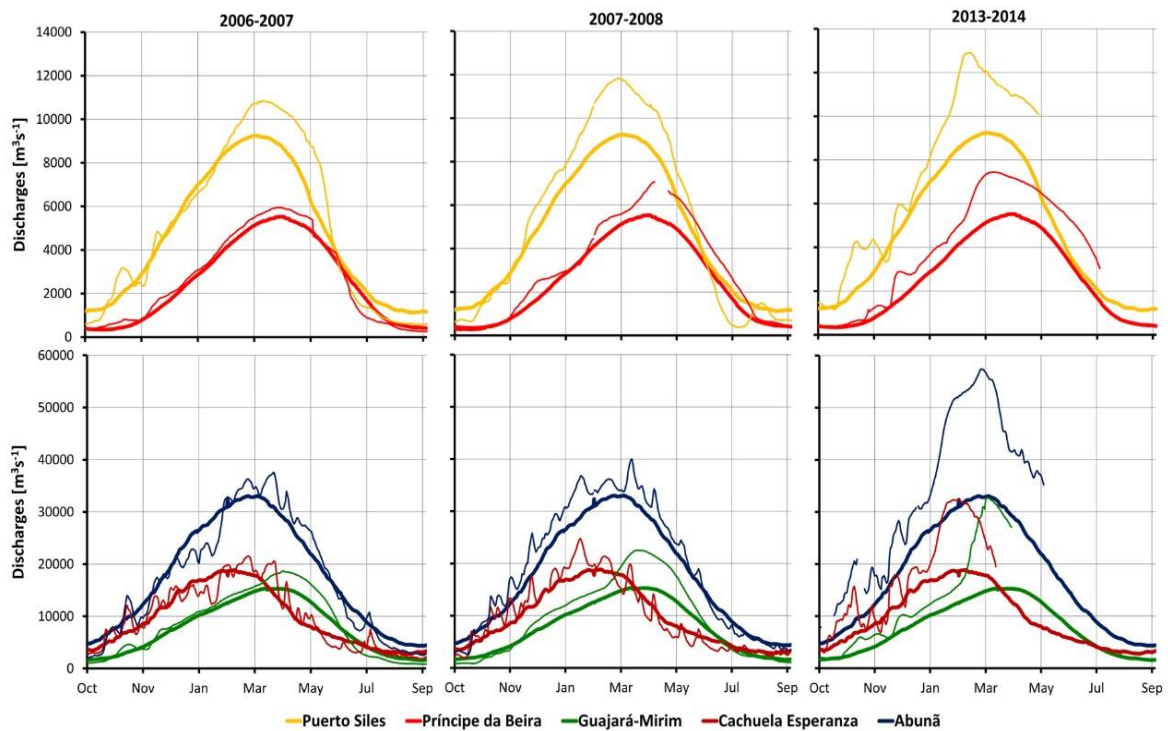
Figure 3.14 – Monthly rainfall anomalies in the Upper Madeira.





a) Monthly rainfall anomalies from October 2006 to January 2007 (left column); October 2007 to January 2008; and October 2013 to January 2014. (b) Monthly rainfall anomalies from February 2007 to April 2007 (left column); February 2008 to April 2008; and February 2014 to April 2014.  
Source: by the author

Figure 3.15 - Hydrographs for different discharge stations: long term monthly mean discharge and during extreme flood events.



Thick lines represent the long term mean, while thin lines represent extreme events during the 2007, 2008 and 2014 flood events.  
Source: by the author

### The flood of 2007.

Rainfall during the rainy season of 2007 was higher than the climatological average mainly over the drainage areas of the Mamoré and Guaporé rivers. Major rainfalls occurred over the headwaters of these basins in January 2007 and over Beni and Madre de Dios basins in February 2007 (Figure 3.14b). These positive rainfall anomalies were responsible for higher than average discharges at Guajará Mirim station from late February through middle June and from early March to middle June in Puerto Siles gauge stations. At Principe da Beira, discharge was also above the mean from the beginning of the rainy season (October) until June. Although the Mamoré River peaked 16 days later than expected from the long-term average in Puerto Siles, the peak in Guajará Mirim occurred only 3 days earlier than the average time. The delay in the time

of the peak that occurred in the Mamoré River in Puerto Siles station reduced the lag time between the peaks of the Mamoré and Guajará Mirim rivers (Figure 3.15), almost superimposing the peaks of the flood waves of the two rivers at Guajará Mirim station, exacerbating the discharge levels close to the peak.

At the Beni River at Cachuela Esperanza stations, higher than average discharges were observed from late February through early June, and the peak discharge was delayed 14 days from the expected average. This delay in the peak reduced the normal time-delay between the contribution of the western and eastern portions of the upper Madeira Basin, and also delayed the peak of the Madeira River at Abunã station. The fact that the contributions of both parts of the basin were “almost in phase” explains the exceptional discharges observed during the 2007 flood.

#### **The flood of 2008.**

During the hydrologic year of 2007-2008, discharges higher than average were observed in Guajara Mirim from December through June due to above average rainfall occurring over the Mamoré - Guaporé basin during the rainy season (Figure 3.14a,b). The larger positive anomalies of precipitation were observed in January 2008 over the basin.

Although discharge data during the peak of the hydrograph in Principe da Beira are missing, a visual analysis of Figure 3.15 indicates that this peak occurred during the first half of May, later than expected. Discharges were above the long-term average from February 2008 until September 2008. Exceptionally higher than long-term average discharge was also recorded in the Mamoré River at Puerto Siles from December through May, and the peak timing was slightly delayed from the average. Due to the severity of the 2008 flood at the Mamoré River, the discharge at Guajará Mirim was well above the long-term average, and the peak occurred 17 days earlier than average, in middle April 2008. The reason for the water stage behavior at Guayará Mirim during 2008 is related to the spatial distribution of rainfall: a large amount of rainfall accumulated during February and March over the lower part of the Mamore basin, downstream of Puerto Siles (Figure 3.14a,b). This anomalous rainfall

located close to Guajar Mirim station suffered almost no attenuation, and it added to the crest of the flood coming upstream from the Mamor River, resulting in the exceptional discharges observed at Guajar Mirim station (Figure 3.15).

In Cachuela Esperanza, the Beni River discharges were higher than the long-term average from October through April, and the maximum discharge was recorded 23 days before the long-term average. However, a secondary peak occurred in early April (09/04), directly associated with the positive rainfall anomalies in the headwaters of the Madre de Dios sub-basin (Figure 3.14b). This second peak almost coincided with the higher discharges recorded at Guajar Mirim station. This second late peak, a few days before the peak at Guajar Mirim, drove water levels in the Madeira River to exceptionally high values at Abun station. Moreover, Abun registered discharges higher than the average from the beginning of the rainy season (October) until early June, and the peak was observed 25 days later than expected from the long-term average.

### **The flood of 2014**

Rainfall above the climatological mean was observed in December 2013 over the confluence area of the Guapor and Mamor rivers. Later, positive rainfall anomalies spread over the whole upper Madeira basin, with the largest values over the drainages areas of the Beni- Madre de Dios River system during January 2014 (Figure 3.14a,b).

This anomalous rainfall produced exceptionally higher than normal discharge in the Mamor River at Puerto Siles in February 2014 and in the Guapore River at Principe da Beira in March 2014. In Puerto Siles, the peak was observed only 9 days before the long-term average, whereas in Principe da Beira, it was 22 days earlier than average. The peak time at Puerto Siles matched the beginning of an abrupt increase of discharge at Guajar-Mirim during the first days of March. Discharge above the average was recorded in Guajar Mirim from the beginning of the rainy season (October), and the hydrograph peak occurred by the end of March, one month earlier than expected from the long-term

hydrograph. The river Beni at Cachuela Esperanza showed discharges exceptionally higher than the long-term average since October 2013. During Mid-January, discharge increased abruptly in response to abundant rainfall in the Beni and Madre de Dios contributed areas. The peak at Cachuela Esperanza station was recorded 14 days earlier than expected from the long-term averaged hydrograph (Figure 3.15).

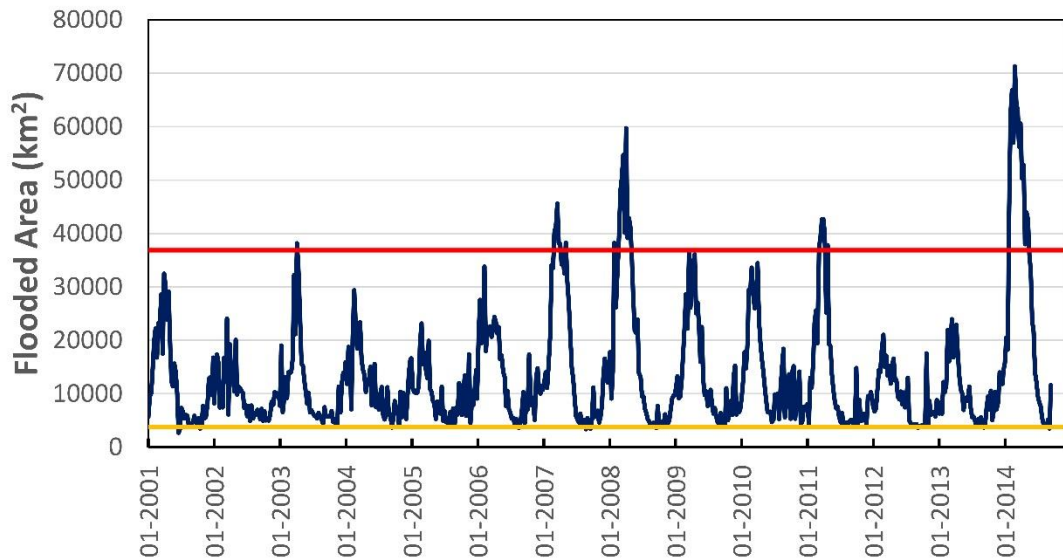
By the time that the flood wave coming from the Mamoré-Guaporé river system had reached its peak at the Guajara-Mirim station, discharge in the Madeira River at Abunã station was well above the long-term average because it was receiving significant flows from the Beni-Madre de Dios River System. Moreover, during 2014, both the Beni-Madre de Dios and Mamoré-Guaporé river systems showed exceptionally high discharges, and both systems peaked at the Madeira confluence almost simultaneously, superimposing the flood waves of the eastern and western upper Madeira Basin. In addition to the fact that the flood waves coming from different areas of the basin were in phase, the flood of the Madeira River at Abunã was exacerbated by intense local rainfall during the peak time.

### **3.3.3 Flood dynamics in the Llanos during the 2007, 2008 and 2014 events.**

#### **3.3.3.1 Spatial and temporal variability of floods**

The multi-temporal series of flood maps obtained from MODIS images for the time slot 2001-2014 allowed to identify the peculiar characteristics of the Llanos de Moxos. Flood peaks tend to occur between March and April, whereas during August-September, floods are primarily related to permanent water bodies (lakes and rivers). A conspicuous degree of interannual variability is observed, with a range of 50293 km<sup>2</sup> between the maximum flood peak (2014) and the minimum flood peak (2012). The average flood peak reaches 36859 km<sup>2</sup> with a standard deviation of approximately 14357 km<sup>2</sup> (Figure 3.16). These metrics clearly show that there is a complex dynamic in terms of flood extension and timing.

Figure 3.16 - Time-variation of the flooded area in the study area during period 2001–2014



The horizontal red line indicates the mean of the flood peaks; the yellow solid line indicates the minimum open water extension.

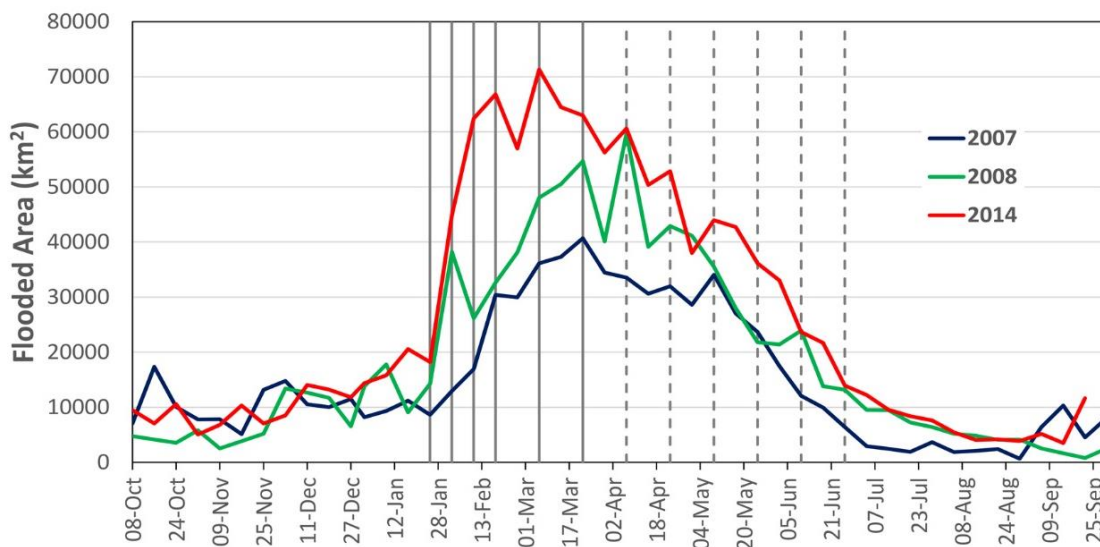
Source: by the author

When comparing these results with those obtained by Hamilton et al., (2004), who performed flood estimations for the period 1978-1987 from passive microwave radiometry, it is possible to note both similarities and disparities. The annual flood cycles are similar (peaks in March-April and minimum in August-September); the maximum flood extension in 2014 (71305 km<sup>2</sup>) is of the same magnitude as Hamilton's estimation for 1982 (78460 km<sup>2</sup>), which can be considered the two major flood events according to local community perceptions. Because no hydrometric information is available for the Llanos before 1983, it is not possible to make an estimation of the maximum extension of the flooding during the 1982 event based on the relationship found in this study. In addition, the permanent open water area values are also similar (approximately 3000 km<sup>2</sup>). However, the mean flooded area for the period 1978-1987 according to Hamilton et al. (2004) is approximately 50000 km<sup>2</sup>, whereas our estimation is 30000 km<sup>2</sup>. These discrepancies can be explained by the differences in the methods, the study area and different periods of study.

In addition, making use of visual interpretation of optical and SAR high resolution images (pixel of about 30-meter size), Bourrel et al. (2009) assessed a flooded area of 30000 km<sup>2</sup> for the 1997 flood. Other maximum flood estimations in the area, such as 150000 km<sup>2</sup> reported by Junk (1993), 100000 km<sup>2</sup> estimated by Hanagarth (1993) or 215171 km<sup>2</sup> estimated by Crespo and Van Damme (2011), are based on floristic and vegetation composition rather than on water detection from remote sensing techniques, and they are not reported in yearly time steps. Hence, no direct comparisons were performed with them.

It is possible to distinguish that the events of 2007, 2008 and 2014 are the most representative of the period 2001-2014 in terms of magnitude and behavior (Figures 3.16 and 3.17). The maximum flooded area was 40676 km<sup>2</sup> on 22/03/2007, exceeding by +27% the mean flood peak for the 2001-2014 period; 59694 km<sup>2</sup> on 07/04/2008, exceeding by +62%; and 71305 km<sup>2</sup> on 06/03/2014, with +93% above the mean.

Figure 3.17 - Time-variation of the flooded area during the 2007, 2008 and 2014 flood events.



Vertical lines indicate the dates of the flood maps of Fig. 3.18 a and b.  
Source: by the author

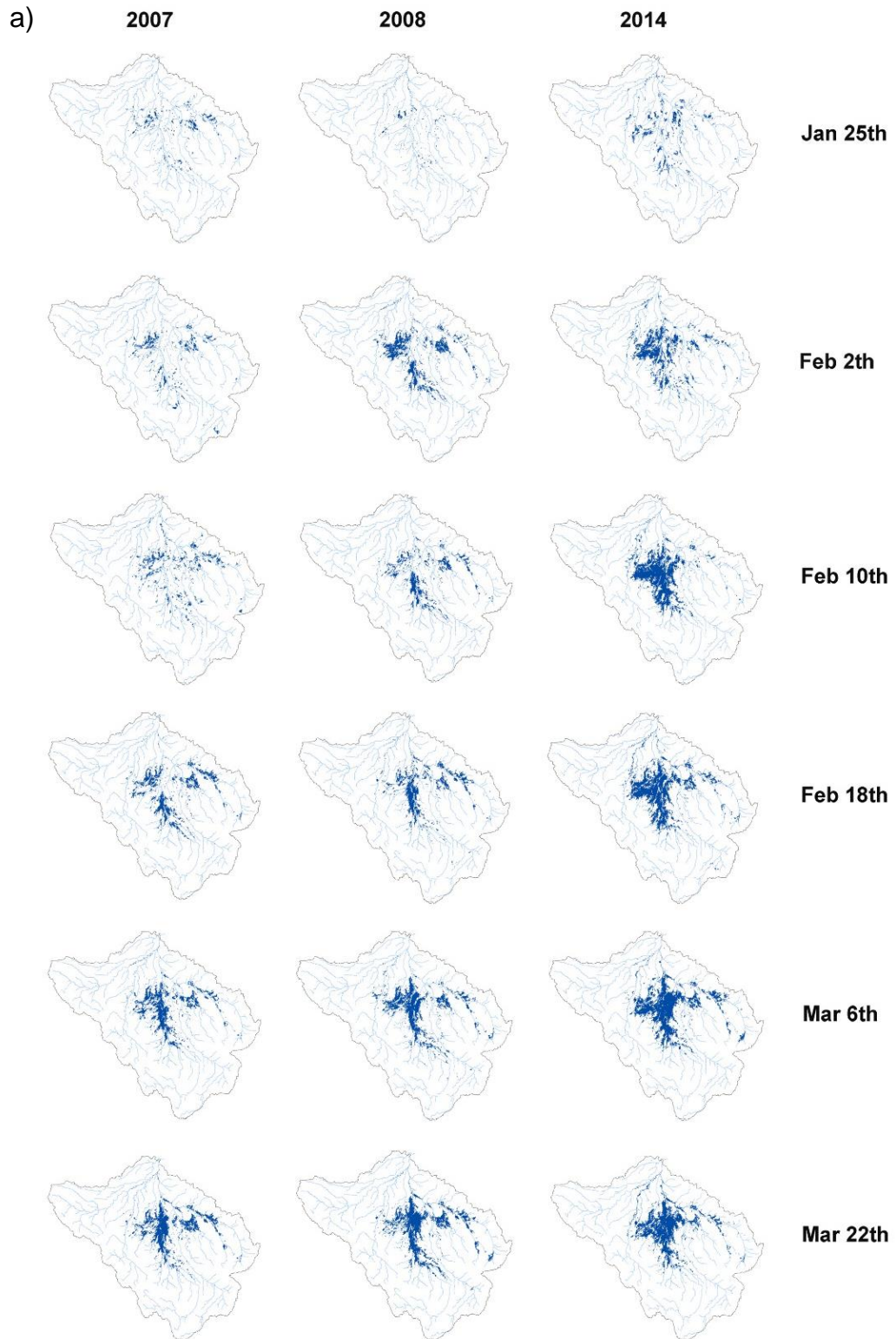
Figures 3.18 a,b show the flood dynamics of the Llanos areas for the 2007, 2008 and 2014 events for different dates, shown as vertical bars in Figure 3.17:

continuous bars indicate that the flooded area is increasing, whereas dotted vertical bars correspond to when the water is receding in the floodplain.

Figure 3.18a shows that the flooding begins in isolated spots in the central area of the Llanos, in endogenous streams, rivers and lakes, suggesting the existence of a threshold storage level in several small lakes that needs to be reached to allow exchange with the drainage network. It is noticeable, in the case of the 2007 and 2008 floods, the displacement and expansion of the flooded area from the southern part to the center of the Llanos, close to Puerto Siles station, a process that occurred along the Mamoré main-stem simultaneously with the movement of the river flood-wave. When this gradually growing flooded area reached the center of the Llanos, the flooding generalized to the whole area of the wetlands. This process was not as evident during the 2014 flood, presumably because the magnitude of the rainfall and consequently the dynamics of the process were so fast that the temporal resolution of the images could not capture that behavior. It is also clear that there were differences in the timing of the three events: although in the 2007 flood event, the increase in the flooded area became evident by the beginning of March, during the 2008 and 2014 events, the flooded area was noticeable already in early February, particularly during 2014. This is related to the fact that in the event of 2007, positive rainfall anomalies were observed in January 2007, whereas in the floods of 2008 and 2014, above-the-mean rainfall was observed from November 2007 and December 2013, respectively (Figure 3.14a, b).

The flooded area in February in the western part of the “Llanos” was much larger in 2014 compared to 2008. However, in the eastern part, particularly between late March and during April, the situation was the opposite (Figure 3.18a,b); thus, the eastern flooded area was larger in 2008 compared to 2014. This illustrates the effect of local rainfall on the dynamics of the wetlands: in January and February 2008, the eastern portion of the Mamoré contribution area was affected by intense localized positive rainfall anomalies. Although in January and February 2014 positive rainfall anomalies were spread over the Mamoré contribution area, very intense rainfall spots were located in the upper Mamoré only in 2008 (Figure 3.18a,b).

Figure 3.18 - Flood dynamics for the 2007, 2008 and 2014 events..



a) From January to March; and b) from April to June.

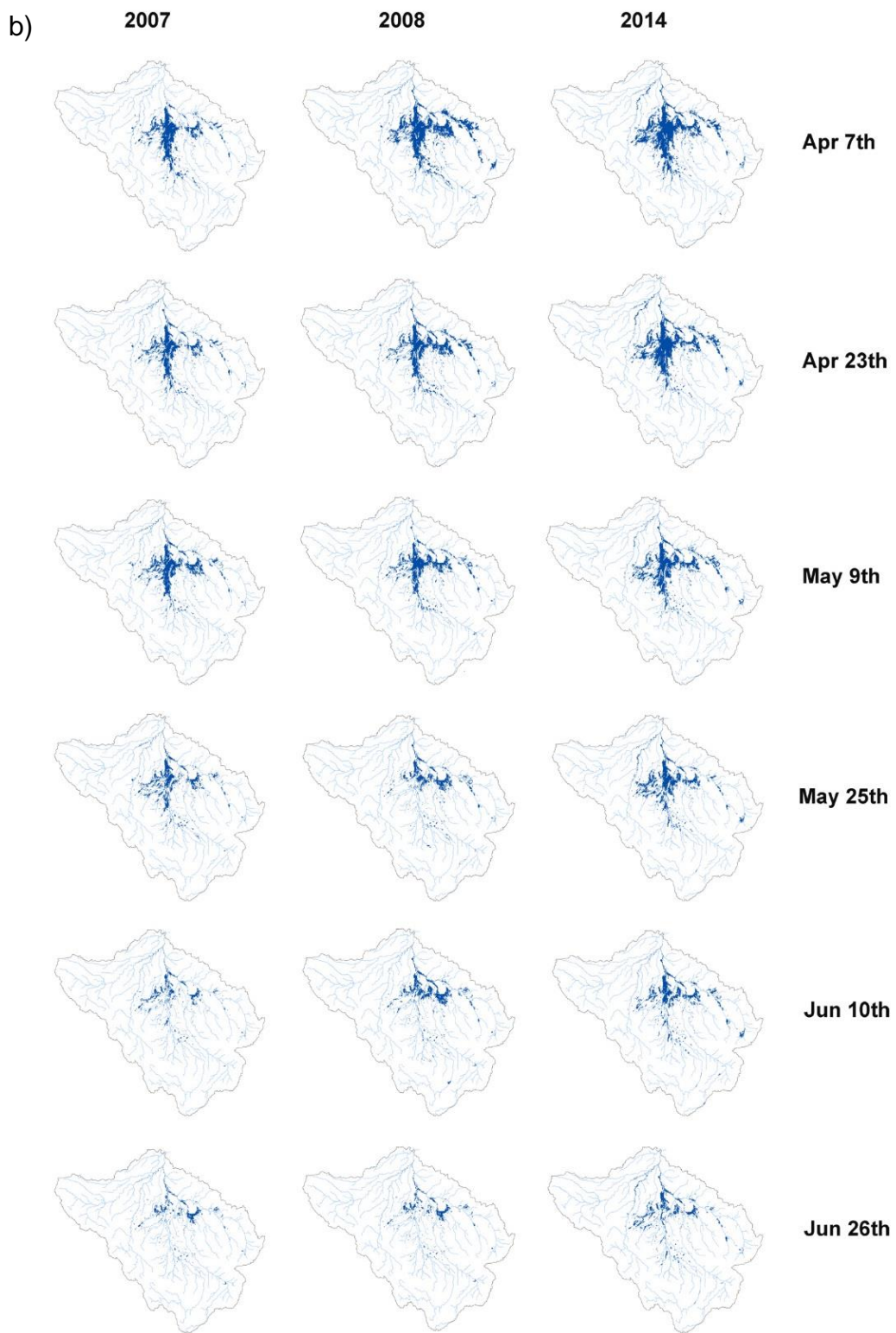


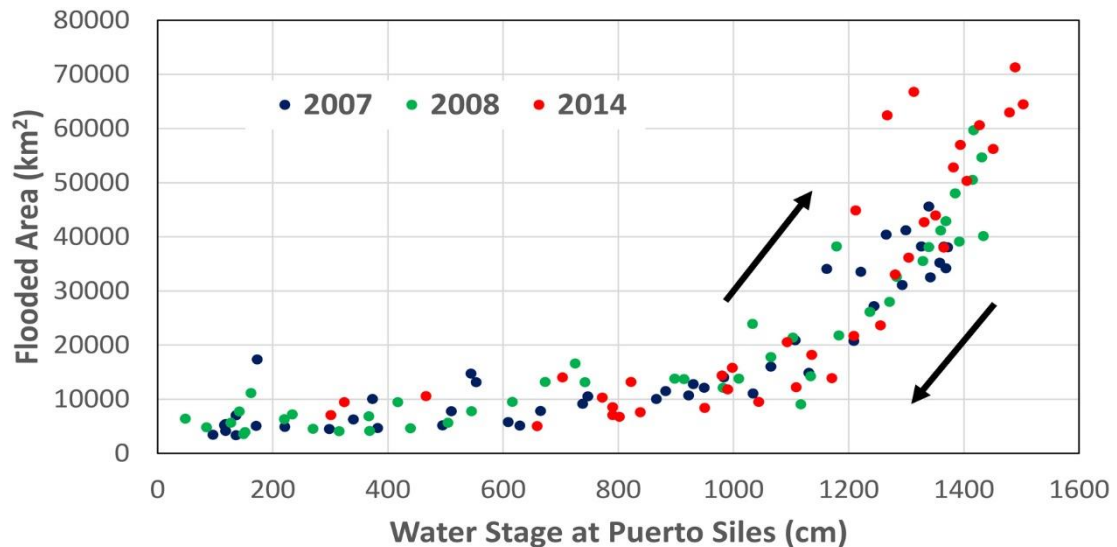
Figure 3.18 (conclusion)  
 Source: by the author

On the other hand, during 2014, the strongest positive rainfall anomalies persisted in the upper Madre de Dios–Beni river system during January and February 2014 (Figure 3.14), explaining why the flood was extended to the west in 2014 compared to 2008. Therefore, localized rainfall is a determinant of the dynamics of a flooded area.

Time variation in the three flood events was also verified during the recession of the flooded area: Figure 3.16 indicates that during the 2007 event, the Llanos had returned to its initial condition of January by June 10<sup>th</sup>, while in the other two events the flooded area was still evident. This is related to the fact that rainfall returned to normal by March 2007, whereas in 2008 and 2014 rainfall higher than the climatological mean persisted over the Beni and Mamoré basins. Therefore, the extension of the flooded area depends not only on the magnitude of rainfall anomalies but is also directly related to the time-persistence of positive rainfall anomalies. Although March marks the end of the wet season and the rainfall amounts are already declining, above normal values during this month have the potential to cause significant surface runoff because the flooded area is usually close to its maximum.

Figure 3.19 shows the relationship between flooded area and the stage at Puerto Siles gauging station. Although there is a clear relationship between the flooded area and the gauging station, a loop in the relationship is also evident with the river's rise and recession observed in the three floods. This behavior is explained by the arrival of the flood pulse coming through the Mamoré River, shown in Figure 6a: the flooded area gradually increases upstream of Puerto Siles station before the gage can detect significant variation of the water stage. However, at the peak time of Puerto Siles, the flooded area reaches its maximum, indicating that the station is a good proxy for the flooded area of the wetlands. Moreover, during the recession, the relationship is stable and well defined regardless of the previous history of the flood event.

Figure 3.19 - Relationship between flooded area and water stage at Puerto Siles during the three floods



Black arrows indicate the time evolution of the floods.

Source: by the author

### 3.3.4 Hydrological functioning of the Llanos

Bourrel et al. (2009) hypothesized that the floods in the Llanos are controlled by two different processes:

- An exogenous process resulting from the arrival of the flood wave from the Mamoré River and other tributaries generated in the Andes piedmont;
- An endogenous process resulting from the outflow of water from the wetlands in response to local precipitation, which can be temporarily blocked by high water levels of the exogenous flood wave at the Mamoré main-stem.

Bourrel et al. (2009) suggested that wetlands dynamics vary markedly from year to year: sometimes, the endogenous process controls almost the entire flood wave, sometimes the flood wave is governed by the exogenous process, and during large floods, it is governed by the combination of the two.

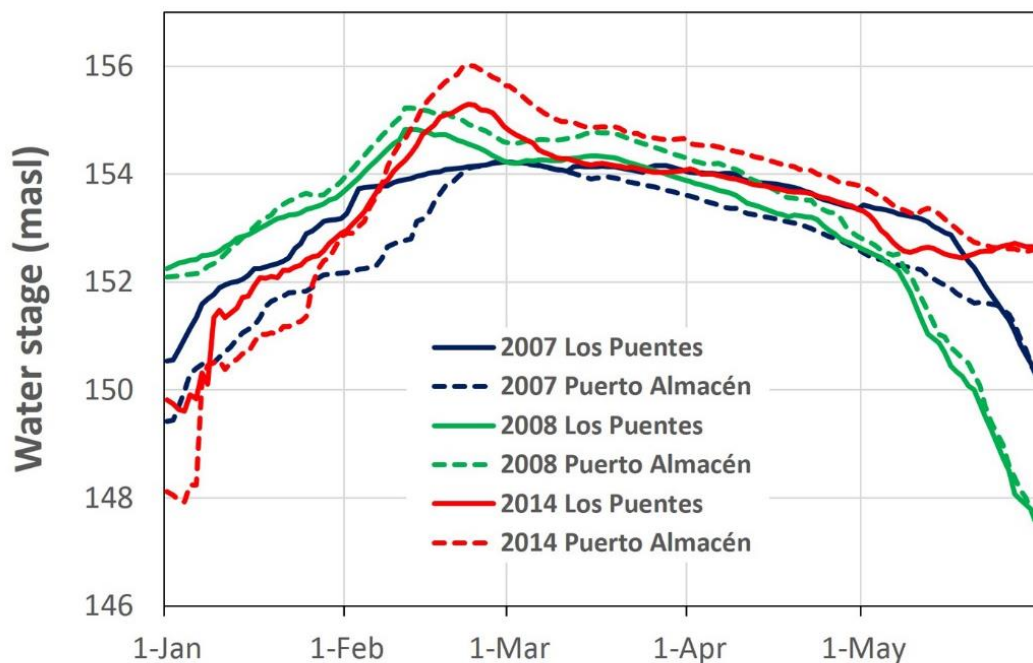
The arrival of the flood wave through the Mamoré River together with the expansion of the flooded area downstream, depicted in Figure 3.18a, b, is a strong indication that the flooding of the Llanos makes an important exogenous contribution to the initial phase of the flood, as suggested by Bourrel et al. (2009).

Although we observed in Figure 3.18a that concomitant with the expansion of the flooding upstream, the flooded area also increased in isolated areas of the endogenous network, the contribution times to the Mamoré River of endogenous streams and lakes are likely to be much longer than the arrival of the flood wave through the Mamoré River. Therefore, in the initial phase, the flooding of the Llanos should occur mainly from the river main stem toward the floodplain.

To check for potential hydrodynamic effects in the exchange between the Mamoré main stem and the wetlands, we compared the water stages of the Mamoré River at Los Puentes and the Ibaré River, an endogenous tributary of the Mamoré River, at the Station of Puerto Almacén (Figure 3.1) during the floods of 2007, 2008 and 2014. Because the two stations are relatively close, comparison of their water stage behavior provides an indication of the magnitude and direction of the river main-stem and floodplain exchange. Water stage was expressed in meters above sea level based on the altitude of the gauge's zero as estimated by (KOSUTH; BLITZKOW; COCHONNEAU, 2006). Figure 3.20 indicates that, at the beginning of the rising limb of the flood, the water stage at the Mamoré River at Los Puentes was higher than in the Ibaré River at Puerto Almacén, suggesting that the direction of the flow was from the river to the floodplain. As the flood progressed, the water stage at the gauge station located at the wetlands was higher than the station in the Mamoré main-stem particularly during the 2008 and 2014 floods, indicating that the flow was from the wetlands toward the river. This process continues during the peak and for most of the recession of the flood wave. Finally, when the recession became more pronounced, differences in water level between the two stations gradually reduced and eventually inverted, suggesting a return to the initial conditions. Although the water stages during 2007 flood were similar in behavior, thus is, a

steeper raise in Puerto Almacén gauge stations close to the peak-time, the water stages in this station remained only slightly higher than Los Puentes station and for a shorter time- period. This suggests that the flow from the wetlands toward the river was less important in magnitude and duration during 2007 compared to the other two events.

Figure 3.20 – Comparison of water stages of the Mamoré and Ibaré Rivers.



Water stage at the station of the Mamoré River at Los Puentes (continuous lines) and the Ibaré River at Puerto Almacén (dotted lines) during the 2008 (green lines) and 2014 (red lines) floods.

Source: by the author

Our data confirm the hypothesis of Bourrel et al. (2009) with respect to the combination of exogenous and endogenous processes during large floods. In addition, the data suggest that, during major floods, the exogenous process is relatively short-lived and dominates only the first part of the rising phase. Because at peak time the difference in water stage between the wetlands and main stem is at its maximum (Figure 3.20), lateral contribution from the wetlands to the river (endogenous process) appears to determine the

magnitude and duration of the flooding. Moreover, the larger the flood, the more significant the flows from the wetlands towards the river: the 2014 flood produced the largest positive gradients from the wetlands to the river main stem and for a longer time-period, followed by the 2008 flood and finally the 2007 event. However, despite the reduced duration of the exogenous phase, it is clear that it plays a crucial role in damping the flood by transferring water to the wetlands during the initial phase of the event.

### **3.4 Conclusions**

Major flood events in the upper Madeira are characterized by the superposition of flood waves originating in the Beni-Madre de Dios River system (western upper Madeira) and the Mamoré–Guaporé river system (eastern upper Madeira). The concomitant peaks reaching the Madeira River at Abunã station, exacerbated by abundant local rainfall, result in higher peak discharges such as those observed during the 2007, 2008 and 2014 flood events. In the case of the 2007 event, the peak of the Madeira was enhanced due to a delay in the discharge of the Beni-Madre de Dios River system, which was in phase with the contribution of the Mamoré-Guaporé system. During the 2008 flood, the peak of the Madeira River at Abunã resulted from the superposition of a late secondary peak from the Beni-Madre de Dios system with the peak of the Mamoré-Guaporé system, and it was augmented by intense local rainfall at Abunã station. Finally, in the 2014 flood, the flood wave from the Mamoré-Guaporé river system was faster and “in phase” with the contribution coming from the Beni-Madre de Dios river system. Because the discharges of the two river systems were the maximum recorded in the available series, the Madeira reached peak discharges never observed in the available series.

In terms of flooded area, this study corroborated the estimations of Hamilton et al. (2004) in terms of the maximum flooded area. However, discrepancies were noted in terms of the mean flooded area, presumably due to differences in the methodology used for image processing.

The dynamics of the flooded area in the Llanos are strongly dependent on the timing and spatial distribution of positive rainfall anomalies. The magnitude of

the flooding, on the other hand, is strongly dependent not only on the spatial distribution of the positive anomalies but also on the location of intense rainfall spots. This can be explained by the fact that flooded areas transform all rainfall into runoff, and therefore localized intense rainfall has an immediate and abrupt influence on river discharge. Obviously, this effect is more pronounced in the middle of the wet season, when the flooded area is enough large that the hydrological response cannot be attenuated by soil water storage. In addition, the persistence of positive rainfall anomalies in March determines the duration of the flooding.

As suggested by Bourrel et al. (2009), floods in the Llanos are a combination of an exogenous process, which is a flood wave originating in the Mamoré upper drainage area; and an endogenous process, which is the contribution of the flooded area of the Llanos. Although the exogenous process appears to be important in the early phase of the flooding, dampening the incoming flood wave from the Andes piedmont, the endogenous process appears to be the most important in determining the magnitude and duration of the flooding of major floods.



## **4 SATELLITE ALTIMETRY AND MULTITEMPORAL FLOOD MAPS TO SUPPORT PROCESS UNDERSTANDING**

### **4.1 Introduction**

The large extension and remoteness of the Amazon wetlands limits the establishment of a dense network of in situ hydrometric measuring stations, which could provide complementary information for remote sensing studies and/or inputs for hydrological or hydrodynamic models. This explains why satellite altimetry are widely used to complement existent local observations of water levels in ungauged rivers and wetlands (CALMANT; SEYLER, 2006; FRAPPART et al., 2006; ALSDORF et al., 2007; SEYLER et al., 2009; JUNG et al., 2010; DASILVA et al., 2012). Also, satellite altimetry data is being extremely important not only as the main information for observational studies, but also for improving hydrological-hydrodynamic models (WILSON et al., 2007a; GETIRANA, 2010; PAIVA et al., 2013b; GARAMBOIS et al., 2016; PARIS et al., 2016)

Recently, the HYBAM-OS project and the Brazilian Water Agency – ANA have integrated satellite altimetry estimations in virtual stations to the Amazon River network, either to retrieve historical records, either for real time monitoring of rivers and floodplains ([www.hidrosat.ana.gov.br/](http://www.hidrosat.ana.gov.br/)). Although there is an increased number of virtual water stage stations along the Amazon and the LM, water level information within the wetlands and its main characteristics in terms of flood depth, flood extension and water storage are still limited.

In this study, multi-temporal flood maps (from MODIS -Moderate Resolution Imaging Spectroradiometer) data were combined with floodplain water level time series data derived from satellite altimetry (ENVISAT & SARAL) to answer key questions of the hydrological functioning of the LM including the spatial and temporal distribution of flooding; the relative contribution of exogenous floods created by the flood wave from the Andes, as well as endogenous floods originated in the lowlands; and estimations of temporarily water storage in the floodplains during floods.

Findings of this study provide support for previous hypotheses regarding the dynamics of the floods in the region, and constitutes preliminary information for future altimetry projects, such as the Surface Water and Ocean Topography (SWOT) mission (DURAND et al., 2010)., which is expected to provide information of continental waters in an unprecedented way and support hydrological/hydrodynamical modeling.

## **4.2 Methods**

### **4.2.1 Multitemporal flood maps**

Multi-temporal maps of flooded areas for the period 2001-2014 were derived using both active and optical systems: the MODIS M\*D09A1 product, the PALSAR L1.5 product, and ScanSar HH images. The M\*D09A1 product includes seven spectral bands in the 400 nm to 2500 nm spectral region at a spatial resolution of 500 m (<http://modis.gsfc.nasa.gov>). The near infrared (NIR-841-576 nm) and middle infrared (MIR-1230-1250 nm) channels capture the variation of the floodplain surface during the hydrological cycle as a function of vegetation growth, water availability and flooding. PALSAR is an active L-band sensor on board the Land Observation Satellite (ALOS) launched in 2006 by the Japanese National Space Agency (JAXA). PALSAR data detect water under the vegetation canopy with relative independence from atmospheric conditions because of the L-band double bounce effect (WOODHOUSE, 2005). Classification was based on an object-based image analysis (OBIA) approach (BLASCHKE, 2010), using segments or clusters-based mapping algorithms rather than pixel-based schemes. Image segmentation was achieved by exploring spatial connectivity and spectral similarity between pixels to form groups of homogeneous pixels. The statistical mean was calculated at the cluster level and then used in the flood mapping algorithm. Spatial segmentation was performed using the PALSAR image dataset because it presented the finest spatial resolution, and the results were subsequently applied to the MODIS images that were registered to the same geometry.

Details regarding the image treatment, classification and validation can be found in section 3.2.2.

In total, 632 multi-temporal flood maps were used to generate a flood frequency map, which represents the amount of time a floodplain is flooded, and a floodplain flashiness index map, which reflects the rapidity and frequency of short-term changes in the extent of flooding.

Thus, for every mapping unit (cluster) the following equation was applied to obtain the frequency of flooded days:

$$FFp = \frac{NFD}{Ns} \quad (4.1)$$

where  $FFp$  represents the frequency of flooded days,  $NFD$  represents the number of flood days and  $Ns$  represents the total number of days in the multi-temporal flood map series.

Regarding the flashiness index, we applied an adaptation of the Richards-Baker Flashiness Index (known as the R-B index) (BAKER et al., 2004), which was originally designed for streamflow data, using the following equation:

$$R - B \text{ flood} = \frac{\sum_{i=1}^n |a_i - a_{i-1}|}{\sum_{i=1}^n a_i} \quad (4.2)$$

where  $R-B \text{ flood}$  represents the R-B index for flood extension in floodplains and  $a$  is the flooded area at time step  $i$ .

## 4.2.2 Altimetric water stage time series

### 4.2.2.1 Altimetric principles and data

Satellite altimetry measurements are based on the time of flight of a radar pulse emitted by an altimeter and the echo reflected by the water surface directly below. The electromagnetic pulse is a radar emission in the Ku and Ka bands, with frequencies of 13-17 Ghz and 26.5-40 Ghz, respectively. One half the time interval required for this pulse to be reflected back to the altimeter is used to measure of the distance between the satellite and the Earth's surface (FU;

CAZENAVE, 2001). The height  $H$  of the earth's surface with respect to the geodetic reference, considering corrections related to the delayed propagation through the atmosphere and ionosphere, is estimated as follows:

$$H = a_s - p + C_{iono} + C_{dry} + C_{wst} + C_{st} + C_{pt} \quad (4.3)$$

where  $a_s$  is the satellite altitude with respect to a reference ellipsoid,  $p$  is the distance between the satellite and the earth's surface,  $C_{iono}$  is the correction for delayed propagation through the ionosphere,  $C_{dry}$  and  $C_{wst}$  account for delayed propagation through the atmosphere, and  $C_{st}$  and  $C_{pt}$  are corrections for crustal vertical motions because of solid and polar tides, respectively.

Although satellite altimetry was initially conceived for monitoring ocean level variations, its usefulness for monitoring the level of continental waters has been demonstrated since the end of the 1970s (CALMANT; SEYLER; CRETAUX, 2008; DASILVA et al., 2012). Subsequently, the application of satellite altimetry has evolved in a noticeable way. Currently, its applications in continental hydrology encompass diverse areas, such as water stage variations in rivers and lakes, densification, reconstruction and correction of in situ time series and studies on river slopes and its applications in hydrodynamic modeling (CALMANT; SEYLER; CRETAUX, 2008; PAIVA et al., 2013b; DOMENEGHETTI et al., 2016; PARIS et al., 2016; TOURIAN et al., 2016). The future launch in 2020 of the US-French SWOT mission (<https://swot.cnes.fr/fr>, <https://swot.jpl.nasa.gov/mission>), which will apply a Ka band interferometric swath altimeter, will provide unprecedented high spatial resolution and temporal sampling observations of continental waters, thus extending the data for current sampling locations.

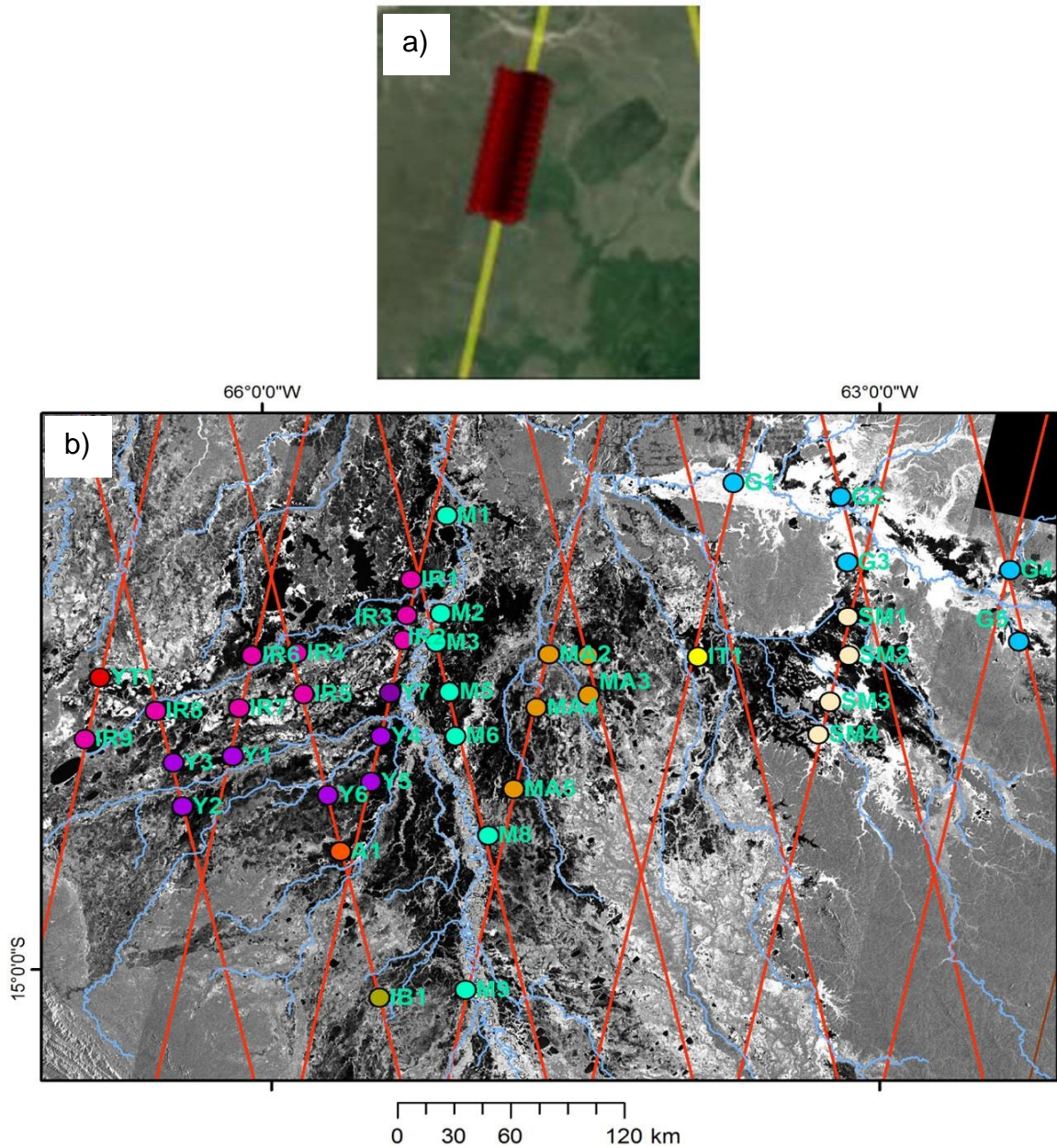
Data from the RA-2 altimeter on board the ENVISAT satellite (launched in 2002) have been combined with data from the AltiKa altimeter on board the SARAL satellite (launched in 2013), which has the same orbit as the ENVISAT. Thus, altimetry data based on water stage time series for the period 2002-2014 are obtained via cycles 6 to 94 of the ENVISAT RA-2 altimeter (cycles 95–113 are not considered because ENVISAT was in a drifting orbit and incompatible with SARAL) and via cycles 1 to 17 from the SARAL AltiKa. We obtained

ENVISAT/RA-2 Geophysical Data Records (GDRs) version V 2.1 from the Center for Topographic Studies of the Ocean and Hydrosphere (CTOH) [www.ctoh.legos.obs-mip.fr](http://www.ctoh.legos.obs-mip.fr). SARAL data, version IGDR-T, were obtained from the AVISO (Archiving, Validation and Interpretation of Satellite Oceanographic, [www.aviso.altimetry.fr](http://www.aviso.altimetry.fr)) database.

#### **4.2.2.2 Altimetric virtual stations within the floodplains and water stage time series**

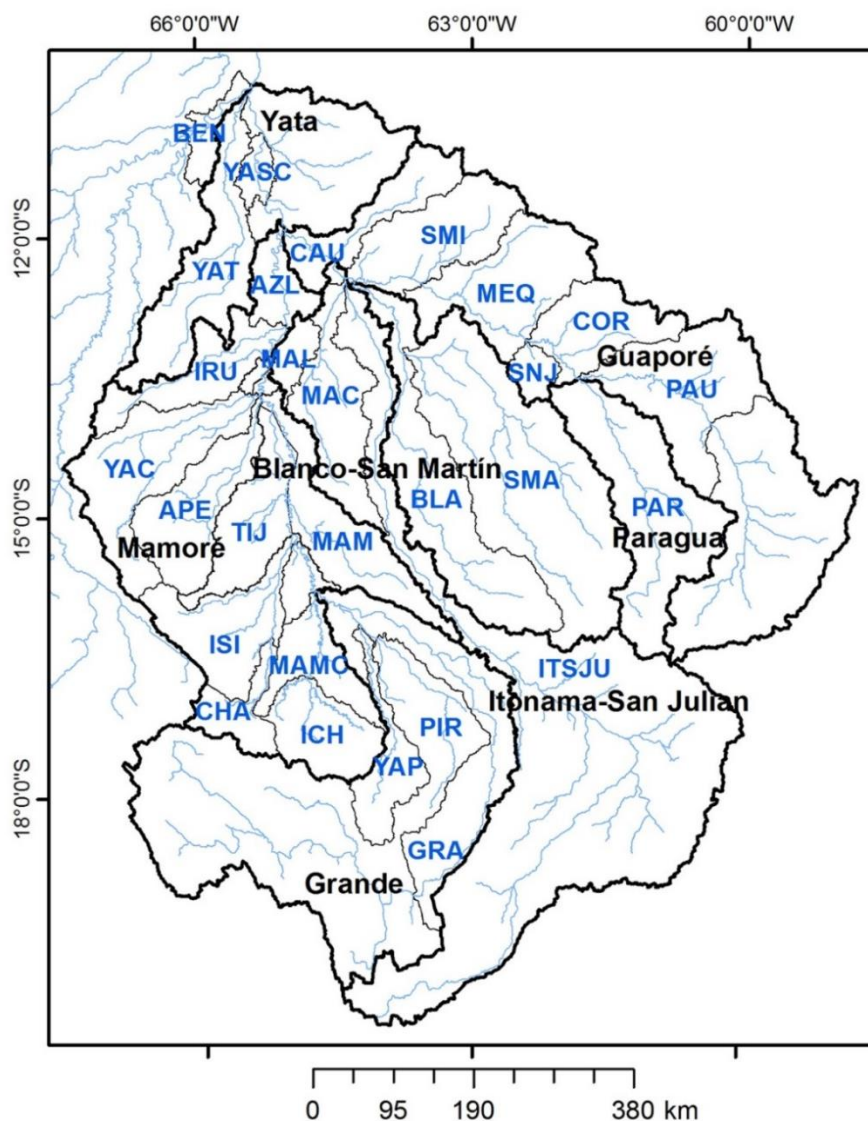
The intersections between the satellite track and a body of water are widely known as altimetric virtual stations (AVSs), in which water stage time series data are generated from radar measurements with each pass (FRAPPART et al., 2006; DASILVA et al., 2010). We compiled information on 41 AVSs distributed along different rivers in the LM: Mamore River (9 AVSs), Iruyañez River (9 AVSs), Yacuma River (6 AVSs), Guaporé–Iténez River (5 AVSs), Blanco–San Martin (4 AVSs) and the Apere and Yata rivers (1 AVS each). Thus, 20 AVSs were located in rivers outside the influence of the Andes, and 21 AVSs were located in rivers whose source is the Andes and its piedmont areas. The AVSs along the Mamore, Yacuma and Ibaré rivers are believed to have a stronger dependence on the meteorological conditions in the Andean slope and piedmont regions than the AVSs at the Iruyanez, Yata and Guapore-Iténez rivers, which are primarily governed by local conditions (Figure 4.2 and Table 4.1).

Figure 4.1– Satellite tracks, measurement points and Location of altimetric virtual stations along floodplains in the Llanos de Moxos;



a) Detail of satellite track and satellite measurement points (red dots) in a floodplain; b) Location of different altimetric virtual stations (AVS) along floodplains in the Llanos de Moxos; red lines indicate the satellite track. AVS distribution among different basins are presented in Table 4.1. Source; by the author

Figure 4.2 – Detail of the different basins and subbasins according to Pfafstetter (1989).



Basin (level 3)	Subbasin (level 2)	CODE	Basin (level 3)	Subbasin (level 2)	CODE
Mamoré	Apere	APE	Blanco-San Martín	Blanco	BLA
	Chapare	CHA		San Martín	SMA
	Tijamuchi	TIJ	Guaporé	Cautario	CAU
	Ichilo	ICH		Corumbiara	COR
	Isiboro – Secure	ISI		Mequéns-Massaco	MEQ
	Yacuma	YAC		Paucerna-Verde	PAU
	Mamorecillo	MAMC		San José	SNJ
	Irupaya	IRU	Sao Miguel	SMI	
	Arroyo Azul	AZL	Paragua	Paragua	PAR
	Mamoré	MAM	Itonamas San Julian	Machupo	MAC
	Mamoré-Lagunas	MAL		Itonamas-San Julian	ITSJU
	Grande	Grande Bajo	GRA	Yata	Yata
Piraí		PIR	Yata-Santa Cruz		YASC
Yapacaní		YAP			

Source: by the author

Table 4.1 - Major basins, subbasins and codification of AVS.

Major Basin (level 4)	Basin (level 3)	Subbasin (level 2)	CODE	AVS code
Guapore - Itenez	Blanco-San Martín	Blanco	BLA	----
		San Martín	SMA	SM1, SM2, SM3, SM4
	Guaporé	Cautário	CAU	----
		Corumbiara	COR	G4, G5
		Mequéns-Massaco	MEQ	G1, G2, G3
		Paucerna-Verde -	PAU	----
		San José	SNJ	----
		Sao Miguel	SMI	G1
	Paragua	Paragua	PAR	----
	Itonamas - San Julian	Machupo	MAC	MA1, MA2, MA3, MA4, MA5
		Itonamas-San Julian	ITSJU	IT1
Mamore	Mamoré	Apere	APE	A1
		Chapare	CHA	----
		Tijamuchi	TIJ	IB1
		Ichilo	ICH	----
		Isiboro – Secure	ISI	----
		Yacuma	YAC	Y1. Y2, Y3, Y4, Y5, Y6, Y7
		Mamorecillo	MAMC	----
		Iruyañez	IRU	IR1, IR2, IR3, IR4, IR5, IR6, IR7, IR8, IR9
		Arroyo Azul	AZL	----
		Mamoré	MAM	M5. M6, M8, M9
		Mamoré-Lagunas	MAL	M1, M2
	Yata	Yata	YAT	YT1
		Yata-Santa Cruz	YASC	----
	Grande	Grande Bajo	GRA	----
		Pirafí	PIR	----
		Yapacaní	YAP	----

Source: by the author

The altimetric pulses of AltiKa and RA-2 were processed using the ICE-1 algorithm (WINGHAM; RAPLEY; GRIFFITHS, 1986), which has been reported to perform better over continental water bodies than other algorithms (FRAPPART et al., 2006; CALMANT et al., 2013). We used the Virtual Altimetry Station (VALS 2010) software, which is specialized for altimetry, VALS can import, analyze, correct and select a group of altimetric measurements to generate water stage time series. This process is appropriate for floodplains, in

which water is not confined to river channels. Therefore, ancillary information, such as flood maps, a digital elevation model (DEM) and radar color composites, were employed (in Appendix 1, Figure A4, an example of altimetric measurements within VALS is provided). To obtain continuous time series measurements from the ENVISAT RA-2 and SARAL AtiKa satellites, several adjustments were applied to both data sets. Following the recommendations of Calmant et al. (2013), a global bias correction of  $-1.044 \pm 0.212$  m was applied to the ENVISAT RA-2 data. In addition, a global bias of  $0.263 \pm 0.18$  m was applied to the SARAL AltiKa data (SANTOS DA SILVA et al., 2015b). Concerning the bias in ENVISAT/SARAL, a 0.75 m bias was applied to SARAL values, as recommended by Santos da Silva et al (2015a).

#### **4.2.2.3 Flood signatures**

Water depth time series in the floodplains were estimated by analyzing the total variations along the water stage time series. We constructed a flood duration curve (FLDC) for every AVS. An FLDC is a plot that shows the percentage of time that the flood depth in a floodplain is likely to equal or exceed some specified value of interest. Similar to curves derived from streamflow data, the FLDC and its derived metrics can be important when characterizing the hydrological functioning of floodplains. Thus, in this study, we adapted the following set of metrics and signatures used to characterize ephemeral streamflow data (BAKER et al., 2004; KENNARD et al., 2009; TRANCOSO et al., 2016), these are:

- The 10th percentile flood depth – F10, which accounts for high flood intensity and variability. This metric is related to the magnitude of high floods, F10 represents the water height value which 10% of the time is equaled or exceeded.

Moreover, we obtained additional metrics from the altimetric water stage time series.

- The coefficient of variation (CV) is a measure of dispersion that provides information on the magnitude of variations in the water level within the floodplains..

$$CV = \frac{STDV}{H} \quad (4.4)$$

where *STDV* represents the standard deviation of the data (when >0), and *H* represents the mean of the series.

- Rising limb density (RLD) denotes the ratio between the number of rising limbs within the water depth series and the total amount of time steps in the series (increments in the water stage that exceed the 40<sup>th</sup> percentile were not considered as rising limbs). Higher RLD values correspond to higher flashiness and a greater regularity of floods.

$$RLD = \frac{NRL}{T} \quad (4.5)$$

where *NRL* represents the number of rising limbs within series *s* and *T* represents the total of number of records.

- The flashiness index (BAKER et al., 2004), is applied to the water stage time series using the following equation:

$$R - B \text{ Stage} = \frac{\sum_{i=1}^n |h_i - h_{i-1}|}{\sum_{i=1}^n h_i} \quad (4.6)$$

where *R–B index* represents the R-B index for the flood stage in the floodplains and *h* represents the water stage at time step *i*.

A cluster analysis was performed to group similar water stage time series. Thus, an expectation maximization (EM) algorithm initialized via model-based hierarchical clustering (MHC) was employed based on the water stage time series signatures and the RLD, F10N, VC and R-B index values. The MHC algorithm can automatically infer the number of clusters and employs a Bayesian scheme for model selection (HELLER; GHAHRAMANI, 2005). This clustering approach has been proven to be useful for grouping streamflow data using FLDC-derived signatures (TRANCOSO et al., 2016).

When comparing water stage time series with flood dynamics for a given AVS, the extent of flooding was calculated by considering an area of 625 km<sup>2</sup> surrounding the virtual station. This spatial discretization coincides with a regular cell scheme with a 25 km resolution, and this scheme is also employed in hydrological models (SIQUEIRA-JÚNIOR; TOMASELLA; RODRIGUEZ, 2015) or regional circulation models (RCMs), which are currently applied for the region, such as in the Brazilian Regional Atmospheric Modeling System (BRAMS) (GARCÍA SKABAR; SALIO; NICOLINI, 2012). Because the available hydrological models use DEMs to simulate floodplain dynamics, we compared Shuttle Radar Topography Mission (SRTM) altitude data with the combination of remote sensing altimetry-floodplain mapping within those selected rectangular areas.

#### **4.2.3 Surface water storage in floodplains**

Water depth information combined with multi-temporal flood maps was used to generate the time series of water storage volumes in the floodplains. Estimations for the Beni and Madre de Dios basins are missing because AVS data were not employed for these basins. The spatial statistics of the interpolated flood depth values were calculated at the cluster level to obtain surface water volumes within the floodplains.

Streamflow for the period 2002-2014 from the hydrological stations Puerto Siles (Mamore River) and Principe da Beira (Guapore) (Figure 3.1) were employed in order to estimate the total water volume generated by these basins. With this, comparisons between the amounts of surface water stored in floodplains during flood peaks against the total volume of water generated by the respective basin during the hydrological year was possible.

### **4.3 Results**

#### **4.3.1 Complex flooding processes**

As explained in section 3.3, the different climatic regimes, extensions and topographies of the four main tributaries of the Bolivian Amazon, determines the particular discharge regimes that governs the flooding process in the area. the

steeper topography and smaller contribution area of the Madre de Dios River creates a faster hydrological response that has a strong influence on the peak and shape of the flood waves of the Beni River. The Mamoré River flows along the vast wetlands, reducing the peaks and significantly delaying the travel time of the flood waves from the Andes. Thus, the peak discharge at the Cachuela Esperanza Station in the Madre de Dios-Beni River system generally occurs 54 days before the peak at the Guajar-Mirim Station in the Mamor-Guapor River system. At the Abun Station in the Madeira River, the peak discharge generally occurs 8 days after the peak at Cachuela Esperanza and 46 days before the peak in the Mamor-Guapor River system. The time difference between the peaks of the Madre de Dios-Beni River system from the west part of the study area and the Mamor-Guapor River system from the east attenuates the discharge of the upper Madeira and prevents the occurrence of extremely high river levels at the Abun Station (OVANDO et al., 2016).

Floods in the LM are a combination of an exogenous process, which is a flood wave originating in the Mamor upper drainage area that occurs in response to rainfall in the Andes range and its piedmont, and an endogenous process, which is the contribution of the flooded area of the wetlands (BOURREL ET AL., 2009). The exogenous process is referred to as an overbank spilling from the main river channel, whereas the endogenous process results from the outflow of groundwater from the floodplain as a result of local precipitation. Nevertheless, the processes involved are more complex in reality because the hydrodynamic control exerted by the Mamore on its floodplain tributaries varies in importance depending on the characteristic of the hydrological year. Therefore, Bourrel et al. (2009), had subdivided the endogenous process into three types: "sensu stricto", "controlled" and "combined". The sensu stricto type refers to floods in floodplain tributaries in response to local precipitation; the controlled type refers to the floods of an endogenous river caused by the hydrodynamic control exerted by the Mamore River; and the combined type refers to an overflow of an endogenous river caused by the inflow of water from the Mamore River (BOURREL ET AL., 2009).

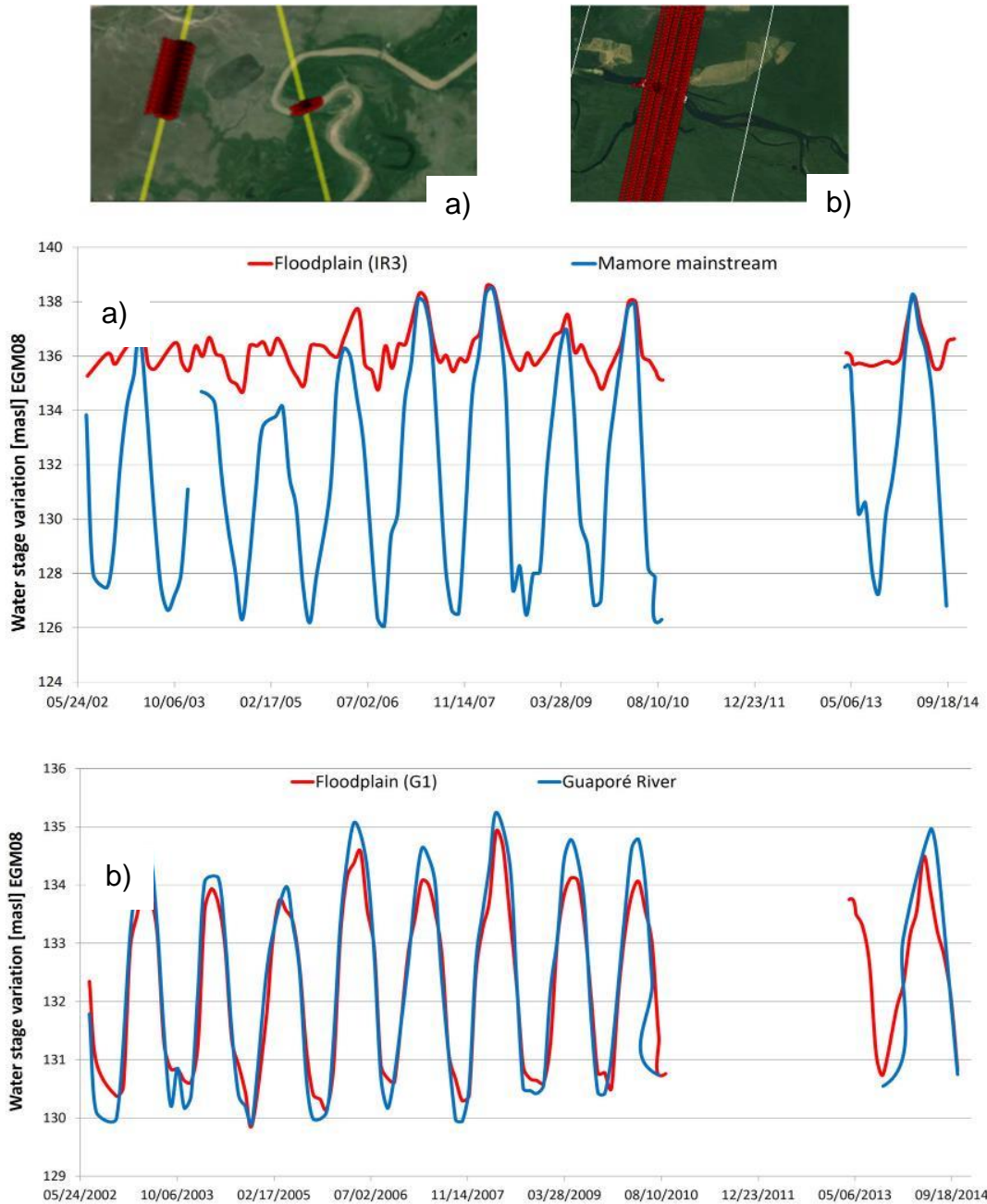
The exogenous process appears to be important in the early phases of flooding because it dampens the incoming flood wave from the Andes piedmont area, and the endogenous process appears to be important in determining the magnitude and duration of major floods (OVANDO et al., 2016).

Satellite altimetry time series of the water stage within floodplains and rivers illustrate the particularities of the endogenous and exogenous processes. When comparing the water stage time series from the mainstream Mamore River with an adjacent floodplain tributary, clear differences can be observed. As expected, the amplitude of water stage variations within the Mamore mainstream is higher than that of the floodplain. For instance, at a site near the confluence of the Iruyañez and Mamore rivers (AVS code IR3) (Figure 4.3), the water stage varies up to 2-3 m in the Iruyañez floodplains and 8-10 m in the Mamore River channel. In most of the years the water stage in both the Mamore mainstream and Iruyañez floodplain are generally independent, which is an example of a *sensu stricto* endogenous process, where flood dynamics in the floodplain is more regular without abrupt changes in water stage. However, connection between the two systems is obvious when the Iruyañez floodplain and the Mamore main stream attain the same level during extreme flooding events, thus suggesting a controlled endogenous process. In this case, more intense water stage changes are visible in the floodplain. Considering that the Mamoré River water height shows larger amplitudes than the Iruyañez, it is likely that the interactions between the river and the floodplain in certain parts along the Mamoré main-stream can be classified as combined.

In other words, the settle of an endogenous, exogenous or combined process and its importance varies from year to year depending on the meteorological conditions. This alternation of endogenous/exogenous process was also described in section 3.2.2 - Figure 3.20 – when comparing observational data from the Mamore and the Ibare rivers. In a frequently flooded site located the Iténez-Guapore (Figure 4.3), on the other hand, the differences between the river and its floodplain show an amplitude of about 0.5 m to 0.8 m. In this case the water stage during flood peaks at the river channel is always higher than the

floodplain, suggesting direct river contribution. So, this site is representative of a purely exogenous flood that occurs every wet season.

Figure 4.3 - Comparison between water stage variations in floodplain and in the river mainstream.



Satellite track, Measuring points and time series: a) Mamore River (b) and Iténez-Guapore River.

Source: by the author

### 4.3.2 Flood extension, variability and frequency

The estimated flood extension for the flood peaks during the 2001-2014 period illustrates the total flooded area and the interannual variability of flooding processes within each basin in the region. The estimates show that the total flooded area in each of the basins varies from year to year, and in certain subbasins, the flood peak occurred in 2014, whereas in others, the peaks occurred in 2008 or even during minor events (Table 4.2). As shown in section 3.3.3, the distribution of rainfall and the occurrence of rainfall anomalies in different areas was not uniform over time and represents a determinant of the flood peak variability, although the river–floodplain connectivity may also play a relevant role.

The largest interannual variation can be found in the Itonamas-San Julian and Mamoré basins, which also have the largest extension of flooded areas, and in these basins, the total flooded area ranges from approximately 1600 km<sup>2</sup> to 12243 km<sup>2</sup> and 8600 km<sup>2</sup> to 37649 km<sup>2</sup>, respectively. In both cases, the total flooded area represents more than a 100% change with respect to the annual mean. In the other basins, the maximum flooded areas do not show greater than 65% increases from their respective mean annual flooded areas (Table 4.2). In the Mamoré Basin, most of the tributaries attained their maximum flood extension during the 2014 event. In the piedmont tributaries and the Yacuma, Apere, Chapare, Ichilo, Isiboro-Secure and Ibare rivers, the total extent of flooding in 2014 was 15900 km<sup>2</sup>, whereas in the floodplains of the Rio Grande subbasin, which drains a portion of the Andean west-oriented slopes, the extent of flooding reached 1805 km<sup>2</sup>. The extent of flooding of the Iruyañez and Yata rivers, which are disconnected from the piedmont area, was 6000 km<sup>2</sup> and 3668 km<sup>2</sup> in 2014, respectively. In the central floodplains of the Mamoré, which are formed by the Arroyo Azul, Mamoré and Mamoré Lagunas subbasins, the total extent of flooding was 14893 km<sup>2</sup>.

In the Itenez-Guapore Basin, considerable flooding (10950 km<sup>2</sup>) was reported for floodplains in the Blanco-San Martin Basin in 2008, and the Andes did not contribute to the flooding. In the Itonama-Machupo Basin, the highest flooding (San Julian subbasin) reached up to 3250 km<sup>2</sup> in 2008. In the lower Machupo

subbasin, flooding reached 12498 km<sup>2</sup> in 2014. The Parapeti River is believed to have only contributed to the flooding extent of the San Julian subbasin during years with extreme rainfall levels (ARGOLLO, 2006). In other tributaries, which include the Brazilian portion of the basin, flooding reached approximately 7339 km<sup>2</sup> in different years.

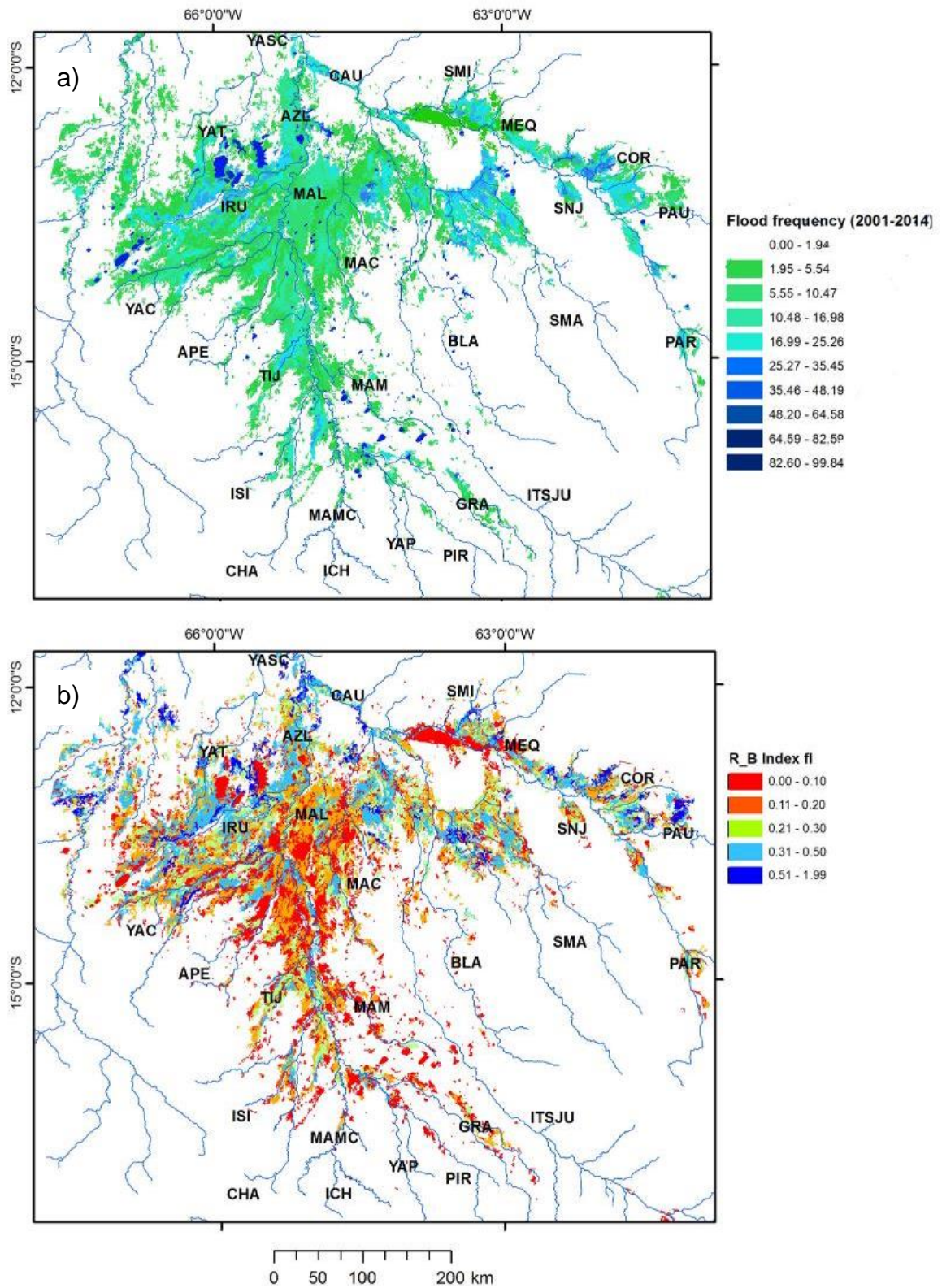
Table 4.2 - Maximum flooded area in the different tributaries, and subbasins division in accordance (Pfafstetter (1989).

Major Basin (level 4)	Basin (level 3)	Subbasin (level 2)	Maximum flood [km <sup>2</sup> ]	Year
Guapore - Itenez	Blanco-San Martín	Blanco	2336.10	2008
		San Martín	8614.49	2008
	Guaporé	Cautário	634.60	2014
		Corumbiara	3038.75	2008
		Mequéns-Massaco	2196.03	2008
		Paucerna-Verde	1011.60	2004
		San José	449.55	2006
	Sao Miguel	8.93	2010	
	Paragua	Paragua	809.00	2008
	Itonamas - San Julian	Machupo	12498.64	2014
Itonamas-San Julian		3254.32	2008	
Mamore	Mamoré	Apere	3078.69	2014
		Chapare	49.62	2014
		Ibare-Tijamuchi	3750.60	2014
		Ichilo-Mamoré	20.10	2014
		Isiboro - Secure	1737.59	2014
		Yacuma	6984.54	2014
		Mamorecillo	373.16	2014
		Iruyañez	6782.31	2014
		Arroyo Azul	3226.29	2014
		Mamoré	10504.38	2014
		Mamoré-Lagunas	1162.68	2014
	Yata	Yata	3437.81	2014
		Yata-Santa Cruz	231.01	2008
	Grande	Grande Bajo	1648.01	2008
		Piraí	107.04	2014
		Yapacaní	50.51	2014

Source: by the author

Both the flood frequency and flood flashiness metrics provide complementary details on the hydrological functioning of floodplain (Figure 4.4). The flood frequency represents the amount of time that a floodplain is flooded, whereas the R-B flood index reflects the rapidity and frequency of short-term changes in flood extension (higher R-B flood index values correspond to a flashier response of the floodplain). Most of the areas with higher flood frequency areas ( $FFp > 25$ ) are located in the floodplains of the Iruyañez, Yacuma, San Martin Blanco, Itonama and Guaporé rivers and coincide with areas with high R-B flood index values ( $> 0.3$ ). Thus, high R-B values indicate that floods mainly occur as a response to local processes, such as local rainfall, saturation excess overland flow and overbank events of small tributaries, indicating local short-term changes in the extent of flooding. According to the maps (Figure 4.4) these patterns occur mostly in frequently flooded sites, where floods are driven by local conditions. However, lower R-B flood index values are associated with occasionally flooded sites ( $FFp < 10$ ), where floods depend on the arrival of flood waves from upstream tributaries. These characteristics describe the sites in the middle portion of the Mamoré River and the Itonamas River, where flood processes are primarily linked to overbank flows. In the next section, satellite altimetry data are used to assess variations in the water level within the floodplains.

Figure 4.4 - Flood frequency and R-B Flood maps.



Flood frequency map (2001-2014);b) R-B Flood flashiness Index. Subbasin codes are detailed in Table 4.1.

Source: by the author

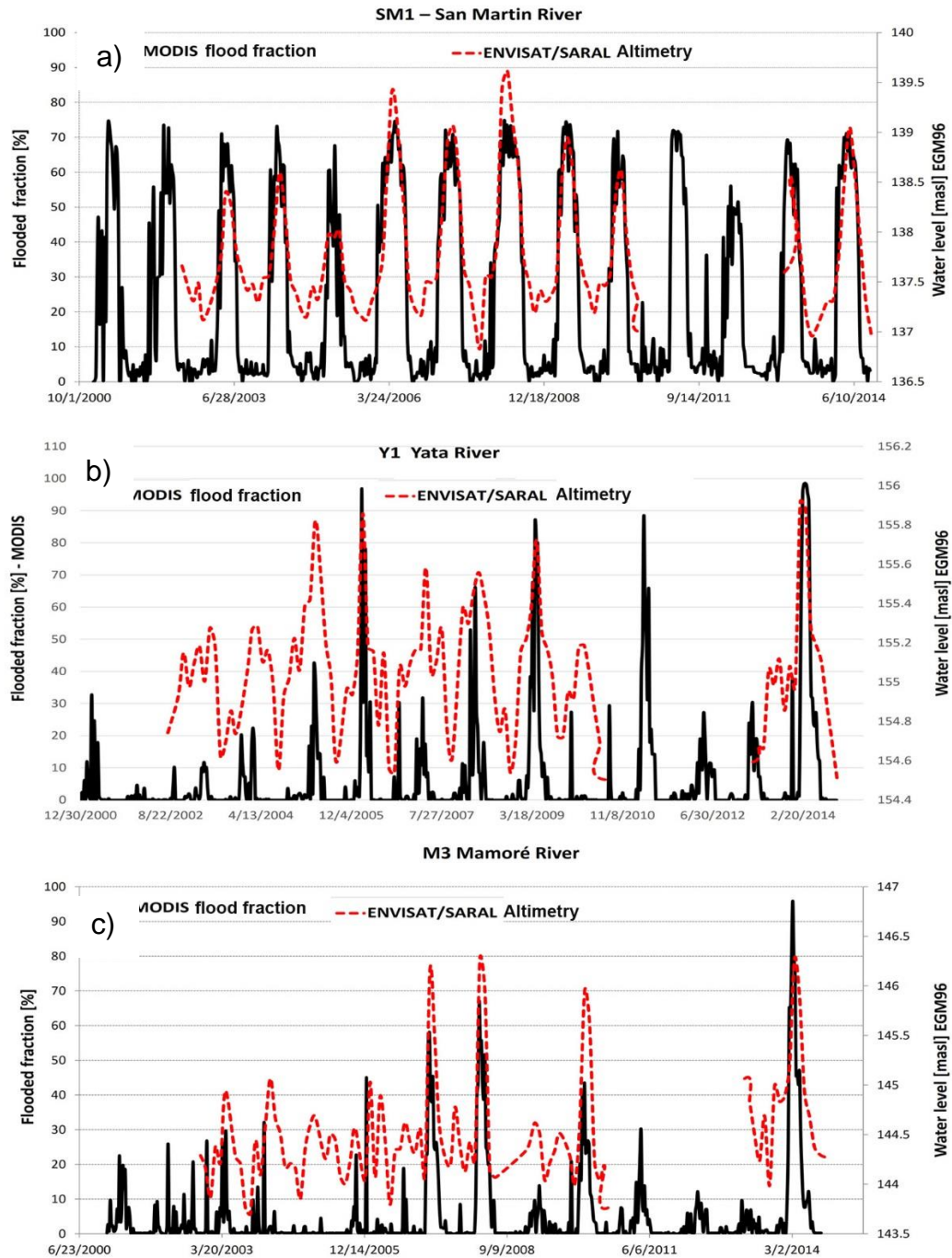
### 4.3.3 Water depth in the floodplains

Water stage variations of altimetric time series data were used to estimate and characterize the water depth of the LM floodplains, and they provided a vertical dimension to the multi-temporal flood maps derived from MODIS. Thus, in this section we augment earlier information with key data regarding the water depth in floodplains, such as i) the shape of the altimetric series, which is denoted by the RLD; ii) the CV, which is a signature derived from the FLDCs (normalized 10th percentile); iii) the maximum and mean water depths; and iv) the estimated surface water storage in the floodplains.

A comparison of the time series of water stages derived from satellite altimetry data, which used flooded fractions of 0.25 regular polygons (approximately 625 km<sup>2</sup>) estimated from MODIS, showed that these independent measures were consistent. Thus, the flood fraction time series corroborates the water stage patterns and captures extreme events and smaller floods. In zones mapped as experiencing regular or frequent floods, the water stage series generally present peaks during every wet season and a high RLD (> 0.8) (Figure 4.5a). However, for sites with medium to low flood frequencies, peaks are restricted to extreme flood events, such as in 2007, 2008, 2010 and 2014, and lower RLD values are observed (Figure 4.5b-c). High RLD values are primarily observed in the floodplains of the Guapore, Blanco, San Martin and Itonama rivers; medium RLD values are primarily observed in the Iruyañez, Yacuma and Ibare rivers; and low RLD values are primarily observed in the central Mamore floodplains (Figure 4.5c). High CV values, which might be considered an indicator for strong interactions between rivers and floodplains, are located mainly along the central Mamoré in mapped areas with a low or medium flood frequencies. Low CV values are indicative of a greater influence of endogenous processes and less river-floodplain interactions. These sites are consistent with more frequent and predictable floods and are primarily located across the Guapore, Blanco, San Martin and Iruyañez rivers (Figure 4.6a). Intermediate and high CV values in the Yacuma, Itonama and Mamore floodplains indicate more active river-floodplain interactions. R-B index estimates from altimetry time series data follow the same patterns as those estimated from multi-temporal flood maps

(MODIS). Thus, low R-B index values are associated with occasionally flooded areas along the Mamoré River, and high values are associated with the Iruyañez and Guapore rivers (Figure 4.6b)

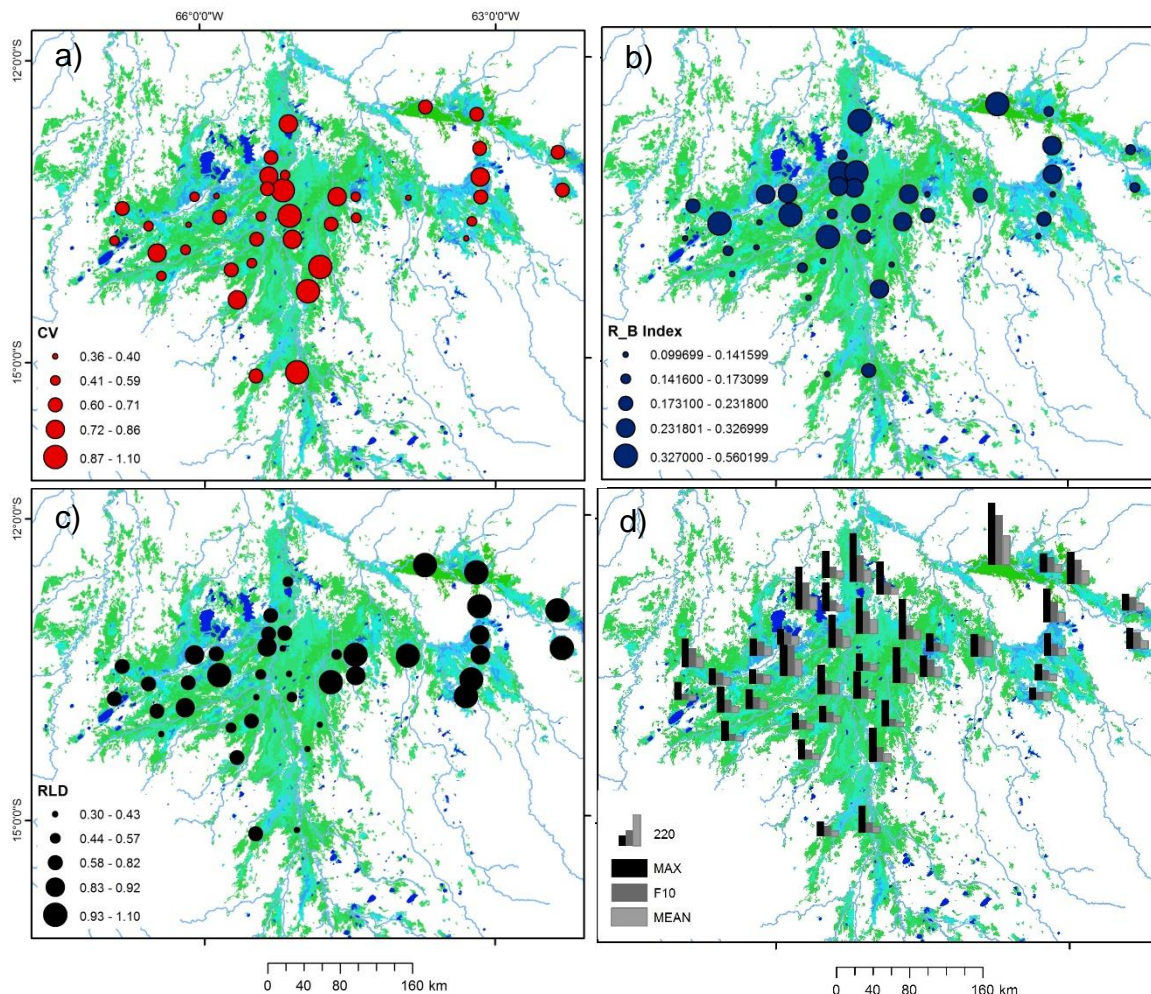
Figure 4.5 - Water stage and flooded fraction time series.



Water stage 2001-2014 (SARAL-Altika and ENVISAT RA-2) and flooded fraction for a surrounding cell of 25 km size. a) for high frequently flooded site,  $RLD > 0.9$  (b); medium frequency,  $RLD > 0.8$ ; and (c) and low frequency,  $RLD 0.3 - 0.55$   
 Source: by the author

The variation of water depth at every AVS show conspicuous extreme water levels during extreme events and regular interannual variations. In general, a floodplain's mean water depth in the wet season ranges from 30 cm to 100 cm, whereas the maximum values during extreme events may reach up to 100-200 cm, although water depths as high as 450 cm are observed at specific sites (Figure 4.6d). Because maximum depths are representative for the massive flood event of 2014 (see Appendix 1, Figure A5), they represent the most likely extreme flood depth values that can occur in the region and provide a measure of risk exposure. The large differences between the maximum depth with its respective F10 and mean values primarily observed along the Mamore River (Figure 4.6d), indicate that extreme depths are restricted to intense flooding events in which water levels rise conspicuously above the normal water depth because of rainfall anomalies in the Andes and piedmont area. Smaller differences between the maximum and F10 or mean values, which are mainly found across the Blanco–San Martin, Iruyañez, and Itonama rivers, indicate more regular and frequent flooding events that are fed by local rainfall over the lowlands.

Figure 4.6 – Signatures from water stage time series



Signatures derived from altimetric water stage time series over a map of flood frequency: a) Coefficient of Variation (CV); b) *R-B Stage*; c) Rising Limb Density (RLD); d) Maximum, mean water depth and *F10* signatures.

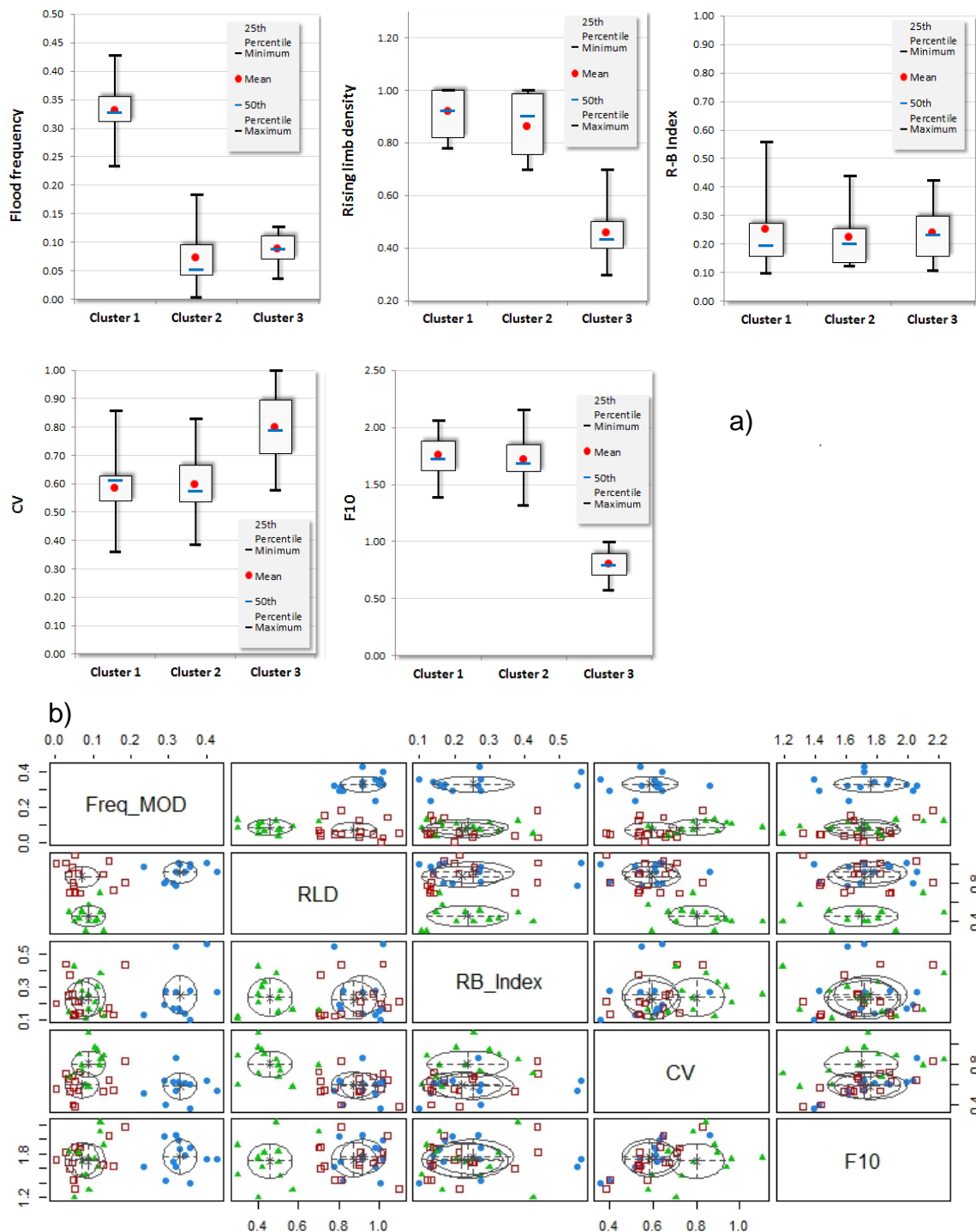
Source: by the author

Hierarchical clustering was employed to differentiate groups of AVSs based on the relationships between the flood frequency and the altimetric signatures described above (RLD, CV, R-B index and F10N). The EM algorithm evaluated 10 models and selected the equal volume and shape model (EEI) as the best option for clustering. As a result, three main clusters were identified that display particular flood patterns (Figure 4.7). The FFp signatures and R-B index values showed more evident differences with respect to Cluster 1, whereas the RLD, CV and F10 showed major differences for Cluster 3. Differences between these variables were influential in separating Cluster 2, which showed an intermediate behavior between Cluster 1 and Cluster 3 (Figure 4.7a).

These signatures and their respective clusters represent local characteristics of the flood regime (details of the clusters minimum, maximum, mean, median and percentiles values are shown in a box & whisker plots - Figure 4.7a). . Based on the spatial distribution of these characteristics (Figure 4.8), certain patterns can be distinguished:

- The first cluster (blue squares in Figures 4.6b and 4.7) is characterized by high *FFp* (mean = 0.33) and high RLD (mean = 0.9) values that indicate regular floods; a medium CV (mean = 0.6) that indicates moderate variations of water depth; an R-B index with high whisker amplitudes (0.10–0.57; mean = 0.28, which was the highest among the clusters) that indicates short-term water level variations; and F10 values (mean = 1.78, which was the highest among the clusters) that indicate a flashier flood regime. This cluster may be representative of floodplains that are not directly connected with the Andes and piedmont areas, such as those of the Guapore, Blanco, San Martin, Yata and Iruyañez rivers.
- The second cluster (red squares) is characterized by noticeably lower *FFp* (mean = 0.08) and lower RLD (mean = 0.85) values that indicate less periodicity of floods; a CV equal to that of Cluster 1 (mean = 0.6) that indicates a moderate variation of water depth; an R-B index with a lower mean (0.21) and smaller whisker amplitudes (0.11–0.42); and lower F10N values (mean = 1.6) that indicate a lower flood flashiness. This intermediary cluster can be considered representative of floodplains that are more dependent on exogenous processes (flood wave from piedmonts) but have a relatively fast response to endogenous processes.
- The third cluster (green triangles) is characterized by low *FFp* (mean = 0.08) and noticeably lower RLD (mean = 0.45) values that indicate sporadic flooding; a high CV (highest among the clusters; mean = 0.8) that indicates a large magnitude of water depth (high variation of water depth) during flood events; and the lowest R-B index (mean = 0.25) and F10N values (mean = 0.75) among the clusters that indicate the irregularity of floods.

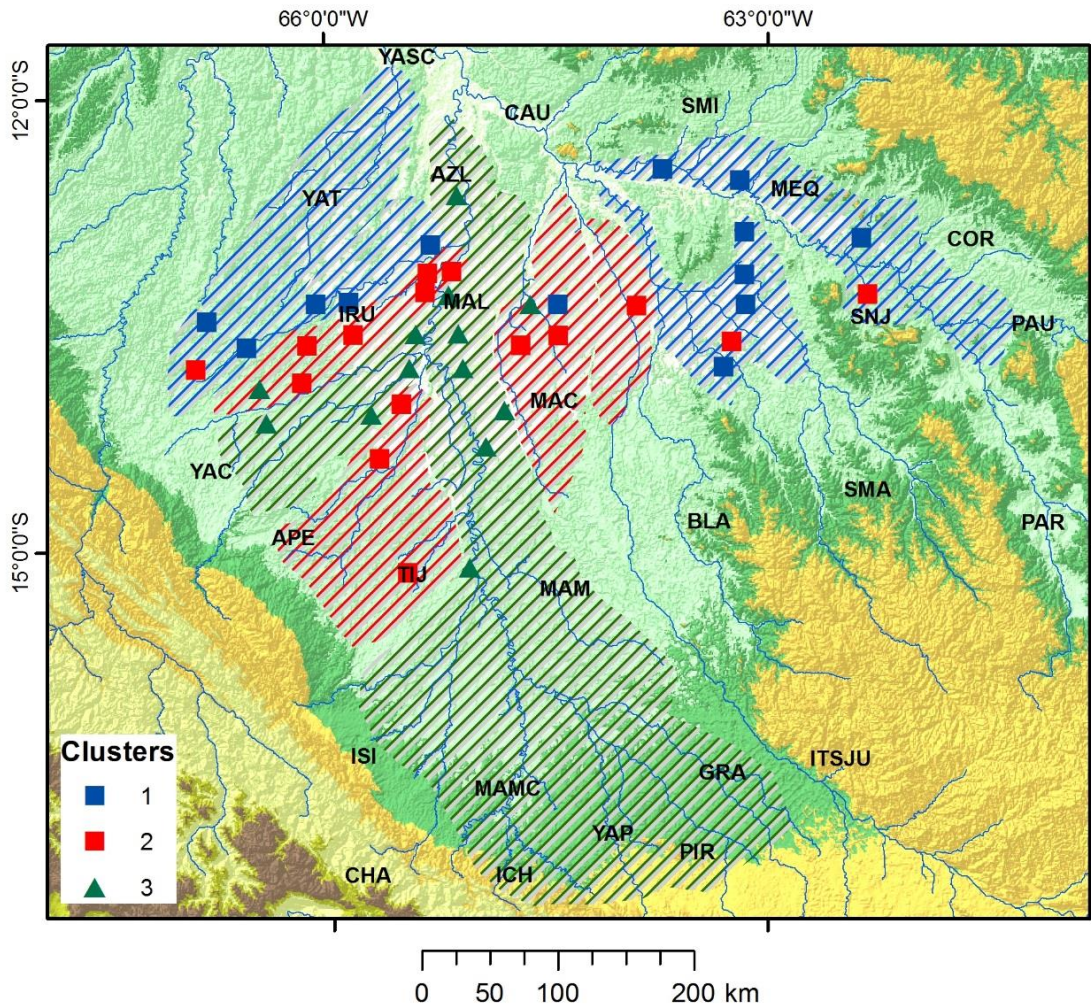
Figure 4.7 – Box-Whisker and scatterplots from different flood signatures.



a) Boxxes are bound by the 25<sup>th</sup> and 75<sup>th</sup> percentiles of the datasets, while the blue mid-line displays the median value and the red dot the mean; b) Scatterplots between the AVS signatures and flood frequency, different symbols and colors indicate the classification results while ellipsoids centers correspond to the component means.

Source: by the author

Figure 4.8 - Clustering results of flood signatures.

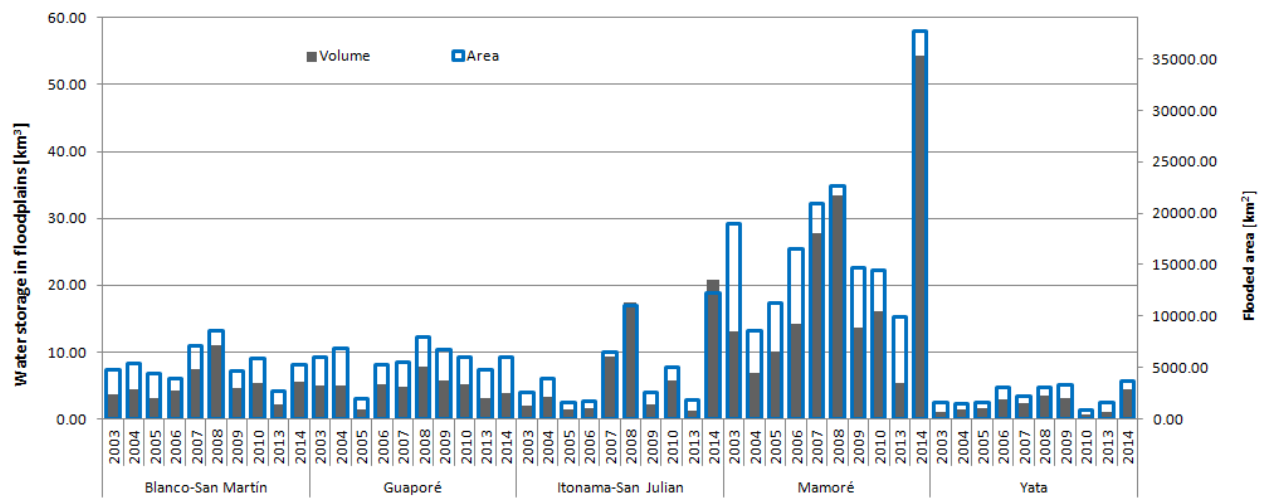


Different clusters derived from *FFp*, *RLD*, *R-B Stage*, and *CV* signatures, shaded areas correspond to representative zones.  
 Source: by the author

Surface water volumes estimated from multi-temporal maps and water depth levels for the flood peaks from 2003-2014 can be used to determine the initial water volume stored in the floodplains along the different basins in the area. As expected, the proportions are similar to that of the extent of flooding revealed in item 4.1 of (Figure 4.9), with the Mamoré Basin presenting the largest storage capacity and its Andean-connected tributaries exhibiting a relevant role. The total volume of surface water stored in the floodplains ranged from 10 km<sup>3</sup> to a maximum of 94 km<sup>3</sup> during the massive flooding event of 2014. The distribution

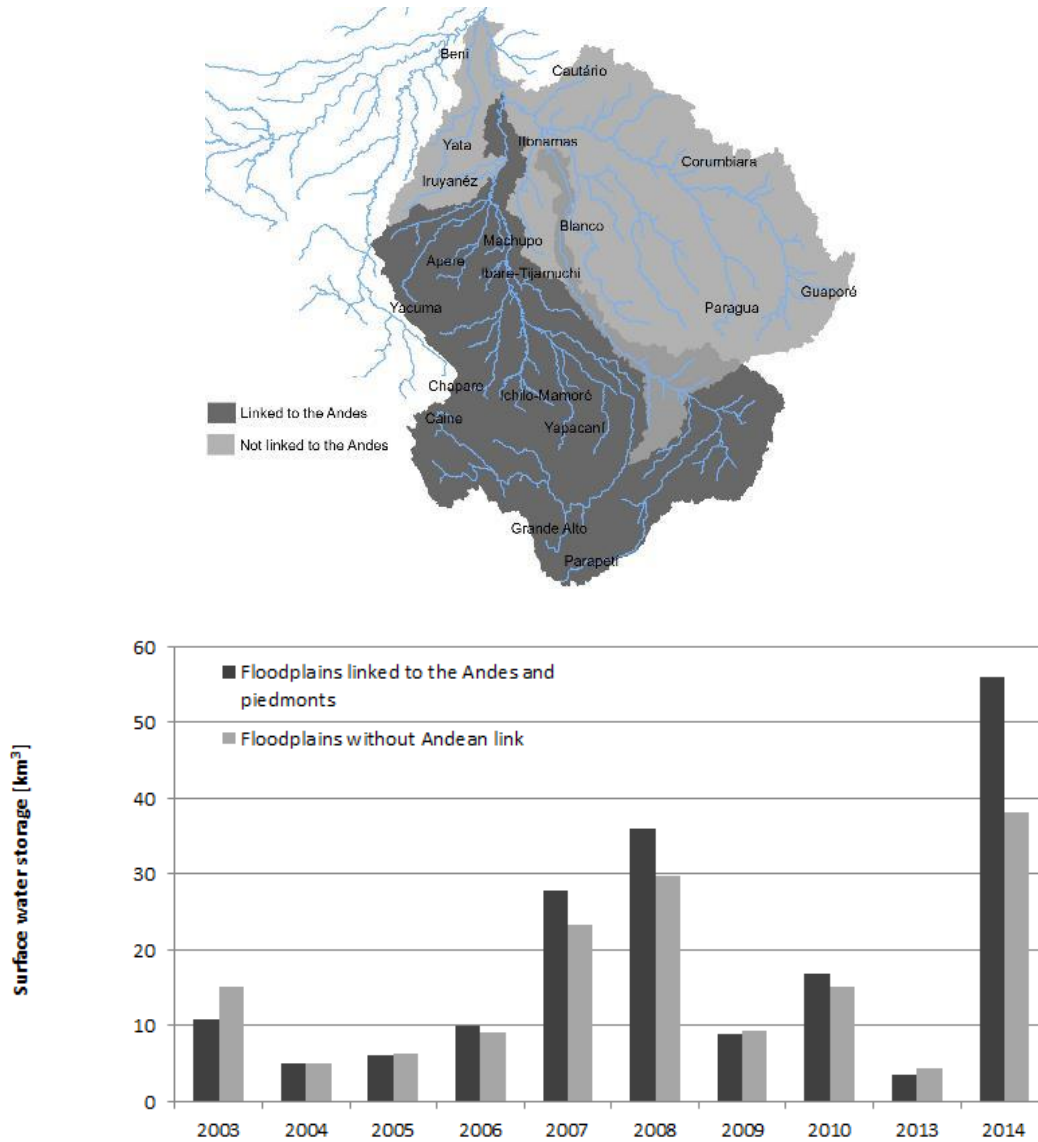
of surface water stored in the different basins (Figure 4.10) shows the relevance of both Andean-connected and Andes-independent floodplains. In most years, the stored surface water is distributed equitably in these basins, although during extreme events (2007, 2008 and 2014), the role of Andes-connected floodplains appears to be more relevant (Figure 4.1).

Figure 4.9 - Flooded area and surface water storage in floodplains during 2003-2014 period.



2001 and 2012 are missing since no altimetric data is available for these years.  
Source: by the author

Figure 4.10 - Contrast between flooded area and surface water storage in floodplains with and without Andean connection.



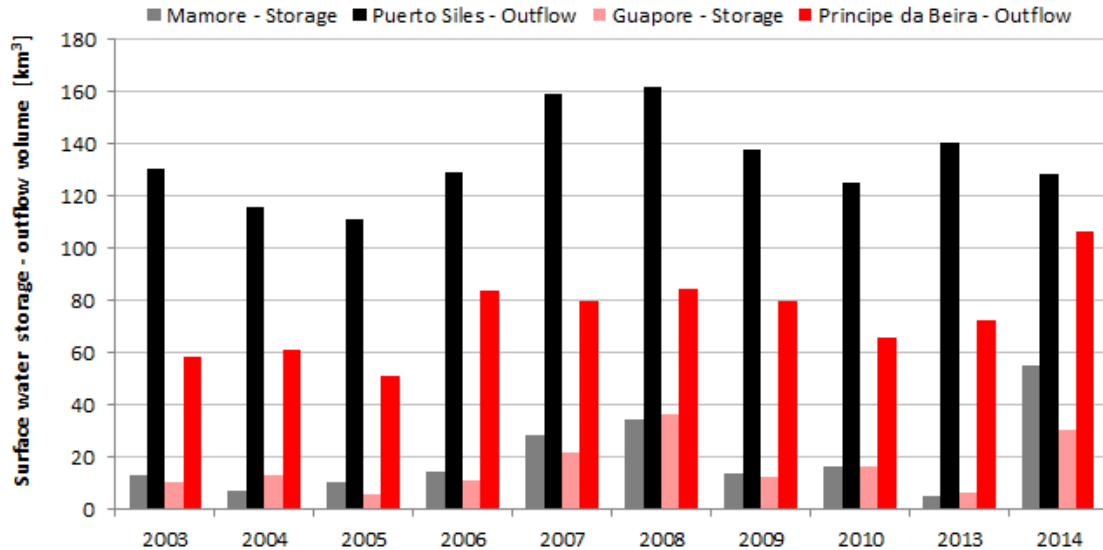
Source: by the author

When comparing the amount of surface water stored in floodplains during flood peaks against the total volume of water generated by the respective basin during the hydrological year, an initial quantification of the river-floodplains interactions could be provided in terms of the water volume that was stored and

drained. In the case of the Mamore Basin floodplain, the volumes range from 6% to 25% of the total volume discharged by the Mamoré at the Puerto Siles Station. In the case of the Guapore Basin, the volumes range from approximately 9% to 28% of the total volume discharged at the Principe da Beira Station (Figure 4.11). Unfortunately, the outflows for 2014 are incomplete because our streamflow time series ended in June 2014.

When considering that major flood events in the region are characterized by the superposition of flood waves in the main tributaries (as explained in Chapter 3), it becomes clear that the floodplains capacity for water storage is determinant for streamflow regulation. The timing and magnitude of the mean monthly discharges at Puerto Siles and Principe da Beira stations (Figure 3.15) illustrate about this, there is possible to visualize that, without floodplain storage, the hydrographs might have different patterns.

Figure 4.11 - Contrast between flooded area and surface water storage in floodplains with and without Andean connection.



Source: by the author

#### 4.4 Discussion and conclusions

Multi-temporal flood mapping has been used to estimate the distribution, extent and timing of floods as well as the surface water storage within different basins in the Bolivian Amazon wetlands. This type of information (Wittman et al., 2015) is important for delimiting the extent of floodplains and defining wetlands of interest for conservation, land use planning or management.

The flooded area was noticeably variable from year to year. The highest flood peaks in the Mamore Basin corresponded to the extreme flooding event in 2014, whereas in most of the tributaries of the Guapore, the flood peaks corresponded to flooding events in 2008 and 2006. The specific distribution of rainfall and the occurrence of rainfall anomalies in the different basins are influenced by the SST (sea surface temperature) in the equatorial Pacific and Atlantic, which determine the flood extent and timing in each of the subbasins (Molina 2017; Villar 2014, Ronchail 2005). The largest extent of flooding is observed in the Mamore Basin as well as the central Mamore and Andes-connected tributaries and the Itonamas and Blanco rivers within the Guapore Basin.

By combining multi-temporal flood maps and satellite altimetry, relevant features of the flood regime were assessed, and three groups with particular characteristics were identified.

The first group is composed of floodplains that are exposed to frequent floods and generally located in rivers without a direct connection with the Andes, such as the Guapore tributary rivers Blanco, San Martín, Iruyañez, and Yata. Seasonal floods are a result of sensu stricto endogenous processes, which may include overbank spilling of lowland tributaries. The rapid response at these sites may also indicate a good connection between the river channels and their floodplains. These characteristics make these sites vitally important to the habitats of many plant and animal species, which rely on regular floods

The second group can be considered representative of floodplains that are more dependent on exogenous processes, such as flood waves originating in

the Andean piedmont area, although they present a relatively fast response to endogenous processes, which is observed in certain floodplains located along the Ibare, Isiboro, and Yacuma rivers (with a contribution by the Andes piedmont) and the endogenous Iruyañez and Yata rivers.

The third group is representative of the floodplains along the Mamore and Yacuma rivers and characterized by occasional flooding, which is a result of flood waves from the Andes. Here, floods occur during extreme events, and high water depths are attained. These wetlands are of great significance when buffering the flood waves from the Andes and piedmont areas. These waves deposit important sediment loads on the floodplain.

A gradient of flood depths is observed along the north-south axis, and higher flood depths are expected at the junction of the Guapore and Mamore rivers at the outlet of the LM.

The amplitude of water stage variations in the rivers and their adjacent floodplains displays interesting features because of the frequency of flooding. Thus, sites with a dominance of endogenous or exogenous flooding processes can be distinguished. Nevertheless, only a few sites offer an opportunity to analyze the altimetric measurements of both river channels and their floodplains.

By combining multi-temporal flood maps and satellite altimetric time series, we were able to estimate the total amount of surface water stored in the floodplains as well as the water distribution within different basins. The total volume of surface water stored in the floodplains ranged from 10 km<sup>3</sup> to a maximum of 94 km<sup>3</sup>, which was observed during the massive event of 2014. Surface water storage estimates can be considered a preliminary method for quantifying the role of floodplains in streamflow regulation (when considering the maximum values) and determining the water demand required for wetlands to maintain a normal flood pulse that guarantees the wetlands' functionality (in the case of minimum and mean values). Previous water storage estimates are not available for this region; thus, comparisons could not be performed. However, the values

obtained here are on the same order of magnitude as those estimated by Alsdorf et al. (2010) for the Amazon central floodplain.

A gross estimate of the river-floodplain interactions could be obtained by comparing the amount of surface water stored in the floodplains during flood peaks against the total volume of water generated by the respective basins during the hydrological year. For the Mamore Basin, 25% of the total volume discharged to Puerto Siles Station was stored in its floodplains during extreme events, and for the Guapore Basin, approximately 28% of the total volume discharged at the Principe da Beira Station was stored in its floodplains.



## **5 TOWARDS INTEGRATING SPATIAL HYDROLOGY AND HYDROLOGICAL MODELING**

### **5.1 Introduction**

In this chapter, we analyzed the performance of the MHD-INPE model (Portuguese acronym of Modelo Hidrológico Distribuído) developed by the National Institute for Space Research (Portuguese acronym INPE) to simulate flooding dynamics of the wetlands. The floodplain routine of the model was parameterized using SRTM data and permanent water bodies defined from MODIS-M\*D09A1 estimated flooded areas. The model was implemented in the Madeira River for climate change studies (SIQUEIRA-JÚNIOR; TOMASELLA; RODRIGUEZ, 2015) for the period 1970-1990 and more recently for the period 2000-2014 (SIQUEIRA-JUNIOR et al., [s.d.]). The purpose of this chapter is to critically analyze the preliminary results of the model for the period 2001-2014 in the upper Madeira basin with focus on the ability of the hydrological model in simulating the wetlands dynamics and to explore how simulations can be improved using additional remote sensing techniques.

### **5.2 Methods**

#### **5.2.1 The MHD-INPE model**

The MHD-INPE was used to simulate streamflow and flood extent in the study area. The MHD-INPE, developed from the MGB-IPH model from the Institute of Hydraulic Research (Portuguese acronym IPH) of the University of Rio Grande do Sul (COLLISCHONN et al., 2007), is composed by grid cells, where every cell is constituted by different blocks which are a unique combination of land use, soil type, and vegetation cover. This concept, similar of the VIC model (LIANG et al., 1994) and the Hydrological Response Units (HRU) (KOUWEN et al., 1993), enables to reduce the number of parameters and input data demand. The hydrologic response of every block is computed independently, and then aggregated at grid level and routed to the river system using the Muskingum-

Cunge method (TAKEUCHI; AO; ISHIDAIRA, 1999). If necessary, specific routines for floodplain simulation are applied.

The MHD-INPE model include three soil layers: A first layer simulating the rapid response in form of subsurface flow: a second layer or “transmission zone” that accounts for the time delay between deep percolation and aquifer recharge and provides the necessary storage to sustain dry season evaporation; a third layer that accounts for baseflow and variable source area dynamics, accounting also for the amount of saturation overland flow. Evapotranspiration is estimated using the Penman Monteith method (MONTEITH, 1965). The MHD-INPE model combines a probabilistic distribution of water columns in a grid, as in (ZHAO, 1992), with the hydrological response principles of the TOPMODEL (BEVEN, 1997).

Further details of the MHD – INPE model water balance and propagation can be found at Rodriguez and Tomasella, (2016) and Siquiera-Júnior et al. (2015). We will describe in more detail the floodplain routine of the model since this component was used in the Bolivian Lowlands for the first time.

#### **5.2.1.1 Floodplain routine of the MHD-INPE model**

The MHD-INPE model represents the river-floodplain processes following the principles of a raster based floodplain simulation (BATES; DE ROO, 2000), where water flows between river channels and floodplains are simulated under a raster based scheme. Thus, simulation of floodplains consists in several differentiated processes: 1) water fluxes between floodplain cells, in the four cardinal directions; 2) fluxes between non-flooded fraction and flooded fraction within a floodplain cell, where the non-flooded fraction of a cell drains into a flooded fraction via surface, subsurface and groundwater flows; and 3) water fluxes between river channel and floodplains.

The model requires previous data preparation and analysis in order to determine the floodable cells where flows exchanges and storage are estimated. For every floodplain cell the following relations are required: i) The water storage volume (VFP) versus the mean water level (HFP); and ii) The

flooded area (AFP) versus VFP. This information can be derived from a Digital Elevation Model (DEM), with finer resolution than the model's grid discretization, by prescribing arbitrary values of water level HFP and calculating the correspondent flooded area AFP and the volume VFP by integration.

Water level in river channels and floodplains, and its fluctuations, are determinant for the water fluxes between them, as represented schematically in figures xx and xx). The floodplain flow is estimated for all interconnected floodable cells (a floodable cell and its four neighbors). The flow between floodplain cells (QFP) is calculated by the following equation, adapted from Bates and De Roo (2000):

$$QFP_{i+1,j}^{t+1} = \pm \frac{QFP_{i+1,j}^t - g(HFP_{i,j}^t - HFP_{i+1,j}^t)h_{flow}^t FW_{fp} \Delta t_{fp}}{1 + \frac{gn_{fp}^2 \Delta t_{fp} |QFP_{i+1,j}^t|}{FW_{fp} \Delta x (h_{flow}^t)^{10/3}}} \quad (5.1)$$

Where:  $QFP$  is the flow between floodplain cell  $i+1, j$  in the time  $t$ ;  $HFP$  is the mean water level in a cell,  $g$  is gravity;  $FW_{fp}$  is the width factor, defined as the relationship between the width of the breach overtopping the floodplain cell  $b_x$  and the total cell side  $\Delta x$  (Equation 2);  $h_{flow}^t$  is the parameter defined as the difference between the highest water level of the two elements ( $HFP_{i+1, j}$  or  $HFP_{i, j}$ ) and the minimum water level at which the floodplains overflow their banks ( $ZTRA_{i+1, j}$  or  $ZTRA_{i, j}$ ) (Equation 2); and  $n$  is the Manning coefficient.

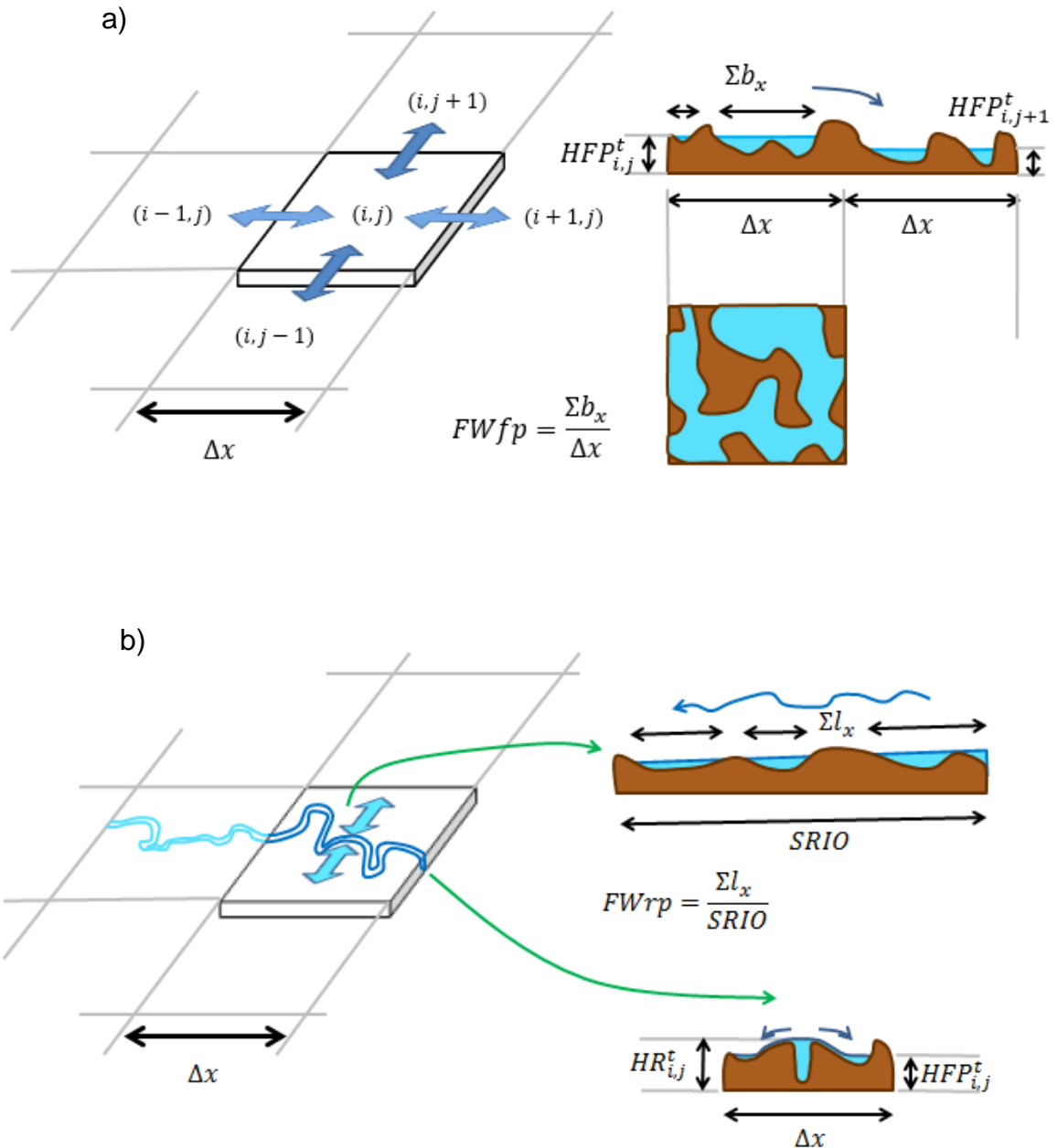
$$FW_{fp} = \frac{\sum b_x}{\Delta x} \quad (5.2)$$

$$h_{flow}^t = \max(HFP_{i+1,j}^t, HFP_{i,j}^t) - \max(ZTRA_{i+1,j}, ZTRA_{i,j}) \quad (5.3)$$

The floodplain overflow water level (ZTRA) indicates when the cell is hydraulically isolated and changes in water volume stored in the cell occurred

only due to precipitation and evaporation, the width factor  $FW_{fp}$  is a key calibration parameter.

Figure 5.1 – a) Schematic representation of water flow between floodplain cells; b) and between river channel and floodplain.



Source: Rodriguez and Tomasella, (2016) and Siquiera-Júnior et al. (2015)

The flow between the river channel and a floodplain cell (QRP) is calculated by

$$QRP_{i+1,j}^{t+1} = \pm \frac{QRP_{i+1,j}^t - g GRAD^t h_{flow}^t FW_{rp} \Delta t_{fp}}{1 + \frac{gn_{fp}^2 \Delta t_{fp} |QRP_{i,j}^t|}{2FW_{rp} SRIO (h_{flow}^t)^{10/3}}} \quad (5.4)$$

Where:  $QRP$  is the flow between the river channel and the floodplain cell  $i+1, j$  in the time  $t$ ;  $g$  is gravity;  $GRAD^t$  is the difference between the river stage  $HR$ , or the water level at which the river overtop its banks,  $ZTRA$ , minus the mean floodplain water level  $HFP$  or the floodplain overflow water level  $ZTRA$  (Equation 5);  $FW_{rp}$  is the width factor, defined as the relation between width of the river-floodplain breach  $l_x$  and the total river length within a cell  $SRIO$  (equation 6);  $h_{flow}^t$  is the parameter defined as the difference between the highest water level either in floodplain or river ( $HR i, j$  or  $HFP i, j$ ) and the floodplain overflow water level ( $ZTRA i, j$ ), (Equation 7); and  $n$  is the Manning coefficient.

$$GRAD^t = \max(HR_{i,j}^t, ZTRA_{i,j}^t) - \max(HFP_{i,j}^t, ZTRA_{i,j}^t) \quad (5.5)$$

$$FW_{rp} = \frac{\sum l_x}{SRIO} \quad (5.6)$$

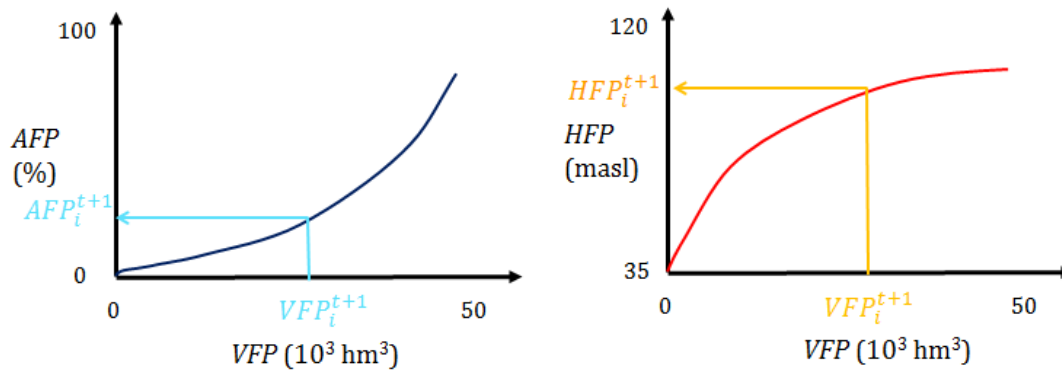
$$h_{flow}^t = \max(HRT_{i,j}^t, HFP_{i,j}^t) - ZTRA_{i,j} \quad (5.7)$$

In this case the  $FW_{rp}$  is also a key parameter to be calibrated

The water level  $HR$  at each river cell is estimated by the streamflow propagation method: if the water stage in the river is lower than the floodplain overflow water level  $HFP$ , then floodplain drain water into a river. Conversely, when water stage at the river is higher than floodplain overflow water level, water flows from the river to the floodplain.

The water balance in terms of volume and the total flooded area for each floodable cell  $(i,j)$  is estimated in every the time step  $t$  (Figure 5,2). The water storage volume in every cell is updated in every time step, as a function of water flows between floodplain cells and the river (Equation 5.7). With this, the calculation of other hydrological process, like runoff, evapotranspiration and moisture uptake, as a result of flood extent variation, is updated every time step (Equation 5.8). With this, the variation of water and energy budget as a result of flood extent variation is included in the simulation

Figure 5.2 – Schematic relationship between volume VFP, area AFP and water stage HFP within a model cell.



Source: Rodriguez and Tomasella, (2016) and Siquiera-Júnior et al. (2015)

$$VPF_i^{t+1} = VPF_i^t + \Delta t_{FP} (\pm QFP_{i+1,j}^{t+1} + \pm QFP_{i,j+1}^{t+1} \pm QFP_{i-1,j}^{t+1} \pm QFP_{i,j-1}^{t+1} \pm QRP_{i,j}^{t+1}) \quad (5.7)$$

$$VPF_i^{t+2} = VPF_i^{t+1} + \Delta t_{MHD} \frac{AFP_i^{t+1}}{100} ACEL_i (PRE_i^{t+1} - EO_i^{t+1}) \quad (5.8)$$

Where  $ACEL$  is cell area;  $PRE$  is precipitation and  $EO$  is evaporation

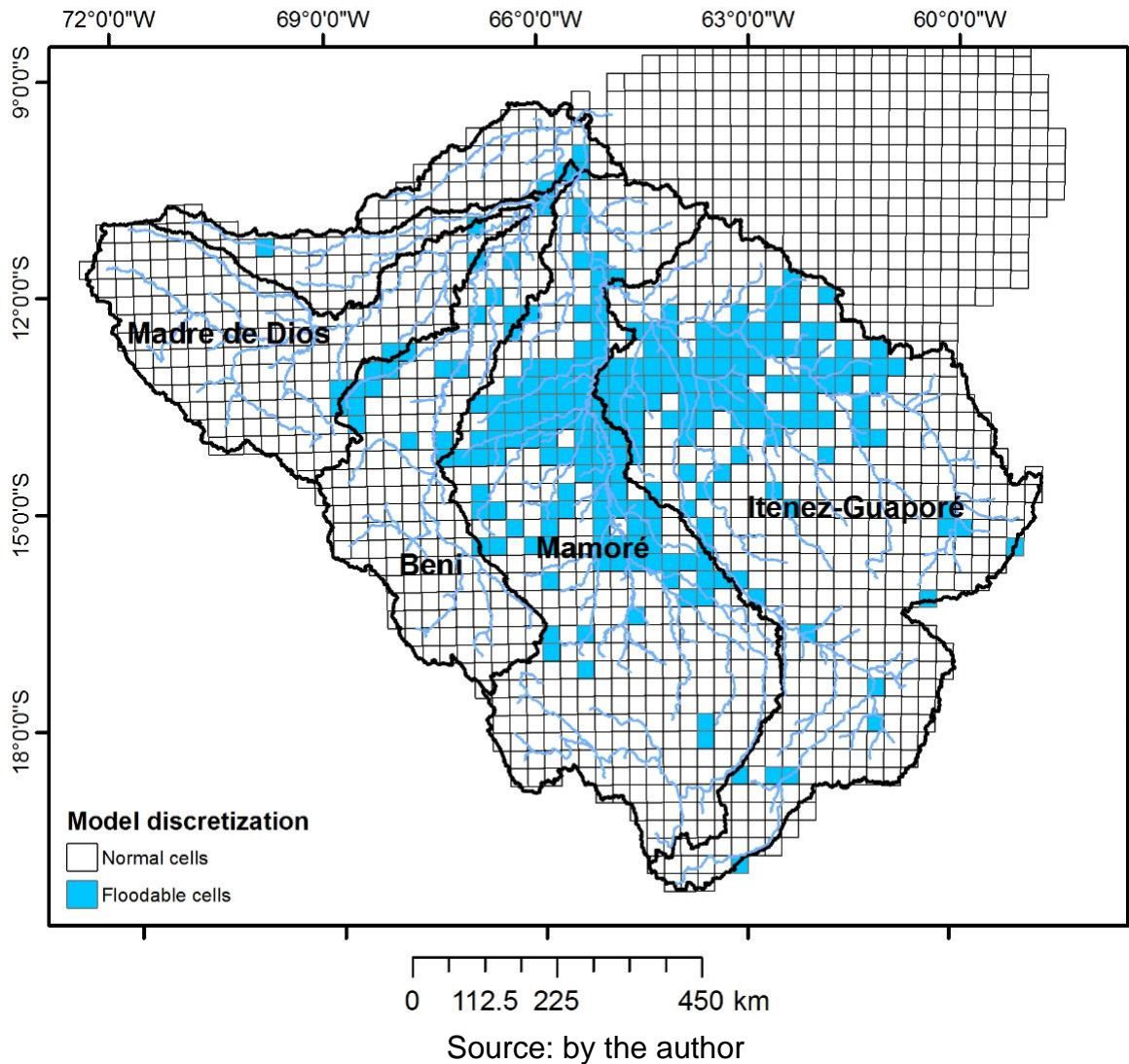
### 5.2.2 Model parameterization

Model parameterization based on remote sensing information (multitemporal flood maps) were employed: Initially, the floodplain component of the MHD-INPE model requires the definition of the floodable cells in order to execute the floodplain routines. In this cells, differentiated estimations of vertical processes as well as river–floodplain and floodplain-floodplain interactions are performed; Additionally, the minimum flooded area that the model employ as a threshold for water fluxes between floodplain cells takes place; and finally the relationships between flooded area, volume and water level.

As explained before, a Digital Elevation Model (DEM), with finer resolution than the model's grid discretization, allows estimating the required relations between VPF, AFP and HFP, in this case the MHD-INPE model employs the SRTM-DEM with 90m resolution (JARVIS et al., 2008).

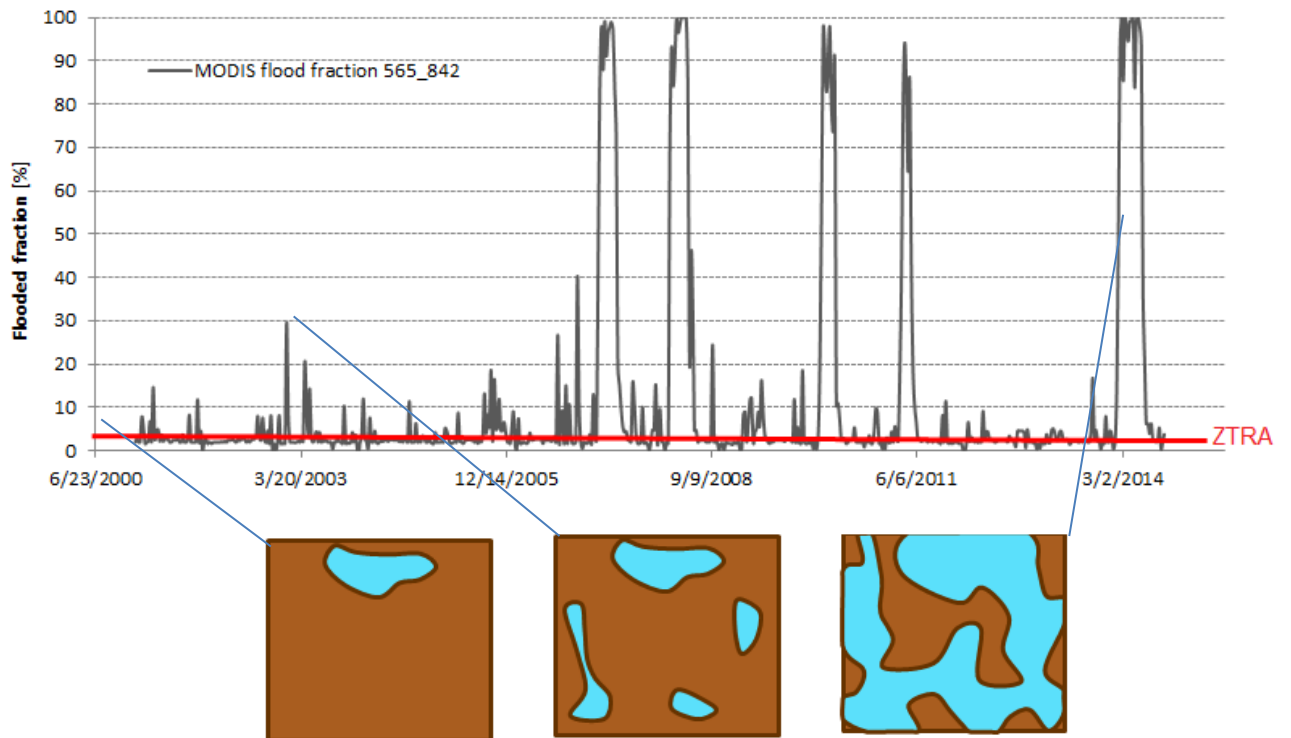
The flood estimates for the 2001-2014 period, derived from MODIS - M\*D09A1 images, for every MHD-INPE model cell grid, were employed as a main input for defining floodable cells in the study area. A threshold of 2% of the flood frequency value were applied to differentiate floodable cells from others, meaning that cells with less than 2% of the time during 2001-2014 were considered as non-floodable (Figure 5.3). Flooded areas were estimated over the grid-cells. To achieve this, two main procedures were done using GIS software: i) Spatial interception between vector files representing the model grid discretization and the polygons (results from the segmentation over radar mosaics), in which the classification were based (details are given in section 3.1.2); and ii) the calculation of the total flooded area for every time step within every grid cell and the flood frequency.

Figure 5.3 - MHD-INPE model cell grid discretization



The flood extension for every grid cell, expressed in percentage of flooded area, was employed for defining what is called in MHD-INPE terminology as *ZTRA*, which, as exposed before, is the threshold level that limits the hydraulic connection of the cell with its floodplain neighbors or with the river. These values were inserted in Floodplain.hig file (Figure 5.4).

Figure 5.4 - Estimation of the flooded fraction for a model grid cell (25 km).



Source: by the author

### 5.2.3 Water stage and flood extent

Since hydrologic and hydrodynamic models in wetlands heavily rely on DEMs to simulate floodplain dynamics and SRTM data is the main source of topographic data in ongoing models applied in the region (PAIVA et al., 2013b; SIQUEIRA-JÚNIOR; TOMASELLA; RODRIGUEZ, 2015). We compared the relationship between flooded areas and water stage derived from SRTM DEM and MODIS/Altimetric water stage. As explained in section 5.1.1, the MHD-INPE model employs a predefined water stage – elevation curve, with this curve (called Floodplain.hig in the MHD\_INPE model terminology) the model estimates the flood extension and water volume within a grid cell at every time step as a function of the water stage. Thus, these volumetric relations estimated from the DEM (SRTM) in this case, are of big relevance for the model performance during the whole simulation. By comparing these water stage-flood extents estimates with independent data sets, in this case MODIS derived

flood maps and satellite altimetry water stages, we intend to have an initial evaluation of the differences between them, and consequently, the potential sources of uncertainty that are inherent to the model when using SRTM derived DEM.

Envisat and SARAL altimetric water stage time series, which commonly are expressed as ellipsoidal heights referred to the ellipsoids WGS 84 and Topex respectively, were transformed into EGM 96 orthogonal heights, using the procedures described in (RAPP, 1982), in order to make them fully comparable with the SRTM derived water stage – flood extent curves.

#### 5.2.4 Model evaluation/validation

The model performance in terms of streamflow estimates were assessed by comparing modeled and observed data according to the recommendations of Moriasi et al., (2007), who suggested a combination of three quantitative statistics, Nash Sutcliffe efficiency (NSE), percent bias (PBIAS) and ratio of the root mean square error to the standard deviation of measured data (RSR) to evaluate the model. NSE (NASH; SUTCLIFFE, 1970) is a normalized statistic that determines the relative magnitude of the residual variance compared to the measured data variance, which indicates the fit between observed and simulated data, and is calculated by the equation 5.9. PBIAS (GUPTA; SOROOSHIAN; YAPO, 1999) is a measure of the average tendency of the simulated data to be larger or smaller than observations, and is estimated by using the equation 5.10. RSR is a standardized root mean square error by using the observation standard deviation (LEGATES; MCCABE, 1999), and is calculated by using equation 5.11.

$$NSE = 1 - \left[ \frac{\sum_{i=1}^n (Y_i^{obs} - Y_i^{sim})^2}{\sum_{i=1}^n (Y_i^{obs} - Y_{mean})^2} \right] \quad (5.9)$$

$$PBIAS = \left[ \frac{\sum_{i=1}^n (Y_i^{obs} - Y_i^{sim}) * 100}{\sum_{i=1}^n (Y_i^{obs})} \right] \quad (5.10)$$

$$RSR = \frac{RMSE}{STDEV_{obs}} = \frac{\left[ \sqrt{\sum_{i=1}^n (Y_i^{obs} - Y_i^{sim})^2} \right]}{\left[ \sqrt{\sum_{i=1}^n (Y_i^{obs} - Y^{mean})^2} \right]} \quad (5.11)$$

Where  $Y_i^{obs}$  is the  $i$ th observation;  $Y_i^{sim}$  is the  $i$ th simulated value;  $Y^{mean}$  is the mean of the observed data; and  $n$  is the total number of observations.

Complementarily, total flood extension estimated by the model was compared with those estimations from multitemporal flood maps. These estimates were assessed in terms of model accuracy (F) (equation 5.12) and bias (BIAS - equation 5.10). These metrics were employed in evaluating model performance in simulating floodplains (HORRITT; BATES, 2001; RUDORFF; MELACK; BATES, 2014):

$$F = 1 - \left( \frac{b+c}{a} \right) * 100 \quad (5.12)$$

Where  $a$  is the total area that was mapped and estimated by the model as flooded;  $b$  is the predicted but not mapped flooded area; and  $c$  is the mapped but not predicted inundated area. For the calculation of BIAS, in equation 5.10,  $Y_i^{obs}$  represents the  $i$ th mapped inundation and  $Y_i^{sim}$  the  $i$ th simulated inundation.

In the next sections we present the results of the model after adjusting the Floodplain.hig input file with information from the multitemporal flood maps.

## 5.3 Results

### 5.3.1 Discharge and flooded area

The statistics for monthly streamflow simulated by the MHD model are enough accurate for all the gauging sites. Values of NSE PBIAS and RSR fit the thresholds proposed by Moriassi et al., (2007), as statistics of an acceptable model performance. In table xx these statistics are summarized showing also the effect of floodplain adjustments in the model performance.

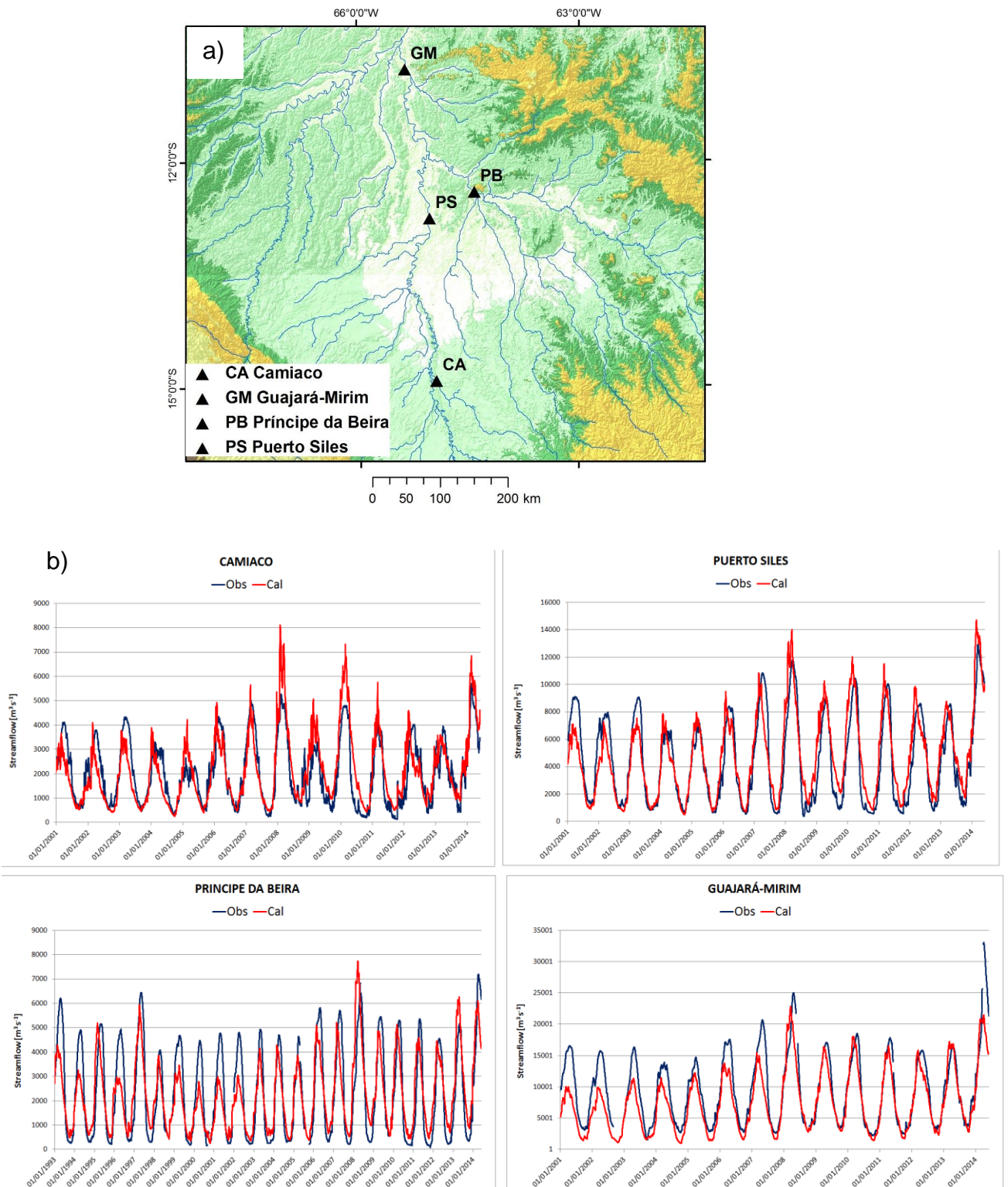
Table 5.1 - Model performance expressed in NSE, RSR and PBIAS.

Criteria	Puerto Siles	Principe da Beira	Camiaco	Guayaramerin	Best combination (Moriassi et al., 2007)
NSE	0.82	0.77	0.74	0.80	0.50
RSR	0.42	0.48	0.51	0.45	0.70
PBIAS	-14.83	-9.76	-13.81	11.92	+25.00

Source: by the author

Overestimates of streamflow, mainly at Puerto Siles and Camiaco gauging stations, coincide with underestimations of total flooded area during 2007, 2008 and 2014, showing the model limitations in generating, maintaining or transmitting water into floodplains in the zone between Camiaco and Puerto Siles during high flood events. Streamflow simulations at Principe da Beira, reflects the model performance for the Guapore River while comparisons at Guajara-Mirim reflects the behavior of the Beni River (Figure 5.5). In both sites the model underestimates are more significant than overestimates with no clear impacts in flood estimates

Figure 5.5 - Modeled and observed streamflow in 4 sites within the study area.

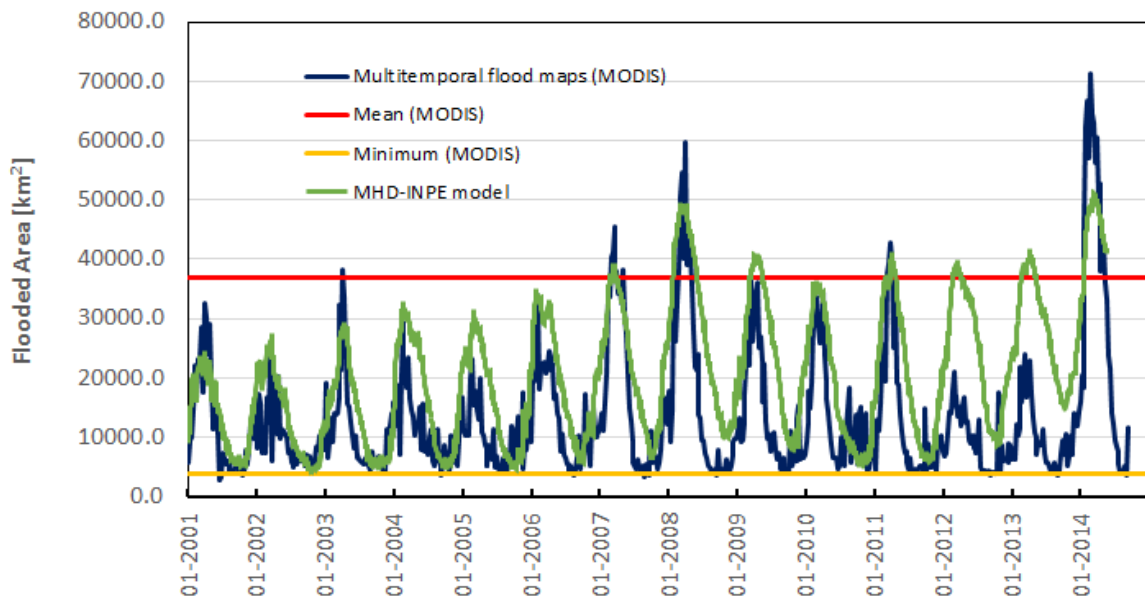


a) Location of gauging stations; b) Comparison between modeled (red lines) and observed streamflow (blue lines).

Source: by the author

Results of the MHD model in terms of flooded area both for the whole basin and at grid cell level are encouraging. In terms of interannual variation, the model is able to capture both the seasonality and magnitude of flood events. However, the recession limbs show slower declines for the model during some years and model overestimates of flood peaks for normal years while noticeable underestimates during extreme events (2003, 2007, 2008 and 2014) (Figure 5.6).

Figure 5.6 - Comparison between total flooded areas estimated by the MHD-INPE model and mapped with MODIS MOD09A1 data.

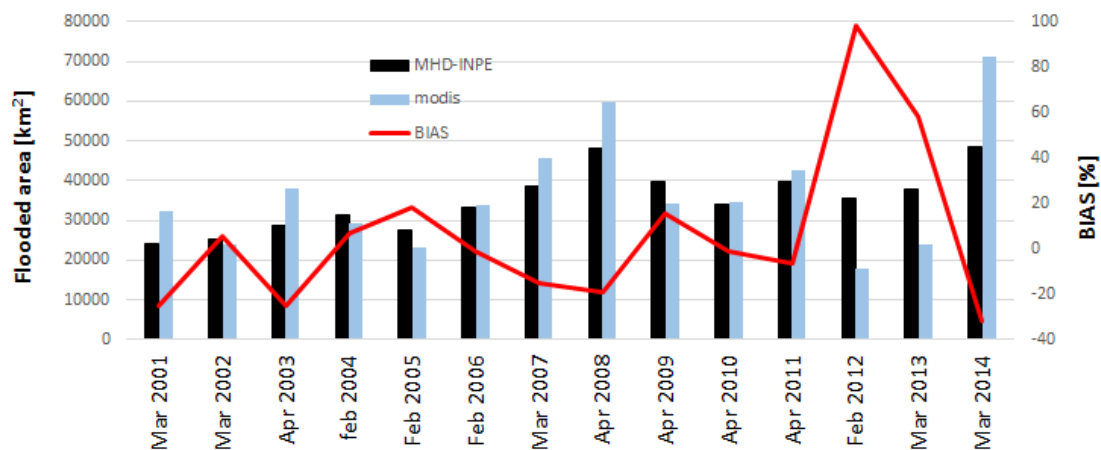


Source: by the author

The model BIAS during flood peaks shows both underestimates and overestimates during the time series. Underestimates, ranging from -1% to -31%, of total flood extent occurs during 8 of the 14 years, in particularly during extreme flood events, while during 6 years overestimates range from +5% to +97%. Excluding the noticeable high overestimates in 2012 and 2013, the model represents floods during normal years with a BIAS +5 to +18% (Figure 5.7). High values of model efficiency  $F$ , up to 98%, are reported for 2006 and 2010, with a mean  $F$  value of 71% for the entire time series. With this, it is possible to conclude that, under this configuration, the model has constraints for simulating extreme events, the higher the magnitude the less model

performance. Especial cases as those of the 2012 and 2013 require deeper analysis.

Figure 5.7 - Estimates of total flooded area by the MHD-INPE model and mapped with MODIS-MOD09A1 during flood peaks.



MHD-Model estimates during flood peaks (back bars), MODIS estimates (blue bars) and model BIAS (red line).  
Source: by the author

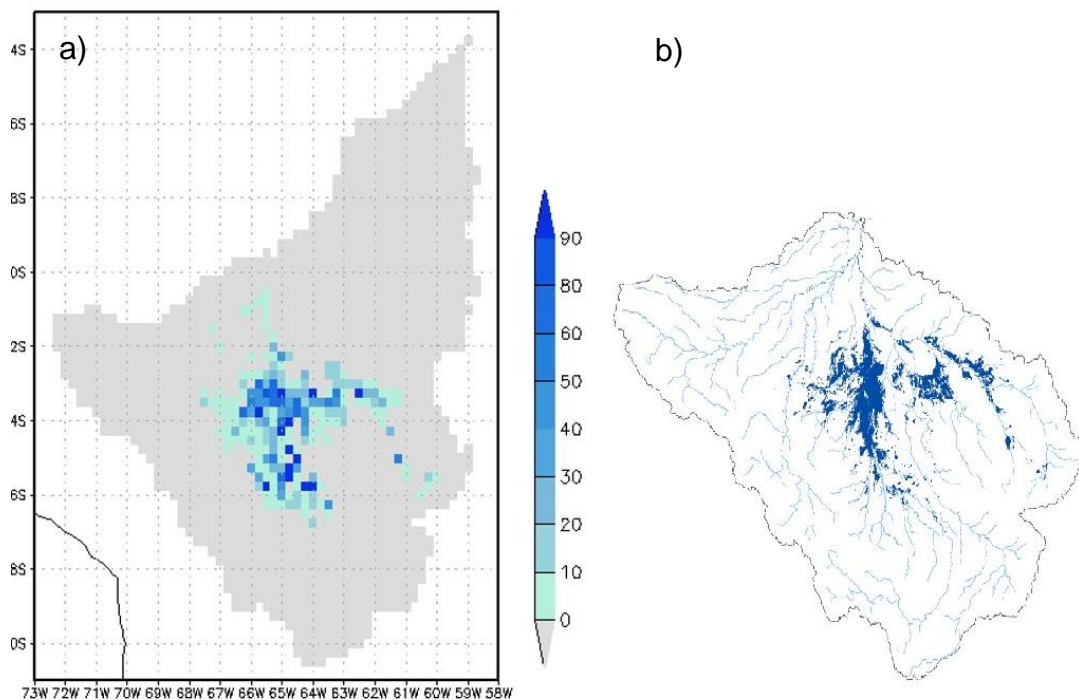
### 5.3.2 Differences between modeled and remote sensing derived flood estimations at cell grid level

As expected, the model has restrictions in the spatial representation of floods as a consequence of the inherent aggregation of flood estimations in a grid-cell of 25 km (Figure 5.8). This is an initial point for understanding differences in modeled and mapped flood extents. Although the floodplains in the study area are predominantly savannas, they present a great complexity derived from diverse factors such as the presence of paleo rivers, gallery forest, forest islands, earth works from ancient cultures and varzeas (forested floodplains) among others. It is also important to highlight that the model estimates the percentage of flooded area inside each cell, not the exact location of floods. In fact, the flooding process is much more complex occurring non-uniformly within a floodplain, as a response of diffuse or channelized water flows (BONNET et al., 2008; RUDORFF; MELACK; BATES, 2014). Thus, when comparing the relations between water stages vs. MODIS flood extensions, and their similar

obtained from a DEM (SRTM in this case), it is possible to distinguish significant differences with direct impacts on hydrological modeling.

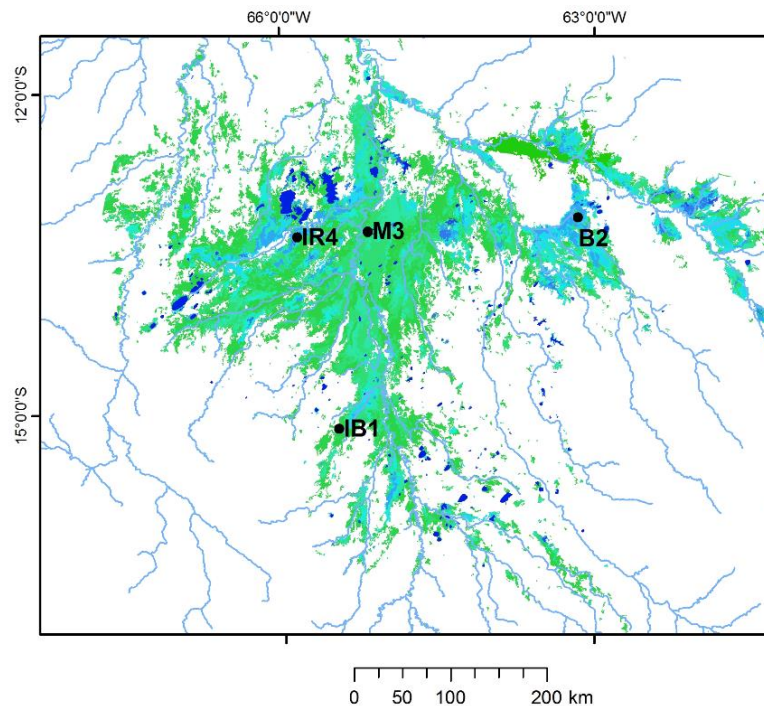
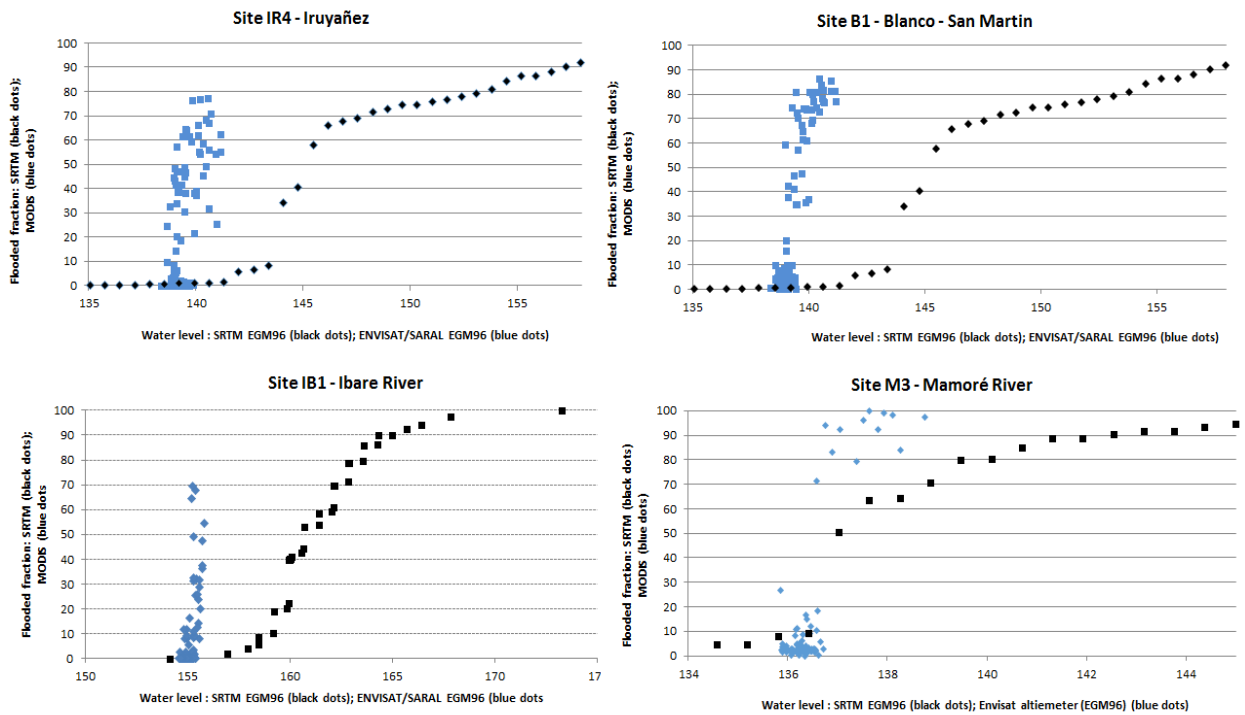
Figure 5.9 shows the flooded fraction as a function of water level derived from SRTM DEM and the flooded fraction estimated from MODIS M\*D09A1 as a function of altimetric data. The steeper slope of the altimetry-MODIS curves indicates that small variations in water stage imply a rapid increase in flood extension, in other words, a more sensitive behavior to variations in water stage (Figure 5.9). Relationships based on SRTM DEM revealed a more gradual variation of flooded areas against altitude, suggesting that SRTM results smooth the topographic variations. In other words the model, based on SRTM DEM, requires much more water volume to reflect water fraction variations within a cell. This has implication in both flood extent and streamflow estimations.

Figure 5.8 – Spatial representation of flooded areas as estimated by the MHD-INPE model and by MODIS MOD09A1 data.



a) Spatial representation of the flood during 22/03/2007 as estimated by the MHD-INPE model; and b) and mapped from MOD09A1 images.  
Source: by the author

Figure 5.9 - Flooded fraction as a function of water stage based in SRTM and satellite altimetry in different sites.



a) Flooded fraction as a function of water stage based in SRTM (black dots) and satellite altimetry/MODIS (blue dots) in different sites; and b) location of the different sites.

Source: by the author

It might be argued that the comparison has limitations due to the fact that the relationship based on satellite altimetry include hydrodynamic effects on the water table, while the relationship based on SRTM is based on a purely kinematic approach. However, considering that river slopes are very low in the area and that the altimetry stations average water stage values over a swath of about 0.5 to 3 km, it follows that inertial effects cannot explain the large differences detected in Figure 5.9.

Also, it is important to take into account the sources of uncertainty in the data that we are comparing. In the case of a SRTM DEM, the most commonly used input for representing topography in large-scale hydrologic models, errors that compromise the flood simulation in floodplains are mainly vegetation artifacts and errors due to interferometric baseline. The influence of dense vegetated areas (known as vegetation artifacts), which comes from the inability of the C band to penetrate dense canopies, implies a difference of about 22.4 m between SRTM and ground elevation, as estimated for the Amazon by Carabajal and Harding (2006), who compared SRTM with ground elevation obtained from laser altimeter (Geoscience Laser Altimeter System - GLAS) on board the ICESat satellite. Errors in the interferometric baseline are referred to averaged errors of about  $\pm 10$  m due to residual motion errors in the interferometric baseline (CARABAJAL; HARDING, 2006). In the case of the MODIS derived multitemporal flood maps, sources of uncertainties are mainly underestimates of flood under dense canopies and variations on the time series due to cloud cover that limits the capture of flood in several time steps (details of both are discussed in section 3.2.2). Regarding errors in satellite altimetry water stage time series, we can mention the inherent errors of the processing algorithms (Ice2), that may imply errors of about 0,55 m (Envisat- RA) and 0,36 m in SARAL-AliKa and errors due to data selection within floodplains in which, unlike rivers and permanent water bodies, we have noticed the effects of vegetation stages and soils moisture content.

These differences and the inherent uncertainties in the data sets illustrate how challenging is integrating flood extent and water stage estimations, from MODIS and satellite altimetry respectively, into hydrologic or hydrodynamic models for

floodplain simulation. To obtain a seamless SRTM DEM, suitable for modeling, appears to be the most obvious first step; however, it is not a simple task and requires a proper characterization of vegetation and estimations of the bias due to interferometric base (BAUGH et al., 2013; RUDORFF; MELACK; BATES, 2014). An overall view of SRTM DEM pretreatment, for representing floodplains accurately, that involves the use of echo sounding tracks for detecting and correcting interferometric bias and vegetation mapping for correcting vegetation artifacts can be found in Rudorff et al. (2014). Corrections and preparation of water extent and water stage time series might require also several steps in function of the integration method.

An option to optimize the MHD-INPE model with flood extent and water stage information from remote sensing techniques, is to construct an alternative Floodplain.hig file replacing the SRTM based water stage – flood extent curve with other based on satellite altimetry and MODIS derived flood extent (Figure 5,9 ); But, as shown in Figure 4.1, the generation of such a curves is limited to those model grid cells that coincides with the satellite track. Thus, the use of flood extent information, which is available for every grid-cell in the model, seems to be more suitable.

#### **5.4 Discussion and conclusions**

As shown in previous sections it is possible to achieve acceptable model improvements even with few adjustments based on multitemporal flood mapping. In this case by setting the values of the floodplain overflow water level (ZTRA), which could be considered a step more than a simple model evaluation by using remote sensing information, but not meaning a sophisticated data assimilation by the model.

The use of long time series of flood maps, with 8-day time step, that reflects both interannual and seasonal variations in flood extension, might be pointed as a factor of relevance that allowed obtaining this model improvement and a robust evaluation of the model performance under different flood regimes. It is worth to highlight that, as explained by Schuman et al. (2016), early efforts in integrating remote sensing information and numerical models were restricted to

the use of dual season wet/dry maps, which had constrained the possibilities of integrating these two information sources.

Although acceptable statistics for streamflow data calibration were obtained, it does not necessarily mean that flood estimations are being represented well. We had found limitations of the MHD-INPE model in estimating flood extent during extreme events, an underestimates of about -15% to -30%, that might hinder the model application for studying extreme events. However, according to the comparisons between flood extent as a function of SRTM DEM and altimetric information, we found that the model might be using extra water volume to reflect water fraction variations within a cell, which have strong implication in both flood extent and streamflow estimations. Therefore, a more accurate representation of the relationship between water level, flooded area and store volume within the floodplain cells should have a huge impact within the MHD-INPE simulations. Figure 5,9 indicates that the cell flooded are is quite sensitive to small variation of water level in the case of the relationship determined by the altimetric data, while SRTM-based relationships require larger variations in water levels to induce the same variation in flooded areas. These differences in behavior can explain why the integrated flooded simulation by the MHD-INPE model (figure 5.6) failed to simulate the sharp variations of flooded areas derived from MODIS.

As explained in section 5.3.1, the complex characteristics of the Llanos de Moxos in terms of vegetation and topography, together with the uncertainties in the SRTM-DEM, constitute the main sources for uncertainties in floodplains routines. These also constrain the assimilation of remote sensing data in a more sophisticated way. Assimilation of flood extent following e temporal resolution of the flood maps (8-day) seems to be feasible, but in that case the model would be totally dependent of flood extension information and thus limited to run for the same period as the multitemporal flood maps. An alternative to tackle this limitation is the use of satellite altimetry and flood maps to modify/edit the relations between water stage and flood extension, synthetized in a Floodplain.hig file (correcting the curve as in Figure 5.9). Nevertheless, since there is not a satellite altimetry time series of every

floodable cell in the model (due to the satellite track coverage limitations – Figure 4,1), this option requires previous analysis for assuming representative curves for all the floodplain cells.

Although the assimilation of altimetric water stage information in river channels had been implemented successfully in hydrologic-hydrodynamic models in the region (PAIVA et al., 2013), the complementary use of water stage information within floodplains still deserves further research. This study constitutes an example of the usefulness of remote sensing information for improving numerical modeling in wetlands. It provides relevant information regarding the challenges and limitations in using altimetric water stage in floodplains.



## 6 GENERAL DISCUSSION AND CONCLUSIONS

### 6.1 About the methods

#### 6.1.1 Multitemporal flood mapping

The combination of optical and microwave remote sensing systems provided the means for the first 15-years mapping, in the region. Firstly, the use of 9 ALOS PALSAR mosaics, with 100 m resolution, for different hydrologic regimes provided the means for performing a robust segmentation, which constitutes the base geometry for the classification of 2248 MODIS M\*D09A1 images. The direct use of MODIS-M\*D09A1 images for segmentation is constrained by the presence of clouds during most of the wet season and its coarser resolution of M\*D09A1 images (500 m). Secondly, by using an OBIA approach, which implies the assumption that a determined satellite signal within a polygon (segment) is representative for its area, together with the use of two images in every time step (MOD09A Terra –morning pass- and MYD09A Aqua -evening pass), the effect of cloud cover was tackled by expanding the possibilities of capturing useful pixel information. In this study we adopt the Multiresolution segmentation method using the thresholds 0.4 and 0.8 (shape and resolution) in order to have a manageable number of resultant polygons on which apply the classification algorithms. Further research is recommended in order to specifically evaluate other segmentation methods.

Parallel classification of ALOS PALSAR images also allowed improving the performance of MODIS classification algorithms and estimating the inability of M\*D09A1 images to capture flood under dense forest. It was calculated an underestimate of about -20% of the total flooded area, mainly corresponding to flooded forest in the Guapore Basin.

The segmentation was done using the original M\*D09A1 coordinate system (Sinusoidal), it allowed to access and process M\*D09A1 images directly in its original format (.hdf), saving lots of memory space of preprocessing products and may be a starting point for a near real time processing system.

### **6.1.2 Satellite altimetry in floodplains**

This study constitutes one of the few examples to explicitly use satellite altimetry within large floodplains in the Amazon. Our results show that, despite the complexity of wetlands in terms of vegetation and soils, determined by the seasonal presence of floodwaters, it was possible to capture relevant characteristics based on water stage variations along the hydrological cycle and along a time slot of about 15 years.

Unlike river channels, floodplains became dry during some months or even years, so the altimetric signal under these circumstances is highly influenced by floodplain vegetation, in their different stages, and by soil moisture content. This made difficult to determine reference values of the floodplain bottom. To tackle this, we adopted a bottom value based in the visual analysis of the altimetric time series. This topic deserves further analysis and, probably the complementary use of other sensors, or techniques, in order to establish a referential floodplain bottom value.

The bias adjustments allowed to constructing continue time series combining both ENVISAT RA2 and SARAL AltiKa data. This task was based in previous studies (CALMANT et al., 2013; SANTOS DA SILVA et al., 2015a, 2015b), which were conducted primarily over rivers. Thus, specific studies of altimetric biases over floodplains in the area are highly recommended.

Since the opportunity to obtain altimetric time series for the different floodplains in the study area was limited to the ENVISAT – SARAL satellite tracks, it is recommended to explore the feasibility to, complementarily, use altimetry data from other missions like JASON. It would expand the possibilities for integrating satellite altimetry and numerical models and to have a better coverage of altimetric information over the study area.

### **6.1.3 Multi-temporal flood maps and satellite altimetry**

As exposed, the combination of satellite altimetry data (ENVISAT-RA2 and SARAL- AltiKa) and multitemporal flood maps derived from MODIS - M\*D09A1 data, provided the means for estimating the floodplains capacity, and role, for

storing surface water during different hydrological regimes. Nevertheless, there are some aspects to be taken into account in future experiences in this topic: Firstly, the time step of the altimetric time series (35 days in this case) do not fully guarantee the capture of maximum flood stage, while flood maps, with 8-day time step, have more chance. Then, for estimating the water depth for certain flood map data it was necessary to assume the information from the closer in time flood stage record. Secondly, flood depth estimations for all the flooded areas rely on previous interpolation of altimetric time series. Thus, accurate volumetric estimations may be achieved in function of both a better coverage of altimetric data and the selection of a proper interpolation method.

#### **6.1.4 Integrating remote sensing and hydrological modeling**

We had provided a relevant example of the usefulness of remote sensing information for improving numerical modeling in wetlands while identifying the main constraints and challenges. We had pointed the use of long time series of flood maps, with 8-day time step, that reflects both interannual and seasonal variations in flood extension, as a factor of relevance that allowed obtaining this model optimization and a robust evaluation of the model performance under different flood regimes. Although satisfactory results have been achieved in terms of calibration with streamflow data, flood estimations have considerable biases and the model is unable to simulate satisfactorily extreme flood events.

By comparing different relations between water stage and flood extension derived from the SRTM-DEM with an independent data set, formed by satellite altimetry data and multitemporal flood maps, it was identified that the main constraints for floodplain simulation are those inherent to the SRTM-DEM. Further research is required to fully understand these limitations and to assess possible effects of finer model resolution, pre-treatment of SRTM-DEM for correcting the floodplain geometry.

## 6.2 Conclusions

This study allows answering the research questions and hypothesis regarding the hydrological functioning of the large wetlands in the Bolivian Amazon.

Initially, we provided new insights regarding the influences of extreme climatic conditions in the region and we had contributed to reduce the gaps between common perception and scientific evidence about extreme floods the region. We had shown that major flood events in the Bolivian Amazon lowlands are characterized by the superposition of flood waves originating in the Beni-Madre de Dios River system (western upper Madeira) and the Mamoré–Guaporé river system (eastern upper Madeira). We also conclude that the dynamics of the flooded area are strongly dependent on the timing and spatial distribution of positive rainfall anomalies, while the magnitude of the flooding is strongly dependent not only on the spatial distribution of the positive anomalies but also on the location of intense rainfall spots. With these, we had debunked previous hypothesis and common perception about the causes of extreme flood events, which include the impacts of hydropower dams in the Brazilian side of the basin, impacts from deforestation and sediment load into the wetlands.

Our results contributes to answering previous hypothesis regarding the flood process: As suggested by Bourrel et al. (2009), floods in the Llanos are a combination of an exogenous process, which is a flood wave originating in the Mamoré upper drainage area; and an endogenous process, which is the contribution of the flooded area of the Llanos. The exogenous process is referred as an overbank spilling from the main river channel while the endogenous process results from outflow of groundwater from the floodplain as a result of local precipitations or over banks of small tributaries. We found that, although the exogenous process appears to be important in the early phase of the flooding, dampening the incoming flood wave from the Andes piedmont, the endogenous process appears to be the most important in determining the magnitude and duration of the flooding.

Multi-temporal flood mapping allowed estimating, for the first time, the distribution, extension and timing of the floods, as well as the surface water

storage within different basins in the Bolivian Amazon. It was found that the total flooded area show a noticeable variability from year to year as a response of particular rainfall distribution and the occurrence of rainfall anomalies in the different basins.

With the complementary use of satellite altimetry, which provided a third dimension (depth) to flood maps, we assessed these processes in more detail, identifying that frequent and predictable floods occur in floodplains without Andean connection where short-term changes in flood depth and extension are reported (flashier floods). On the other hand, floodplains with direct influence of the Andes (Mamoré River) depend on the arrival of flood waves from upstream tributaries (mostly during high events) and show long term changes in flood extension and depth. Another group of floodplains, those with connection to the Andean Piedmonts, shows intermediate behavior in flood frequency and flashiness.

We found that acceptable model improvements can be achieved even with few adjustments based on multi-temporal flood mapping, in this case by defining the floodable cells in the study area and setting the values of the floodplain overflow water level (ZTRA). However, limitations of the MHD-INPE model in estimating sharp variations of flooded area were detected. With the support of MODIS flood estimations and satellite altimetry, we found that the main constraint for these limitations is an inaccurate representation of the relations between water level, flooded area and stored volume within a floodplain cell, which are estimated from a SRTM-DEM. With this, we show that remote sensing information is of major importance for improving and evaluate floodplain simulations. We believe that is necessary to explore new and creative ways of integrating remote sensing and numerical models.

This study provides quantitative and spatial explicit information for improving the knowledge of the hydrology of these large wetlands, valuable elements for supporting its management, conservation and its acknowledgment by the government and society: The flood frequency map might be useful for studying ecosystem connectivity; Maps of maximum and minimum flood extension may

contribute for defining or delimiting wetlands of interest such as the RAMSAR sites; Estimations of surface water storage in floodplains constitute an initial quantification of the wetlands role in buffering the flood wave during extreme events and to support the functioning of the ecosystems during normal years.

## REFERENCES

- ABRIL, G.; MARTINEZ, J.-M.; ARTIGAS, L. F.; MOREIRA-TURCQ, P.; BENEDETTI, M. F.; VIDAL, L.; MEZIANE, T.; KIM, J.-H.; BERNARDES, M. C.; SAVOYE, N. Amazon River carbon dioxide outgassing fuelled by wetlands. **Nature**, v. 505, n. 7483, p. 395–398, 2014.
- ACHA, D.; INIGUEZ, V.; ROULET, M.; GUIMARAES, J. R. D.; LUNA, R.; ALANOCA, L.; SANCHEZ, S. Sulfate-Reducing Bacteria in Floating Macrophyte Rhizospheres from an Amazonian Floodplain Lake in Bolivia and Their Association with Hg Methylation. **Appl. Environ. Microbiol.**, v. 71, n. 11, p. 7531–7535, 2005.
- ALCANTARA, E. H.; STECH, J.; NOVO, E.; SHIMABUKURO, Y.; BARBOSA, C. C. Turbidity in the Amazon Floodplain Assessed Through a Spatial Regression Model Applied to Fraction Images Derived From MODIS/Terra. In: INTERNATIONAL GEOSCIENCE AND REMOTE SENSING SYMPOSIUM, 2008, Barcelona, Spain. **Proceedings...IEEE**, 2008
- ALSDORF, D.; BATES, P.; MELACK, J.; WILSON, M.; DUNNE, T. Spatial and temporal complexity of the Amazon flood measured from space. *Geophysical Research Letters*, v. 34, n. 8, p. L08402, 2007.
- ALSDORF, D. E. Water Storage of the Central Amazon Floodplain Measured with GIS and Remote Sensing Imagery. **Annals of the Association of American Geographers**, v. 93, n. 1, p. 55–66, 2003.
- ALURRALDE, J. C.; CAMPANINI, O.; HERBAS, R.; VAN DAMME, P. A.; DIAZ, CARLOS; VARGAS, C. El agua en Bolivia - Documento de trabajo. La Paz: Ministerio del Agua, 2008.
- ANDREADIS, K. M.; SCHUMANN, G. J.-P. Estimating the impact of satellite observations on the predictability of large-scale hydraulic models. **Advances in Water Resources**, v. 73, p. 44–54, 2014.
- ARGOLLO, J. The Parapeti River and the Izozog swamps, Bolivia. **Revista UNG Geociencias**, v. 5, n. 1, p. 38–44, 2006.
- ARNESEN, A. S.; SILVA, T. S. F.; HESS, L. L.; NOVO, E. M. L. M.; RUDORFF, C. M.; CHAPMAN, B. D.; MCDONALD, K. C. Monitoring flood extent in the lower Amazon River floodplain using ALOS/PALSAR ScanSAR images. **Remote Sensing of Environment**, v. 130, n. 0, p. 51–61, 2013.
- ARNÉZ, A. M. El impacto de la construcción de represas en las enfermedades de transmisión vectorial. In: ARNÉZ, A. M.; MAMANI, E.; NOVOA, G.;

- MOLINA, J.; LEDEZMA, F.; VAUCHEL, P.; CANESE, R. (Eds.). **Bajo el caudal- El impacto de las represas del rio Madera en Bolivia**. La Paz-Bolivia: Foro Boliviano de Medio Ambiente FOBOMADE, 2009.
- ARONICA, G.; BATES, P. D.; HORRITT, M. S. Assessing the uncertainty in distributed model predictions using observed binary pattern information within GLUE. **Hydrological Processes**, v. 16, n. 10, p. 2001–2016, jul. 2002.
- ARRAUT, E. M.; SILVA, T. S. F.; NOVO, E. M. Secas extremas na planicie de inundacao amazônica: alguns impactos sobre a ecologia e a biodiversidade. In: BORMA, L. D. S.; NOBRE, C. (Eds.). **Secas na Amazônia** - causas e consequências. Sao Paulo: Oficina de textos, 2013.
- AYLWARD, B.; BANDYOPADHYAY, J.; BELAUSTEGUIGOTIA, J.-C. Freshwater ecosystem services. In: CHOPRA, K.; LEEMANS, R.; KUMAR, P.; SIMONS, H. (Eds.). **Ecosystems and human well-being: policy responses**. Washington, Island Press, 2005. v. 3. (Millennium Ecosystem Assessment)
- BAKER, D. B.; RICHARDS, R. P.; LOFTUS, T. T.; KRAMER, J. W. A NEW FLASHINESS INDEX: CHARACTERISTICS AND APPLICATIONS TO MIDWESTERN RIVERS AND STREAMS. **Journal of the American Water Resources Association**, v. 40, n. 2, p. 503–522, abr. 2004.
- BATES, P. D.; DE ROO, A. P. J. A simple raster-based model for flood inundation simulation. **Journal of Hydrology**, v. 236, n. 1–2, p. 54–77, 2000.
- BATES, P. D.; HORRITT, M. S.; SMITH, C. N.; MASON, D. Integrating remote sensing observations of flood hydrology and hydraulic modelling. **Hydrological Processes**, v. 11, n. 14, p. 1777–1795, 1997.
- BAUGH, C. A.; BATES, P. D.; SCHUMANN, G.; TRIGG, M. A. SRTM vegetation removal and hydrodynamic modeling accuracy. **Water Resources Research**, v. 49, n. 9, p. 5276–5289, set. 2013.
- BECK, S.; ZENTENO-RUIZ, F.; LÓPEZ R.; LARREA-ALCÁZAR, D.; UZQUIANO, J.; ANTEZANA, A. **Estudio del impacto del fenómeno ENSO (El niño Oscilación del Sur) en la diversidad biológica de Beni y Pando**. Viceministerio de Biodiversidad, Recursos Forestales y Medio Ambiente., 2008.
- BELLAMY JA; JOHNSON, A. K. L. Integrated resource management: moving from rhetoric to practice in Australian agriculture. **Environmental Management**, v. 25, n. 3, p. 265–280, 2000.
- BEVEN, K. TOPMODEL: a critique. **Hydrological Processes**, v. 11, n. 9, p. 1069–1085, 1997.
- BIANCAMARIA, S.; BATES, P. D.; BOONE, A.; MOGNARD, N. M. Large-scale

coupled hydrologic and hydraulic modelling of the Ob river in Siberia. **Journal of Hydrology**, v. 379, n. 1, p. 136–150, 2009.

BIRKETT, C. M. The contribution of TOPEX/POSEIDON to the global monitoring of climatically sensitive lakes. **Journal of Geophysical Research**, v. 100, n. C12, p. 25179, 1995.

BIRKINSHAW, S. J.; O'DONNELL, G. M.; MOORE, P.; KILSBY, C. G.; FOWLER, H. J.; BERRY, P. A. M. Using satellite altimetry data to augment flow estimation techniques on the Mekong River. **Hydrological Processes**, v. 24, n. 26, p. 3811–3825, 30 dez. 2010.

BLASCHKE, T. Object based image analysis for remote sensing. *ISPRS Journal of Photogrammetry and Remote Sensing*, v. 65, n. 1, p. 2–16, 2010.

BOJSEN, B. H.; BARRIGA, R. Effects of deforestation on fish community structure in Ecuadorian Amazon streams. **Freshwater Biology**, v. 47, n. 11, p. 2246–2260, nov. 2002.

BOLEE, E. (Ed). **Ecosystems for water and food security**. Nairobi: United Nations Environment Programme Colombo: International Water Management Institute, 2011.

BONNET, M. P.; BARROUX, G.; MARTINEZ, J. M.; SEYLER, F.; MOREIRA-TURCQ, P.; COCHONNEAU, G.; MELACK, J. M.; BOAVENTURA, G.; MAURICE-BOURGOIN, L.; LEÓN, J. G.; ROUX, E.; CALMANT, S.; KOSUTH, P.; GUYOT, J. L.; SEYLER, P. Floodplain hydrology in an Amazon floodplain lake (Lago Grande de Curuaí-). **Journal of Hydrology**, v. 349, n. 1–2, p. 18–30, 2008.

BOUCHEZ, J.; GAILLARDET, J.; LUPKER, M.; LOUVAT, P.; FRANCE-LANORD, C.; MAURICE, L.; ARMIJOS, E.; MOQUET, J.-S. Floodplains of large rivers: Weathering reactors or simple silos? **Chemical Geology**, v. 332-333, p. 166–184, 2012.

BOURREL, L.; PHILLIPS, L.; MOREAU, S. The dynamics of floods in the Bolivian Amazon Basin. **Hydrological Processes**, v. 23, n. 22, p. 3161–3167, 2009.

BRONDIZIO, E.; MORAN, E.; MAUSEL, P.; WU, Y. Land cover in the Amazon estuary: linking of the Thematic Mapper with botanical and historical data. **Photogrammetric Engineering and Remote Sensing**, v. 62, n. 8, p. 921–930, 1996.

CALMANT, S.; DA SILVA, J. S.; MOREIRA, D. M.; SEYLER, F.; SHUM, C. K.; CRÉTAUX, J. F.; GABALDA, G. Detection of Envisat RA2/ICE-1 retracked

radar altimetry bias over the Amazon basin rivers using GPS. **Advances in Space Research**, v. 51, n. 8, p. 1551–1564, abr. 2013.

CALMANT, S.; SEYLER, F. Continental surface waters from satellite altimetry. **Comptes Rendus Geoscience**, v. 338, n. 14, p. 1113–1122, 2006.

CALMANT, S.; SEYLER, F.; CRETAUX, J. F. Monitoring continental surface waters by satellite altimetry. **Surveys in Geophysics**, v. 29, n. 4–5, p. 247–269, 24 out. 2008.

CARABAJAL, C. C.; HARDING, D. J. SRTM C-Band and ICESat laser altimetry elevation comparisons as a function of tree cover and relief. **Photogrammetric Engineering & Remote Sensing**, v. 72, n. 3, p. 287–298, 1 mar. 2006.

CASTELLO, L.; MACEDO, M. N. Large-scale degradation of Amazonian freshwater ecosystems. **Global Change Biology**, v. 22, n. 3, p. 990–1007, mar. 2016.

COMISIÓN ECONÓMICA PARA AMÉRICA LATINA Y EL CARIBE (CEPAL). **Evaluación del Impacto Acumulado y Adicional Ocasionado por la Niña 2008 en Bolivia**. La Paz-Bolivia. 2008. (LC/MEX/R. 919)

CHARRIÈRE, M.; BOURREL, L.; GAUTIER, E.; POUILLY, M. División geomorfológica del Río Mamoré. In: POUILLY, M.; BECK, S. G.; MORAES R., M.; IBAÑEZ, C. (Eds.). **Diversidad biológica en la llanura de inundación del Río Mamoré**. Importancia ecológica de la dinámica fluvial. La Paz: Fundación Simón I. Patiño, 2004. p. 77–94.

CIPCA. Inundaciones: más allá del cambio climático y la deforestación. 2014.

COE, M. T.; COSTA, M. H.; HOWARD, E. A. Simulating the surface waters of the Amazon River basin: Impacts of new river geomorphic and flow parameterizations. **Hydrological Processes**, v. 22, n. 14, p. 2542–2553, 2008.

COE, M. T.; COSTA, M. H.; SOARES-FILHO, B. S. The influence of historical and potential future deforestation on the stream flow of the Amazon River “ Land surface processes and atmospheric feedbacks. **Journal of Hydrology**, v. 369, n. 1–2, p. 165–174, 2009.

COLLISCHONN, W.; ALLASIA, D.; DA SILVA, B. C.; TUCCI, C. E. M. The MGB-IPH model for large-scale rainfall Runoff modelling. **Hydrological Sciences Journal**, v. 52, n. 5, p. 878–895, 2007.

CRESPO, A.; VAN DAMME, P. A. Spatial flood patterns in the Amazon Basin of Bolivia. In: VAN DAMME, P. A.; CARVAJAL, F.; MOLINA, J. (Eds.). **Los Peces y Delfines de la Amazonia Boliviana: Hábitats, Potencialidades y Amenazas**. Cochabamba - Bolivia: Editorial Inia, 2011. p. 15–28.

CUÉLLAR, S.; RODRÍGUEZ, A.; ARROYO, J.; ESPINOZA, S.; LARREA, D. M. **Mapa de deforestacion de las Tierras Bajas y Yungas de Bolivia 2000-2005-2010**. Fundacion Amigos de la Naturaleza, 2012. Disponible em: <<http://www.sayubu.com/fan/?p=1490>>

DASILVA, J. S.; CALMANT, S.; SEYLER, F.; ROTUNNO FILHO, O. C.; COCHONNEAU, G.; MANSUR, W. J. Water levels in the Amazon basin derived from the ERS 2 and ENVISAT radar altimetry missions. **Remote Sensing of Environment**, v. 114, n. 10, p. 2160–2181, 2010.

DA SILVA, J. S.; SEYLER, F.; CALMANT, S.; ROTUNNO FILHO, O. C.; ROUX, E.; ARAÏOJO, A. A. M.; GUYOT, J. L. Water level dynamics of Amazon wetlands at the watershed scale by satellite altimetry. **International Journal of Remote Sensing**, v. 33, n. 11, p. 3323–3353, 2012.

DAVIDSON, E. A.; DE ARAUJO, A. C.; ARTAXO, P.; BALCH, J. K.; BROWN, I. F.; C. BUSTAMANTE, M. M.; COE, M. T.; DEFRIES, R. S.; KELLER, M.; LONGO, M.; MUNGER, J. W.; SCHROEDER, W.; SOARES-FILHO, B. S.; SOUZA, C. M.; WOFSY, S. C. The Amazon basin in transition. **Nature**, v. 481, n. 7381, p. 321–328, 2012.

DE CARVALHO, W. D.; MUSTIN, K. The highly threatened and little known Amazonian savannahs. **Nature Ecology & Evolution**, v. 1, n. 4, p. 100, 23 mar. 2017.

DE LUCIA LOBO, F.; NOVO, E. M. L. M.; BARBOSA, C. C. F.; GALVAO, L. S. Reference spectra to classify Amazon water types. **International Journal of Remote Sensing**, v. 33, n. 11, p. 3422–3442, 2012.

DI BALDASSARRE, G.; SCHUMANN, G.; BATES, P. D. A technique for the calibration of hydraulic models using uncertain satellite observations of flood extent. **Journal of Hydrology**, v. 367, n. 3, p. 276–282, 2009.

DOBSON, M. C.; PIERCE, L.; SARABANDI, K.; ULABY, F. T.; SHARIK, T. Preliminary analysis of ERS-1 SAR for forest ecosystem studies. **IEEE Transactions on Geoscience and Remote Sensing**, v. 30, n. 2, p. 203–211, 1992.

DOMENEGHETTI, A.; TARPANELLI, A.; TOURIAN, M. J.; BROCCA, L.; MORAMARCO, T.; CASTELLARIN, A.; SNEEUW, N. The benefit of multi-mission altimetry series for the calibration of hydraulic models. In: EGU GENERAL ASSEMBLY, 2016, Vienna Austria, Geophysical Research **Abstracts**. EGU, 2016. p.4946, v. 18

DUNNE, T.; MERTES, L. A. K.; MEADE, R. H.; RICHEY, J. E.; FORSBERG, B. R. Exchanges of sediment between the flood plain and channel of the Amazon

River in Brazil. **Geological Society of America Bulletin**, v. 110, n. 4, p. 450–467, 1998.

DURAND, M.; ANDREADIS, K. M.; ALSDORF, D. E.; LETTENMAIER, D. P.; MOLLER, D.; WILSON, M. Estimation of bathymetric depth and slope from data assimilation of swath altimetry into a hydrodynamic model. **Geophysical Research Letters**, v. 35, n. 20, p. L20401, 2008.

DURAND, M.; FU, L.-L.; LETTENMAIER, D. P.; ALSDORF, D. E.; RODRIGUEZ, E.; ESTEBAN-FERNANDEZ, D. The surface water and ocean topography mission: observing terrestrial surface water and oceanic submesoscale eddies. **Proceedings of the IEEE**, v. 98, n. 5, p. 766–779, maio 2010.

ESCURRA, J. J.; VAZQUEZ, V.; CESTTI, R.; DE NYS, E.; SRINIVASAN, R. Climate change impact on countrywide water balance in Bolivia. **Regional Environmental Change**, v. 14, n. 2, p. 727–742, 22 abr. 2014.

ESPINOZA, J. C.; MARENGO, J. A.; RONCHAIL, J.; MOLINA, J.; NORIEGA, L.; GUYOT, J. L. The extreme 2014 flood in south-western Amazon basin: the role of tropical-subtropical South Atlantic SST gradient. **Environmental Research Letters**, v. 9, n. 12, p. 124007, 2014.

ESPINOZA VILLAR, J. C.; RONCHAIL, J.; GUYOT, J. L.; COCHONNEAU, G.; NAZIANO, F.; LAVADO, W.; DE OLIVEIRA, E.; POMBOSA, R.; VAUCHEL, P. Spatio-temporal rainfall variability in the Amazon basin countries (Brazil, Peru, Bolivia, Colombia, and Ecuador). **International Journal of Climatology**, v. 29, n. 11, p. 1574–1594, 2009.

FALKENMARK, M. Freshwater as shared between society and ecosystems: from divided approaches to integrated challenges. *Philosophical Transactions of the Royal Society of London. Series B: Biological Sciences*, v. 358, n. 1440, p. 2037–2049, 2003.

FEARNSIDE, P. M. Viewpoint – decision making on Amazon Dams: politics trumps uncertainty in the Madeira River sediments controversy. **Water Alternatives**, v. 6, n. 2, p. 313-325, 2013.

FINER, M.; JENKINS, C. N. Proliferation of hydroelectric dams in the Andean Amazon and Implications for Andes-Amazon Connectivity. **PLoS ONE**, v. 7, n. 4, p. e35126, 18 abr. 2012.

FORMAN, R.; ALEXANDER, L. Roads and their major ecological effects. *annu. Rev. Ecological Systems*, v. 29, p 207-231, 1998.

FORSBERG, B. R.; ARAUJO-LIMA, C. A. R. M.; MARTINELLI, L. A.;

- VICTORIA, R. L.; BONASSI, J. A. Autotrophic carbon sources for fish of the Central Amazon. **Ecology**, v. 74, n. 3, p. 643–652, abr. 1993.
- FRAPPART, F.; CALMANT, S.; CAUHOPE, M.; SEYLER, F.; CAZENAVE, A. Preliminary results of ENVISAT RA-2-derived water levels validation over the Amazon basin. **Remote Sensing of Environment**, v. 100, n. 2, p. 252–264, 2006.
- FRASER, L. H.; KEDDY, P. **The world's largest wetlands** - ecology and conservation. Cambridge University Press, 2005.
- FU, L.-L.; CAZENAVE, A. **Satellite altimetry and earth sciences** : a handbook of techniques and applications. Academic Press, 2001. 463 p. ISBN(9780080516585).
- FUNDACIÓN-MILENIO. **Perdidas economicas por inundaciones Enero - Febrero 2014**. Disponível em: <[www.fundacion-milenio.org/Informe-Nacional-de](http://www.fundacion-milenio.org/Informe-Nacional-de)>.
- FÜSSEL, H.-M.; KLEIN, R. T. Climate change vulnerability assessments: an evolution of conceptual thinking. **Climatic Change**, v. 75, n. 3, p. 301–329, 2006.
- GARAMBOIS, P.-A.; CALMANT, S.; ROUX, H.; PARIS, A.; MONNIER, J.; FINAUD-GUYOT, P.; MONTAZEM, A.; DA SILVA, J. S. Hydraulic visibility: using satellite altimetry to parameterize a hydraulic model of an ungauged reach of a braided river. **Hydrological Processes**, v. 31, n. 4, p. 756-767, 2016,
- GARCÍA SKABAR, Y.; SALIO, P.; NICOLINI, M. Verificación de los pronosticos del modelo BRAMS centrado en la region subtropical de Sudamerica . **Revista Brasileira de Meteorologia**, v.27, n.3, p. 291 - 306, 2012.
- GETIRANA, A. C. V. Integrating spatial altimetry data into the automatic calibration of hydrological models. **Journal of Hydrology**, v. 387, n. 34, p. 244–255, 2010.
- GIUSTARINI, L.; CHINI, M.; HOSTACHE, R.; PAPPENBERGER, F.; MATGEN, P. Flood hazard mapping combining hydrodynamic modeling and multi annual remote sensing data. **Remote Sensing**, v. 7, n. 10, p. 14200–14226, 27 out. 2015.
- GLOBAL-WATER-PARTNERSHIP. **Effective water governance**: learning from the dialogues. Stockholm: UNDP, 2003.
- GLOOR, M.; BRIENEN, R. J. W.; GALBRAITH, D.; FELDPAUSCH, T. R.; SCHOENGART, J.; GUYOT, J.; ESPINOZA, J. C.; LLOYD, J.; PHILLIPS, O. L.

Intensification of the Amazon hydrological cycle over the last two decades.

**Geophysical Research Letters**, v. 40, n. 9, p. 1729–1733, 2013.

GUIMBERTEAU, M.; DRAPEAU, G.; RONCHAIL, J.; SULTAN, B.; POLCHER, J.; MARTINEZ, J. M.; PRIGENT, C.; GUYOT, J. L.; COCHONNEAU, G.; ESPINOZA, J. C.; FILIZOLA, N.; FRAIZY, P.; LAVADO, W.; DE OLIVEIRA, E.; POMBOSA, R.; NORIEGA, L.; VAUCHEL, P. Discharge simulation in the sub-basins of the Amazon using ORCHIDEE forced by new datasets. **Hydrol. Earth Syst. Sci.**, v. 16, n. 3, p. 911–935, 2012.

GUPTA, H. V.; SOROOSHIAN, S.; YAPO, P. O. Status of automatic calibration for hydrologic models: comparison with multilevel expert calibration. **Journal of Hydrologic Engineering**, v. 4, n. 2, p. 135–143, abr. 1999.

GUYOT, J. L. **Hydrogéochimie des fleuves de l'amazone Bolivienne**. 1993. Bourdeaux: Université de Bourdeaux, 1993.

GUYOT, J. L.; FILLZOLA, N.; QUINTANILLA, J.; CORTEZ, J. Dissolved solids and suspended sediment yields in the Rio Madeira basin, from the Bolivian Andes to the Amazon. In: Walling, D. E.; Webb, B. W. (Eds.). **Erosion and sediment yield: global and regional perspectives**. Exeter UK: IAHS, 1996.

HALL, A. C.; SCHUMANN, G. J. P.; BAMBER, J. L.; BATES, P. D. Tracking water level changes of the Amazon Basin with space-borne remote sensing and integration with large scale hydrodynamic modelling: a review. **Physics and Chemistry of the Earth, Parts A/B/C**, v. 36, n. 7 -8, p. 223–231, 2011.

HAMILTON, S. K.; SIPPEL, S. J.; MELACK, J. M. Comparison of inundation patterns among major South American floodplains. **Journal of Geophysical Research: Atmospheres (1984 - 2012)**, v. 107, n. D20, p. LBA 5-1-LBA 5-14, 2002.

HAMILTON, S. K.; SIPPEL, S. J.; MELACK, J. M. Seasonal inundation patterns in two large savanna floodplains of South America: the Llanos de Moxos (Bolivia) and the Llanos del Orinoco (Venezuela and Colombia). **Hydrological Processes**, v. 18, n. 11, p. 2103–2116, 2004.

HANAGARTH, W. **Acerca de la geocología de las sabanas del Beni en el noreste de Bolivia**. La Paz, Bolivia: Instituto de Ecología, 1993.

HELLER, K. A.; GHAMRANI, Z. Bayesian Hierarchical Clustering. In: INTERNATIONAL CONFERENCE ON MACHINE LEARNING (ICML '05), 2005, New York, NY, USA. **Proceedings...** New York, NY, USA: ACM, 2005, Disponible em: <<http://doi.acm.org/10.1145/1102351.1102389>>

HESS, L. L.; MELACK, J. M.; AFFONSO, A.; BARBOSA, C. C. F.; GASTIL, M.;

NOVO, E. M. **LBA-ECO LC-07 Wetland extent, vegetation, and inundation: lowland Amazon Basin**. Oak Ridge, Tennessee, USA: ORNL DAAC, 2015a.

HESS, L. L.; MELACK, J. M.; NOVO, E. M. L. M.; BARBOSA, C. C. F.; GASTIL, M. Dual-season mapping of wetland inundation and vegetation for the central Amazon basin. **Remote Sensing of Environment**, v. 87, n. 4, p. 404–428, 2003.

HESS, L.; MELACK, J.; AFFONSO, A.; BARBOSA, C.; GASTIL-BUHL, M.; NOVO, E. L. M. Wetlands of the lowland Amazon Basin: extent, vegetative cover, and dual-season inundated area as mapped with JERS-1 Synthetic Aperture Radar. **Wetlands**, v. 35, n. 4, p. 745–756, 2015b.

HORRITT, M. .; BATES, P. . Effects of spatial resolution on a raster based model of flood flow. **Journal of Hydrology**, v. 253, n. 1, p. 239–249, 2001.

JARVIS, A.; REUTER, H. I.; NELSON, A.; GUEVARA, E. **Hole-filled SRTM for the globe Version 4. CGIAR-CSI SRTM 90m Database**. 2008. Disponível em: <<http://srtm.csi.cgiar.org>>

JONES, J. A.; SWANSON, F. J.; WEMPLE, B. C.; SNYDER, K. U. Effects of roads on hydrology, geomorphology, and disturbance patches in stream networksefectos de carreteras en la hidrología, geomorfología y parches de perturbación en redes de arroyos. **Conservation Biology**, v. 14, n. 1, p. 76–85, 2000.

JUNG, H. C.; HAMSKI, J.; DURAND, M.; ALSDORF, D.; HOSSAIN, F.; LEE, H.; HOSSAIN, A. K. M. A.; HASAN, K.; KHAN, A. S.; HOQUE, A. K. M. Z. Characterization of complex fluvial systems using remote sensing of spatial and temporal water level variations in the Amazon, Congo, and Brahmaputra Rivers. **Earth Surface Processes and Landforms**, v. 35, n. 3, p. 294–304, 15 mar. 2010.

JUNK, W. General aspects of floodplain ecology with special reference to Amazonian floodplains. In: JUNK, W. J. (ed). **The Central Amazon Floodplain**. Springer Berlin Heidelberg, 1997. v. 126p. 3–20.

JUNK, W. Current state of knowledge regarding South America wetlands and their future under global climate change. **Aquatic Sciences**, v. 75, n. 1, p. 113–131, 2013.

JUNK, W.; FURCH, K. A general review of tropical South American floodplains. **Wetlands Ecology and Management**, v. 2, n. 4, p. 231–238, 1993.

JUNK, W. J.; BAYLEY, P. B.; SPARKS, R. E. The flood pulse concept in river-floodplain systems. In: INTERNATIONAL LARGE RIVER SYMPOSIUM, 1989,

Ontario-Canada. **Proceedings...** Ontario-Canada: Canadian Special Publication of Fisheries and Aquatic Sciences, 1989

JUNK, W.; WORBES, M. The forest ecosystem of the floodplains. In JUNK, W. (ed.). JUNK, W. J. (ed). **The Central Amazon Floodplain**. Springer Berlin Heidelberg, 1997. v. 126p. 223–265.

KALLIOLA, R.; SALO, J.; PUHAKKA, M.; RAJASILTA, M.; HÄME, T.; NELLER, R. J.; RÄSÄNEN, M. E.; DANJOY ARIAS, W. A. Upper amazon channel migration. **Naturwissenschaften**, v. 79, n. 2, p. 75–79, fev. 1992.

KAYRANLI, B.; SCHOLZ, M.; MUSTAFA, A.; HEDMARK, A. Carbon storage and fluxes within freshwater wetlands: a critical review. **Wetlands**, v. 30, n. 1, p. 111–124, 2010.

KENNARD, M. J.; MACKAY, S. J.; PUSEY, B. J.; OLDEN, J. D.; MARSH, N. Quantifying uncertainty in estimation of hydrologic metrics for ecohydrological studies. **River Research and Applications**, v. 26, n. 2, p. n/a-n/a, 2009.

KOBLINSKY, C. J.; CLARKE, R. T.; BRENNER, A. C.; FREY, H. Measurement of river level variations with satellite altimetry. **Water Resources Research**, v. 29, n. 6, p. 1839–1848, jun. 1993.

KOSUTH, P.; BLITZKOW, D.; COCHONNEAU, G. Establishment of an altimetric reference network over the Amazon Basin using satellite radar altimetry (Topex Poseidon). In: SYMPOSIUM ON 15 YEARS OF PROGRESS IN RADAR ALTIMETRY, 2006, Noordwijk, Netherlands. **Proceedings...** Noordwijk, Netherlands:ESA Special Publication, 2006

KOUWEN, N.; SOULIS, E.; PIETRONIRO, A.; DONALD, J.; HARRINGTON, R. Grouped response units for distributed hydrologic modeling. **Journal of Water Resources Planning and Management**, v. 119, n. 3, p. 289–305, 1993.

LAI, X.; LIANG, Q.; YESOU, H.; DAILLET, S. Variational assimilation of remotely sensed flood extents using a 2-D flood model. **Hydrology and Earth System Sciences**, v. 18, n. 11, p. 4325–4339, 4 nov. 2014.

LE TOAN, T.; BEAUDOIN, A.; RIOM, J.; GUYON, D. Relating forest biomass to SAR data. **IEEE Transactions on Geoscience and Remote Sensing**, , v. 30, n. 2, p. 403–411, 1992.

LEGATES, D. R.; MCCABE, G. J. Evaluating the use of “goodness-of-fit” Measures in hydrologic and hydroclimatic model validation. **Water Resources Research**, v. 35, n. 1, p. 233–241, jan. 1999.

LEON, J. G.; CALMANT, S.; SEYLER, F.; BONNET, M. P.; CAUHOPÉ, M.; FRAPPART, F.; FILIZOLA, N.; FRAIZY, P. Rating curves and estimation of

average water depth at the upper Negro River based on satellite altimeter data and modeled discharges. **Journal of Hydrology**, v. 328, n. 3–4, p. 481–496, 2006.

LIANG, X.; LETTENMAIER, D. P.; WOOD, E. F.; BURGESS, S. J. A simple hydrologically based model of land surface water and energy fluxes for general circulation models. **Journal of Geophysical Research: Atmospheres (1984-2012)**, v. 99, n. D7, p. 14415–14428, 1994.

LOMBARDO, U.; DENIER, S.; MAY, J.-H.; RODRIGUES, L.; VEIT, H. Human–environment interactions in pre-Columbian Amazonia: The case of the Llanos de Moxos, Bolivia. **Quaternary International**, v. 312, p. 109–119, out. 2013.

LUBIANA, A.; FERREIRA JÚNIOR, P. D. Pivotal temperature and sexual dimorphism of *Podocnemis expansa* hatchlings (Testudines: Podocnemididae) from Bananal Island, Brazil. **Zoologia (Curitiba)**, v. 26, n. 3, p. 527–533, set. 2009.

MACEDO, M. N.; COE, M. T.; DEFRIES, R.; URIARTE, M.; BRANDO, P. M.; NEILL, C.; WALKER, W. S. Land-use-driven stream warming in southeastern Amazonia. *Philosophical Transactions of the Royal Society of London B: Biological Sciences*, v. 368, n. 1619, 2013.

MARENGO, J. A.; SOARES, W. R.; SAULO, C.; NICOLINI, M. Climatology of the low-level jet east of the Andes as derived from the NCEP&NCAR reanalyses: characteristics and temporal variability. **Journal of Climate**, v. 17, n. 12, p. 2261–2280, 2004.

MARTINEZ, J.-M.; LE TOAN, T. Mapping of flood dynamics and spatial distribution of vegetation in the Amazon floodplain using multitemporal SAR data. **Remote Sensing of Environment**, v. 108, n. 3, p. 209–223, 2007.

MATGEN, P.; HOSTACHE, R.; SCHUMANN, G.; PFISTER, L.; HOFFMANN, L.; SAVENIJE, H. H. G. Towards an automated SAR-based flood monitoring system: Lessons learned from two case studies. **Physics and Chemistry of the Earth, Parts A/B/C**, v. 36, n. 7, p. 241–252, 2011.

MATGEN, P.; SCHUMANN, G.; PAPPENBERGER, F.; PFISTER, L. Sequential assimilation of remotely sensed water stages in flood inundation models. In: SYMPOSIUM HS3007 AT IUGG2007, 2007, Perugia. **Proceedings... IAHS Publication**,, 2007.

MAURICE-BOURGOIN, L.; QUIROGA, I.; CHINCHEROS, J.; COURAU, P. Mercury distribution in waters and fishes of the upper Madeira rivers and mercury exposure in riparian Amazonian populations. **The Science of The Total Environment**, v. 260, n. 1–3, p. 73–86, 2000.

MEI, R.; WANG, G. Rain follows logging in the Amazon? Results from CAM3–CLM3. *Climate Dynamics*, v. 34, n. 7, p. 983–996, 2009.

MELACK, J. M.; FORSBERG, B. Biogeochemistry of Amazon floodplain lakes and associated wetlands. In: MCCLAIN, M. E.; VICTORIA, R. L.; RICHEY, J. E. (Eds.). **Biogeochemistry of the Amazon Basin and its role in a changing world**. New York: Oxford Univ. Press, 2001. p. 235–276.

MELACK, J. M.; HESS, L. L. Remote sensing of the distribution and extend of wetlands in the Amazon Basin. In: JUNK, W. J.; PIEDADE, M. T. F.; WITTMAN, F.; SCHÖNGART, J.; PAROLIN, P. (Eds.). **Amazonian Floodplain Forests ecophysiology, biodiversity and sustainable management**. [s.l.] Ecological Studies, 2010. v. 210.

MERTES, L. A. K.; DANIEL, D. L.; MELACK, J. M.; NELSON, B.; MARTINELLI, L. A.; FORSBERG, B. R. Spatial patterns of hydrology, geomorphology, and vegetation on the floodplain of the Amazon river in Brazil from a remote sensing perspective. **Geomorphology**, v. 13, n. 4, p. 215–232, 1995.

MICHAILOVSKY, C. I.; MILZOW, C.; BAUER-GOTTWEIN, P. Assimilation of radar altimetry to a routing model of the Brahmaputra River. *Water Resources Research*, v. 49, n. 8, p. 4807–4816, ago. 2013.

MITCH, W. J.; GOSSELINK, J. **Wetlands**. [s.l.] John Wiley & Sons Inc., 2007.

MITCHELL, B. Integrated water resource management, institutional arrangements, and land-use planning. **Environment and Planning A**, v. 37, n. 8, p. 1335–1352, 2005.

MOLINA-CARPIO, J.; ESPINOZA, J. C.; VAUCHEL, P.; RONCHAIL, J.; GUTIERREZ CALOIR, B.; GUYOT, J.-L.; NORIEGA, L. Hydroclimatology of the Upper Madeira River basin: spatio-temporal variability and trends. **Hydrological Sciences Journal**, p. 1–17, 17 jan. 2017.

MONTEITH, J. L. Evaporation and environment. **Symp. Soc. Exp. Biol**, v. 19, p. 157-184, 1965.

MORIASI, D. N.; ARNOLD, J. G.; VAN LIEW, M. W.; BINGNER, R. L.; HARMEL, R. D.; VEITH, T.-L. Model evaluation guidelines for systematic quantification of accuracy in watershed simulations. **Transactions of the ASABE**, v. 50, n. 3, p. 885–900.

NASH, J. E.; SUTCLIFFE, J. V. River flow forecasting through conceptual models part I — A discussion of principles. **Journal of Hydrology**, v. 10, n. 3, p. 282–290, abr. 1970.

NAVARRO, G.; MALDONADO, M. **Geografía ecológica de Bolivia**,

**vegetación y ambientes acuáticos.** Santa Cruz, Bolivia.: Editorial Centro de Ecología Difusión Simón I. Patiño. , 2004.

NOVO, E. M.; SHIMABUKURO, Y. E. Identification and mapping of the Amazon habitats using a mixing model. **International Journal of Remote Sensing**, v. 18, n. 3, p. 663–670, 1997.

OSAVA, M. **Deforestation in the Andes Triggers Amazon “Tsunami”** | Inter Press Service. 2014.

OVANDO, A. Deforestacion e Inundaciones en la cuenca del rio Itenez como indicadores de la contaminacion por mercurio. In: VAN DAMME MALDONADO, M. , POUJILLY, M. , DORIA, C., P. A. (Ed.). **Agua del Itenez o Guapore, Recursos Hidrobiologicos de un patrimonio binacional (Bolivia-Brasil)**. Cochabamba - Bolivia: Editorial INIA, 2012. p. 59–78.

OVANDO, A.; TEJADA, G.; TOMASELLA, J. Environmental Change and water ecosystem services in the Bolivian Amazon Lowlands (Llanos de Moxos). **GLP newsletter**, v. 12, p. 30–36, 2016.

OVANDO, A.; TOMASELLA, J.; RODRIGUEZ, D. A.; MARTINEZ, J. M.; SIQUEIRA-JUNIOR, J. L.; PINTO, G. L. N.; PASSY, P.; VAUCHEL, P.; NORIEGA, L.; VON RANDOW, C. Extreme flood events in the Bolivian Amazon wetlands. **Journal of Hydrology: Regional Studies**, v. 5, p. 293–308, 2016.

PAIVA, R. C. D.; BUARQUE, D. C.; COLLISCHONN, W.; BONNET, M.-P.; FRAPPART, F.; CALMANT, S.; BULHÕES MENDES, C. A. Large-scale hydrologic and hydrodynamic modeling of the Amazon River basin. **Water Resources Research**, v. 49, n. 3, p. 1226–1243, 2013a.

PAIVA, R. C. D.; COLLISCHONN, W.; BONNET, M.-P.; DE GONÇALVES, L. G. G.; CALMANT, S.; GETIRANA, A.; SANTOS DA SILVA, J. Assimilating in situ and radar altimetry data into a large-scale hydrologic-hydrodynamic model for streamflow forecast in the Amazon. **Hydrology and Earth System Sciences**, v. 17, n. 7, p. 2929–2946, 24 jul. 2013b.

PAIVA, R. C. D.; COLLISCHONN, W.; BUARQUE, D. C. Validation of a full hydrodynamic model for large-scale hydrologic modelling in the Amazon. **Hydrological Processes**, p. 333–346, 2012.

PAIVA, R. C. D.; COLLISCHONN, W.; TUCCI, C. E. M. Large scale hydrologic and hydrodynamic modeling using limited data and a GIS based approach. **Journal of Hydrology**, v. 406, n. 3–4, p. 170–181, 2011.

PARIS, A.; DIAS DE PAIVA, R.; SANTOS DA SILVA, J.; MEDEIROS MOREIRA, D.; CALMANT, S.; GARAMBOIS, P.-A.; COLLISCHONN, W.;

BONNET, M.-P.; SEYLER, F. Stage-discharge rating curves based on satellite altimetry and modeled discharge in the Amazon basin. **Water Resources Research**, v. 52, n. 5, p. 3787–3814, maio 2016.

PAZ, A. R. **Simulação de rios com grandes planícies de inundação**. 2010. 257 p. Tese (Doutorado em Recursos Hídricos e Saneamento Ambiental) - Universidade Federal do Rio Grande do Sul, Instituto de Pesquisas Hidráulicas, 2010.

PEKEL, J.-F.; COTTAM, A.; GORELICK, N.; BELWARD, A. S. High-resolution mapping of global surface water and its long-term changes. **Nature**, v. 540, n. 7633, p. 418–422, 7 dez. 2016.

PÉREZ, T.; POUILLY, M.; MAURICE, L.; PACO, P.; OVANDO, A.; CÓRDOVA, L. **Sensibilidad del Norte Amazónico a la contaminación por el Mercurio**. La Paz - Bolivia. 2009.

PFRAFSTETTER, O. **Classification of hydrographic basins: coding methodology**. Rio de Janeiro: Departamento Nacional de Obras e Saneamento, 1989.

PHILLIPS, O. L.; ARAGAO, L. E. O. C.; LEWIS, S. L.; FISHER, J. B.; LLOYD, J.; LÓPEZ-GONZALEZ, G.; MALHI, Y.; MONTEAGUDO, A.; PEACOCK, J.; QUESADA, C. A.; VAN DER HEIJDEN, G.; ALMEIDA, S.; AMARAL, I.; ARROYO, L.; AYMARD, G.; BAKER, T. R.; BANKI, O.; BLANC, L.; BONAL, D.; BRANDO, P.; CHAVE, J.; DE OLIVEIRA, Ã. C. A.; CARDOZO, N. D.; CZIMCZIK, C. I.; FELDPAUSCH, T. R.; FREITAS, M. A.; GLOOR, E.; HIGUCHI, N.; JIMENEZ, E.; LLOYD, G.; MEIR, P.; MENDOZA, C.; MOREL, A.; NEILL, D. A.; NEPSTAD, D.; PATIÃ±O, S.; PEÃ±UELA, M. C.; PRIETO, A.; RAMIREZ, F.; SCHWARZ, M.; SILVA, J.; SILVEIRA, M.; THOMAS, A. S.; STEEGE, H. TER; STROPP, J.; VASQUEZ, R.; ZELAZOWSKI, P.; DAVILA, E. A.; ANDELMAN, S.; ANDRADE, A.; et al. Drought Sensitivity of the Amazon Rainforest. **Science**, v. 323, n. 5919, p. 1344–1347, 2009.

PINHO, P. F.; MARENGO, J. A.; SMITH, M. S. Complex socio-ecological dynamics driven by extreme events in the Amazon. **Regional Environmental Change**, v. 15, n. 4, p. 643–655, 14 abr. 2015.

PLOTZKI, A.; MAY, J. H.; VEIT, H. Review of past and recent fluvial dynamics in the Beni lowlands, NE Bolivia. **Geogr. Helv.**, v. 66, n. 3, p. 164–172, 2012.

PLUMMER, R.; LOE, R.; ARMITAGE, D. A Systematic Review of Water Vulnerability Assessment Tools. **Water Resources Management**, v. 26, n. 15, p. 4327–4346, 2012.

POUILLY, M.; BECK, S.; MORAES, M.; IBAÑEZ, C. **Diversidad Biológica de**

**la Llanura de Inundación del Río Mamoré.** Importancia Ecológica de la Dinámica Fluvial. Santa Cruz-Bolivia: 2004.

POUILLY, M.; CÓRDOVA, L.; MARTINEZ, J.-M.; MAURICE, L.; MOLINA, J.; OVANDO, A. **Escenarios de impactos geoquímicos y ecológicos consecuentes a los cambios hidrológicos en la cuenca alta del río Madera.** La Paz-Bolivia: WWF Bolivia, 2009a.

POUILLY, M.; MARTINEZ, J. M.; CÓRDOVA, L.; PÉREZ, T.; DUPREY, J. L.; CARANZAS, B.; OVANDO, A.; GUÉRIN, F.; ABRIL, G. **Dinámica de inundación, emisión de gas y tasa de mercurio en peces en el Norte Amazónico boliviano. Hacia una cuantificación de los impactos del proyecto hidroeléctrico del río Madera.** La Paz: WWF Bolivia, 2009b.

QUEGAN, S.; LE TOAN, T. Analysing multitemporal SAR images. In: SIMPÓSIO BRASILEIRO DE SENSORIAMENTO REMOTO, 9. (SBSR)., 1998, Santos. **Anais...** São José dos Campos: INPE, 1998. p. 1183-1194. CD-ROM. Palestra convidada apresentada na II Jornada de Radar, ocorrida paralelamente ao IX SBSR, Santos, 1998. ISBN 85-17-00015-3. Disponível em: <<http://urlib.net/dpi.inpe.br/lise/2005/01.13.18.00>>..

QUEGAN, S.; LE TOAN, T.; YU, J. J.; RIBBES, F.; FLOURY, N. Multitemporal ERS SAR analysis applied to forest mapping. **IEEE Transactions on Geoscience and Remote Sensing**, v. 38, n. 2, p. 741–753, 2000.

RAPP, R. H. **A Fortran Program for the computation of gravimetric quantities from high degree spherical harmonic expansions.** Columbus: Department of Geodetic Science and Surveying, The Ohio State University, 1982.

RENO, V. F.; NOVO, E. M. L. M.; SUEMITSU, C.; RENNÃO, C. D.; SILVA, T. S. F. Assessment of deforestation in the Lower Amazon floodplain using historical Landsat MSS/TM imagery. **Remote Sensing of Environment**, v. 115, n. 12, p. 3446–3456, 2011.

RICHEY, J. E.; MELACK, J. M.; AUDENKAMPE, A. K.; BALLESTER, V. M.; HESS, L. L. Outgassing from Amazonian rivers and wetlands as a large tropical source of atmospheric CO<sub>2</sub>. **Nature**, v. 416, p. 617–620, 2002.

ROCHE, M.-A.; FERNANDEZ-JAUREGUI, C. Water resources, salinity and salt yields of the rivers of the Bolivian Amazon. **Journal of Hydrology**, v. 101, n. 1–4, p. 305–331, 1988.

RODRIGUEZ, D. A.; TOMASELLA, J. On the ability of large-scale hydrological models to simulate land use and land cover change impacts in Amazonian basins. **Hydrological Sciences Journal**, p. 1–16, 4 maio 2016.

RONCHAIL, J.; BOURREL, L.; COCHONNEAU, G.; VAUCHEL, P.; PHILLIPS, L.; CASTRO, A.; GUYOT, J.-L.; DE OLIVEIRA, E. Inundations in the Mamore basin (south-western Amazon - Bolivia) and sea-surface temperature in the Pacific and Atlantic Oceans. **Journal of Hydrology**, v. 302, n. 1-4, p. 223–238, 2005.

RONCHAIL, J.; BOURREL, L.; MAURICE-BOURGOIN, L.; VAUCHEL, P.; COCHONNEAU, G.; GUYOT, J. L.; PHILLIPS, L.; CASTRO, A. Hydrology and Climate in the Southwestern Amazon Basin (Bolivia). **Geophysical Research Abstracts**, v. 5, n. 10982, 2003.

RUDORFF, C. M.; GALVAO, L. S.; NOVO, E. M. L. M. Reflectance of floodplain waterbodies using EO-1 Hyperion data from high and receding flood periods of the Amazon River. **International Journal of Remote Sensing**, v. 30, n. 10, p. 2713–2720, 2009.

RUDORFF, C. M.; MELACK, J. M.; BATES, P. D. Flooding dynamics on the lower Amazon floodplain: 1. Hydraulic controls on water elevation, inundation extent, and river-floodplain discharge. **Water Resources Research**, v. 50, n. 1, p. 619–634, jan. 2014.

SAMPAIO, G.; NOBRE, C.; COSTA, M. H.; SATYAMURTY, P.; SOARES-FILHO, B. S.; CARDOSO, M. Regional climate change over eastern Amazonia caused by pasture and soybean cropland expansion. **Geophys. Res. Lett.**, v. 34, n. 17, p. L17709, 2007.

SANTOS DA SILVA, J.; CALMANT, STÉPHANE; MEDEIROS MOREIRA, D.; CONCHY, T.; FRAPPART, F.; BECKER, M. The question of the AltiKa/Ice-1 bias over rivers. In: EGU GENERAL ASSEMBLY, 2015, held 12-17 April, 2015 in Vienna, Austria. **Geophysical Research Abstracts**. Vienna: EGU, 2015b id.2832, v. 17.

SANTOS DA SILVA, J.; CALMANT, S.; MEDEIROS MOREIRA, D.; OLIVEIRA, R.; CONCHY, T.; GENNERO, M.-C.; SEYLER, F. Validation of SARAL/AltiKa data in the Amazon basin. In: EGU GENERAL ASSEMBLY, 2015, held 12-17 April, 2015 in Vienna, Austria. **Geophysical Research Abstracts**. Vienna: EGU, 2015b. id.2593, v. 17, 2015b.

SARTORI, L. R.; IMAI, N. N.; MURA, J. C.; NOVO, E. M. L. M.; SILVA, T. S. F. Mapping Macrophyte Species in the Amazon Floodplain Wetlands Using Fully Polarimetric ALOS/PALSAR Data. **IEEE Transactions on Geoscience and Remote Sensing**, v. 49, n. 12, p. 4717–4728, 2011.

SCHUMANN, G.; BATES, P. D.; HORRITT, M. S.; MATGEN, P.; PAPPENBERGER, F. Progress in integration of remote sensing-derived flood extent and stage data and hydraulic models. **Reviews of Geophysics**, v. 47, n.

4, p. n/a-n/a, 2009.

SCHUMANN, G. J.-P.; DOMENEGHETTI, A. Exploiting the proliferation of current and future satellite observations of rivers. **Hydrological Processes**, v. 30, n. 16, p. 2891–2896, 30 jul. 2016.

SCHUMANN, G. J.-P.; MOLLER, D. K. Microwave remote sensing of flood inundation. **Physics and Chemistry of the Earth, Parts A/B/C**, v. 83, p. 84–95, 2015.

SEILER, C. **Implementation and validation of a Regional Climate Model for Bolivia**. Fundacion Amigos de la Naturaleza, 2009.

SEILER, C.; HUTCHES, R. W.; KABAT, P. Climate variability and trends in Bolivia. **Journal of Applied Meteorology and Climatology**, v. 52, 2012.

SEILER, C.; HUTCHES, R. W.; KABAT, P.-. Likely Ranges of Climate Change in Bolivia. **Appl. Meteor. Climatol**, v. 52, p. 1303–1317, 2013.

SEYLER, F.; CALMANT, S.; SILVA, J. DA; LEON, J.-G.; FRAPPART, F.; BONNET, M.-P.; FILIZOLA, N.; ROUX, E.; COCHONNEAU, G.; COSTI, A.-C. Z. New perspectives in monitoring water resources in large tropical transboundary basins based on satellite imagery and radar altimetry. In: BLÖSCHL, G, et al. (eds.). **Improving integrated surface and groundwater resources management in a vulnerable and changing world** : proceedings of symposium JS.3. Wallingford : AISH, 2009. SIQUEIRA-JUNIOR, J. L.; OVANDO, A.; TOMASELLA, J.; RODRIGUEZ, D. A. Optimization of the MHD-INPE model through remote sensing. In preparation,

SIQUEIRA-JÚNIOR, J. L. S.; TOMASELLA, J.; RODRIGUEZ, D. A. Impacts of future climatic and land cover changes on the hydrological regime of the Madeira River basin. **Climatic Change**, v. 129, n. 1–2, p. 117–129, 2015.

TAKEUCHI, K.; AO, T.; ISHIDAIRA, H. Introduction of block-wise use of TOPMODEL and Muskingum-Cunge method for the hydroenvironmental simulation of a large ungauged basin. **Hydrological Sciences Journal**, v. 44, n. 4, p. 633–646, 1999.

TEJADA, G.; DALLA-NORA, E.; CORDOVA, D.; LAFORTEZZA, R.; OVANDO, A.; ASSIS, T.; AGUIAR, A. P.. Deforestation scenarios for the Bolivian lowlands, **Environmental research, Spetial issue: “Provision of Ecosystem”**, v. 144, p. 49-63. 2015.

TOMASELLA, J.; PINHO, P. F.; BORMA, L. S.; MARENGO, J. A.; NOBRE, C. A.; BITTENCOURT, O. R. F. O.; PRADO, M. C. R.; RODRIGUEZ, D. A.; CUARTAS, L. A. The droughts of 1997 and 2005 in Amazonia: floodplain

hydrology and its potential ecological and human impacts. **Climatic Change**, v. 116, n. 3–4, p. 723–746, 2013.

TOURIAN, M. J.; TARPANELLI, A.; ELMI, O.; QIN, T.; BROCCA, L.; MORAMARCO, T.; SNEEUW, N. Spatiotemporal densification of river water level time series by multimission satellite altimetry. **Water Resources Research**, v. 52, n. 2, p. 1140–1159, fev. 2016.

TRANCOSO, R.; LARSEN, J. R.; MCALPINE, C.; MCVICAR, T. R.; PHINN, S. Linking the Budyko framework and the Dunne diagram. **Journal of Hydrology**, v. 535, p. 581–597, 2016.

TRIMBLE. **eCognition Developer 8.7** - reference book. München, Germany: [s.n.].

UDAPE. **Evaluación de daño y perdidas por eventos climaticos** - Bolivia 2013-2014. La Paz - Bolivia. 2015.

VAN DAMME, P. A. **Disponibilidad, uso y calidad de los recursos hídricos en Bolivia**. Cumbre Mundial sobre el Desarrollo Sostenible, Johannesburgo: Comision para la Gestión Integral del Agua en Bolivia CGIAB, 2002.

VAN DAMME, P. A.; CARVAJAL-VALLEJOS, F.; SARMIENTO, J.; BECCERRA, P. Vulnerabilidad de los peces de las tierras bajas de la Amazonia Boliviana. In: VAN DAMME, P. A.; CARVAJAL, F.; MOLINA, J. (Eds.). **Los peces de la Amazonía boliviana: hábitats, potencialidades y amenazas**. Cochabamba - Bolivia: Faunagua, 2010.

VIERS, J.; BARROUX, G.; PINELLI, M.; SEYLER, P.; OLIVA, P.; DUPRÉ, B.; BOAVENTURA, G. R.; DUPRÉ, B.; BOAVENTURA, G. R. The influence of the Amazonian floodplain ecosystems on the trace element dynamics of the Amazon River mainstem (Brazil). **Science of The Total Environment**, v. 339, n. 1, p. 219–232, 1 mar. 2005.

VILLAZON, M.; INTURIAS, D. Modelación hidrológica distribuida con datos satelitales a gran escala, escenarios de precipitación con datos de Tierra y TRMM. Caso de estudio: Cuenca del Rio Mamoré. In: 1ra CONFERENCIA NACIONAL DE ESPECIALISTAS EN SISTEMAS DE INFORMACIÓN GEOGRÁFICA Y TELEDETECCIÓN APLICADO A CUENCAS Y RECURSOS HÍDRICOS, 1., 2015, La Paz - Bolivia. **Anales...** La Paz - Bolivia: 2015WESTERHOFF, R. S.; H KLEUSKENS, M. P.; WINSEMIUS, H. C.; HUIZINGA, H. J.; BRAKENRIDGE, G. R.; BISHOP, C. Automated global water mapping based on wide-swath orbital synthetic-aperture radar. **Hydrol. Earth Syst. Sci**, v. 17, p. 651–663, 2013.

WILLIAMS, M. R.; FISHER, T. R.; MELACK, J. M. Solute dynamics in soil water

and groundwater in a central Amazon catchment undergoing deforestation. **Biogeochemistry**, v. 38, n. 3, p. 303–335, 1997.

WILSON, M.; BATES, P.; ALSDORF, D.; FORSBERG, B.; HERRITT, M.; MELACK, J.; FRAPPART, F.; FAMIGLIETTI, J. Modeling large-scale inundation of Amazonian seasonally flooded wetlands. *Geophysical Research Letters*, v. 34, n. 15, p. L15404, 2007a.

WILSON, M.; BATES, P.; ALSDORF, D.; FORSBERG, B.; HERRITT, M.; MELACK, J.; FRAPPART, F.; FAMIGLIETTI, J. Modeling large-scale inundation of Amazonian seasonally flooded wetlands. **Geophysical Research Letters**, v. 34, n. 15, ago. 2007b.

WINGHAM, D. J.; RAPPLEY, C. G.; GRIFFITHS, H. New techniques in satellite altimeter tracking systems. In: ESA INTERNATIONAL GEOSCIENCE AND REMOTE SENSING SYMPOSIUM(IGARSS'86) ON REMOTE SENSING: TODAY'S SOLUTIONS FOR TOMORROW'S INFORMATION NEEDS, 1986, **Proceedings...** ESA, 1986. v. 3, p 1339-1344

WITTMANN, F.; HOUSEHOLDER, E.; LOPES, A.; OLIVEIRA WITTMANN, A.; JUNK, W. J.; PIEDADE, M. T. F. Implementation of the Ramsar Convention on South American wetlands: an update, **Journal of Research and reports in biodiversity studies**. V4, P 47- 58, 2015.

WOODHOUSE, I. H. **Introduction to microwave remote sensing**. CRC press, 2005. ISBN(0415271231).

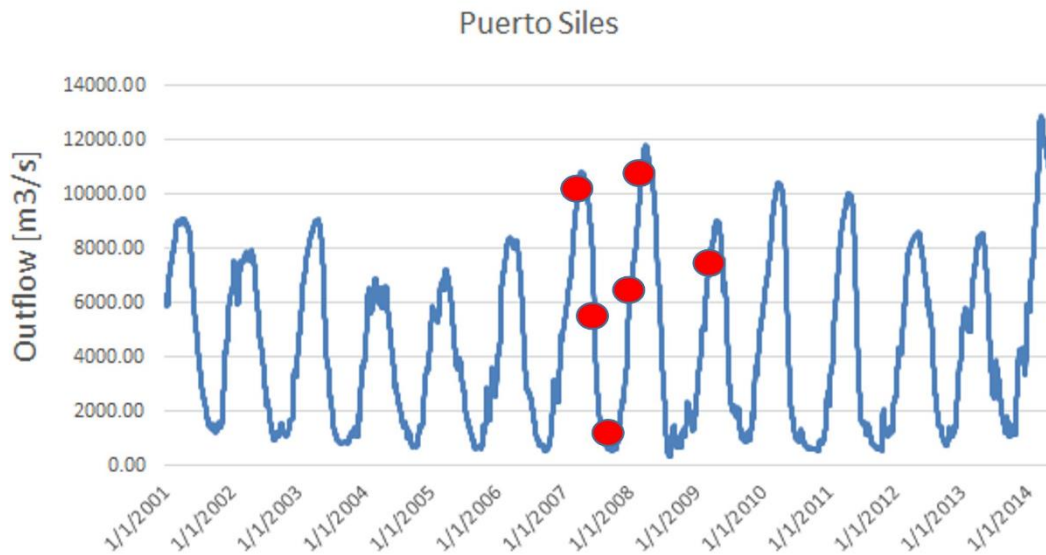
WWF. Bolivia designates world's largest protected wetland Washington, 2017.

ZHAO, R. J. The Xinanjiang model applied in China. **Journal of Hydrology**, v. 135, n. 371–381, 1992.



## APPENDIX 1

Figure A1 – Detail of altimetric measurements along a satellite track:



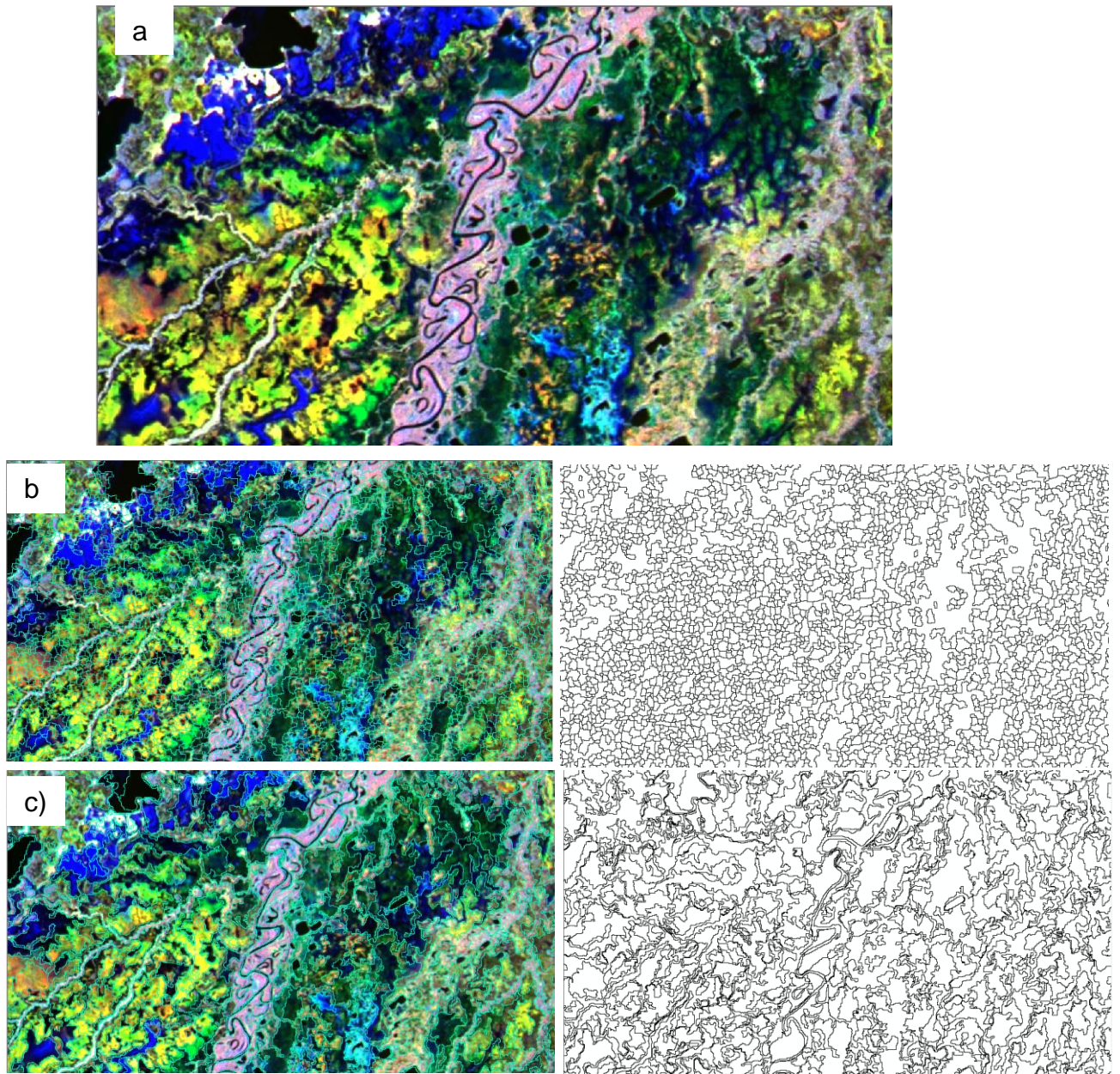
Source: by the author

Table A1 - List of ALOS PALSAR images for each date, and coverage of the study area

<b>Mosaic</b>	<b># scenes</b>	<b>Spatial coverage (% of the area)</b>
Mar 07	8	100%
Jun 07	8	100%
Sep 07	8	98% (Missing small portion for the Paragua)
Dec 07	8	100%
Mar 08	7	98% (Missing small portion for the Paragua)
Mar 09	6	100%

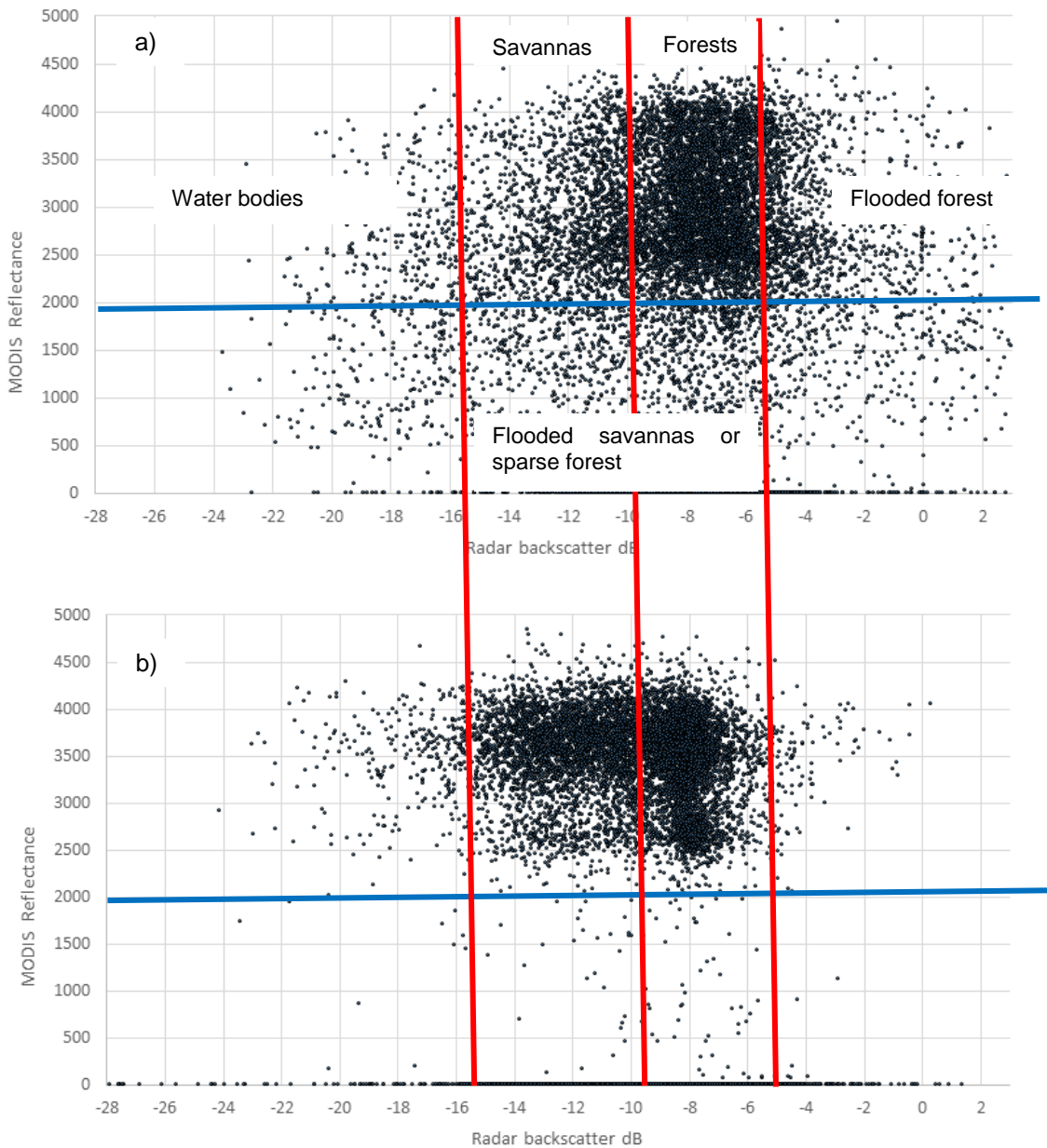
Source: by the author

Figure A2 – Contrast between segmentation methods.



Contrast between segmentation methods: a) RGB (Mar07, Dec07, Sep07); b) multi shape. 0.2, color 0.5 – spec 0.015; c) multi shape.0 , col 0.8.  
Source: by the author.

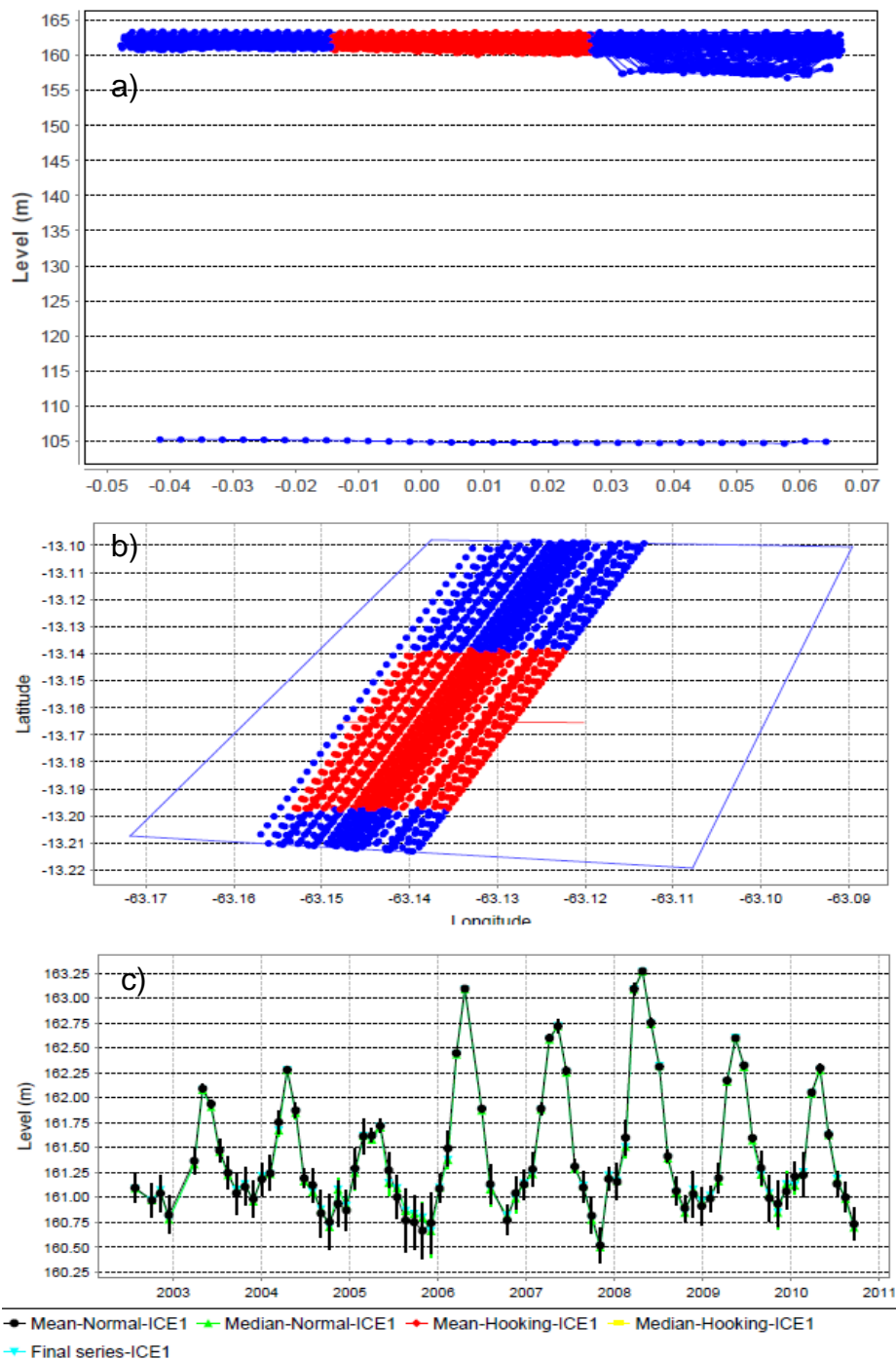
Figure A3. – Scatter plot between MODIS reflectance (MIR band) and radar backscatter during wet and dry season.



a) Noticeable dispersion of radar signal and MODIS reflectance during wet month (Mar-2007); b) Less dispersion of radar and MODIS during dry season (Sep-2007). Red lines show the threshold values for differentiating land cover units (mean backscatter in the classification algorithm). Blue lines are possible MODIS thresholds. Values with 0 are cloud covered objects.

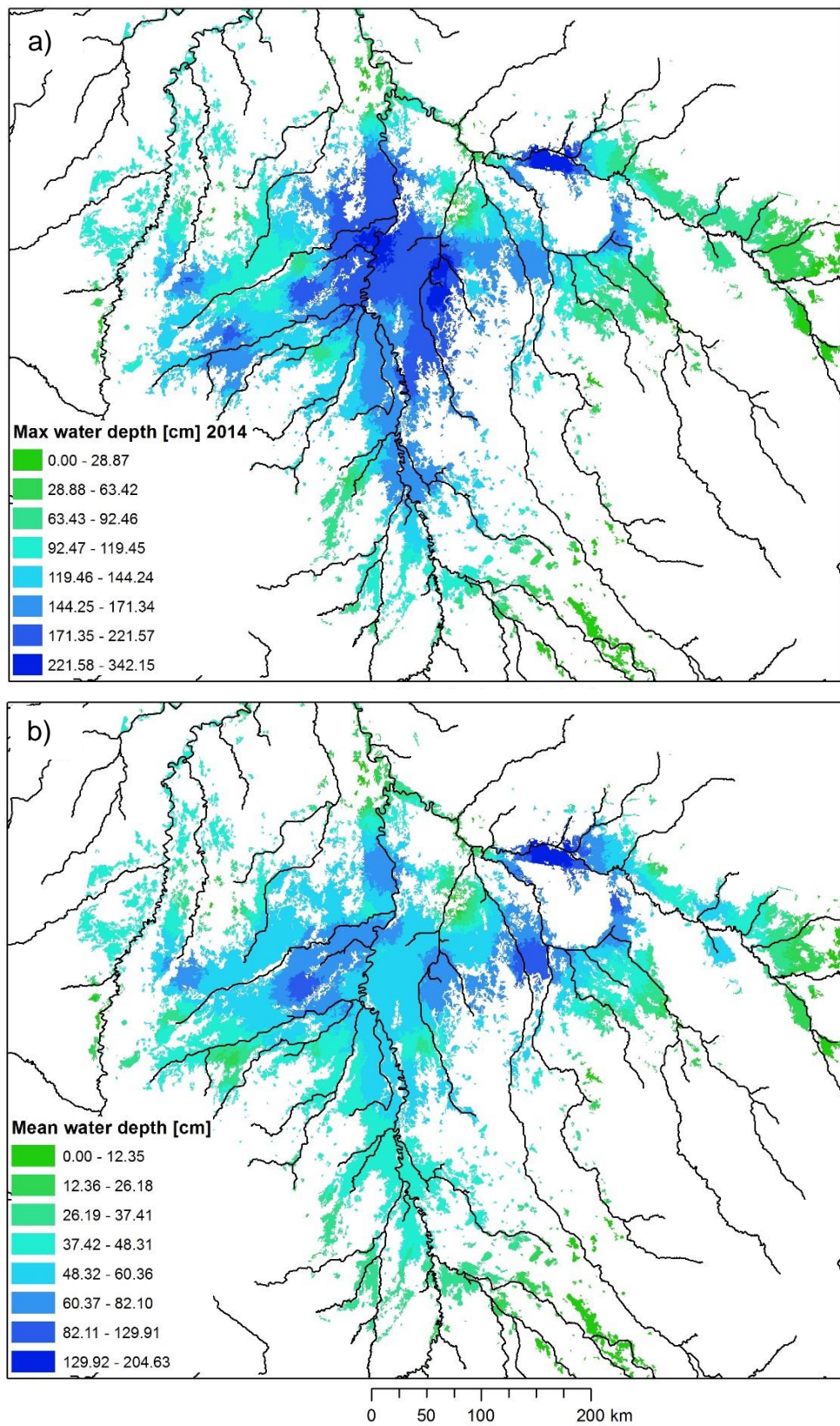
Source: by the author

Figure A4 – Detail of altimetric measurements along a satellite track.



a) Chart of the projected altimetric measurements; b) Geographical position; and c) Final time series. Red points indicate the selected measurements.  
Source: by the author

Figure A5, - Maximum and mean water depth estimates.



Source: by the author